Pyridopyrimidinones as *Cryptosporidium parvum* Calcium Dependent Protein Kinase 1 (*Cp*CDPK1) Inhibitors

by

Dr. Elise Marie Waldron-Young, PharmD.

A dissertation submitted to the Department of Pharmacology and Pharmaceutical Sciences,

College of Pharmacy

in partial fulfillment of the requirements for the degree of

Doctor of Philosophy

in Pharmacology with Emphasis in Medicinal Chemistry

Chair of Committee: Dr. Gregory Cuny Ph.D.

Committee Member: Dr. Nicolas Beyda PharmD.

Committee Member: Dr. Ming Hu Ph.D.

Committee Member: Dr. Meghana Trivedi PharmD. Ph.D.

Committee Member: Dr. Louis Williams Ph.D.

University of Houston

December 2021

DEDICATION

I would like to dedicate my dissertation to my grandparents: Dr. Howard Waldron, Ph.D. and Grace Waldron (my Grandad and Peege). Before I was born, my grandmother was asked what she wanted to be called. She hated “grandmother”, or “granny”, so her friend asked her, what do you want your grandkids to know you for, or remember you as? Reading – she got her love of reading from a woman named Peege. That’s where the name Peege came from. I do not have a lot of memories of my grandparents – they were the old Victorian-type grandparents. However, I have fond memories of sharing books with Peege. I would buy a secondhand book, and if I liked it, I would mail it to her. She would tell my mum what she thought. We did this for years, until I started University and got too busy reading for school. But nevertheless, she taught me my love of reading. On the other hand, my grandad passed when I was a young kid, but he always had a saying, “a doctor can make a mistake and harm one person, but if an engineer or scientist makes a mistake, thousands can be harmed”. He was referring to an engineering blunder that occurred in Canada. A new bridge collapsed, and hundreds of people perished. To remind the engineers of their importance, they are all given a ring made from the bridge. The same philosophy applies to science – a mistake can result in the harm of thousands. But a job well done can benefit sustainably more people than a physician or a doctor. This is why I chose to pursue a Ph.D.; this is why I was never satisfied with a PharmD. I wanted to make a bigger difference.

ACKNOWLEDGMENTS

Submitting this document marks the completion of my dual degree program. I started this PharmD/PhD program when I was only nineteen years old. So, I would like to take this time to thank the College of Pharmacy for the opportunity and for taking the chance on me, allowing me to grow and flourish. I want to acknowledge the faculty and staff who have taken the time to not only educate me and instill their passion onto me, but also took the time to get to know me and my passions. This college has been like a home to me for the last seven years. I have been in the college at all hours of the day and night, working on my PhD, studying for PharmD exams, taking part in student organizations, meetings with faculty and staff trying to improve the college, and just hanging out with friends.

I want to personally thank my mentors over the years. I have reached out to Dr. Vincent Tam more than I care to admit. He has been a significant help in my training and support. I also would like to acknowledge Dean Pitman and Dean Prichard, whom have both taken the time to listen to my thoughts and concerns, especially with the challenges during the pandemic. Both Dr. Tam and Dr. Pitman took time to review my CV and helped me put it together for the Express Scripts Scholarship, which I received in 2019. I would like to acknowledge my committee and its members. Dr. Beyda was my mentor in SSHP. Dr. Ming Hu was more of a co-PI at times. Since the beginning of the program, I would go to Dr. Trivedi about the dual degree program and transition into translational research. My final committee member, who I could not have gotten to this point without is Dr. Williams. He inspired me as a first-year pharmacy student and continues to as my committee member. Dr. Williams encouraged me to apply for scholarships, grants, and pursue my passions within infectious diseases. Lastly, I would like to acknowledge my PI, who has helped me write my first grant, my defense, thesis, and everything in between.

On a personal note, I would like to acknowledge my friends and family who have supported me and encouraged me to pursue my degree and continue through this program. My parents have enabled me to pursue my dreams in science. They raised me to explore and test my scientific curiosities and sent me to science camps annually growing up. They were understanding when I was busy with school and let that take priority. I would also like to acknowledge my friends who were a major support system throughout this program. They listened to my complaints about experiments not working and helped me troubleshoot whenever they could.

I would not have been able to make it through this program without all these people pushing me along!

TABLE OF CONTENTS

DEDICATION **1**

ACKNOWLEDGMENTS **2**

TABLE OF CONTENTS **4**

ABSTRACT **9**

LIST OF TABLES **11**

LIST OF FIGURES **12**

1. INTRODUCTION **14**

2. REVIEW OF LITERATURE **16**

2.1. *Cryptosporidium* **16**

2.2. Approaches to *Cryptosporidium* inhibition **19**

2.2.1. Current therapy for treating cryptosporidiosis **19**

2.2.1.1. Special populations **20**

2.2.2. Novel approaches for treating cryptosporidiosis **21**

2.3. t-RNA synthetase inhibitors for *Cryptosporidium* inhibition 22

2.3.1. t-RNA synthetases **22**

2.3.2. Amino acid inhibitors for *Cryptosporidium* inhibition **23**

2.4. Calcium-dependent protein kinase-1 (CDPK1) inhibitors for *Cryptosporidium* **27**

2.4.1. Protein kinases **27**

2.4.2. Structure of protein kinases 28

2.4.3. Types of protein kinase inhibitors 29

2.4.4. *Cryptosporidium* calcium-dependent protein kinase-1 (CDPK1) inhibitors 30

3. MATERIALS AND METHODS 34

3.1. Assessing t-RNA inhibitors for *Cryptosporidium* inhibition 34

3.1.1. Screening library composition 34

3.1.2. *Cryptosporidium* cellular assay and screening 34

3.1.3. Structure-activity relationship study of boron derivatives 36

3.2. Assessing kinase inhibitors for CpCDPK1 and *Cryptosporidium* inhibition 36

3.2.1. Kinase screening library composition for CpCDPK1 and Cp growth inhibition 36

3.2.2. CDPK1 and Src enzymatic assays 37

3.2.3. Preliminary structure-activity relationship analysis 38

3.2.4. Molecular docking studies 38

3.2.5. Expansion of structure-activity relationship analysis 39

3.2.5.1. General experimental conditions 40

3.2.5.2. Synthesis of UH15_16 and other analogs 41

3.3. *In Vitro* pharmacokinetic metrics of UH15_16: Solubility, absorption, distribution, and metabolism 54

3.4. UH15_16 kinase profiling 54

3.5. Formulation studies 55

3.5.1 Development of intravenous formulation. 55

3.5.2 Development of oral formulation 1. 55

3.5.3 Development of oral formulation 2. 55

3.5.3.1 UH15_16 docking with cyclodextrin 55

3.5.3.2 Oral formulation 2 56

3.5.4. Development of oral formulation 3 57

3.5.4.1. Simulated gastric fluid.....57

3.5.4.2. Simulated intestinal fluid 57

3.5.4.3. Fed-state simulated intestinal fluid (FeSSIF).....57

3.5.4.4. Fasted-state simulated intestinal fluid (FaSSIF).....58

3.5.4.5. Anti-precipitation assay.....58

3.5.4.6. Oral formulation 3 59

3.6. Formulation Assessments.....**60**

3.6.1. Bioanalytical method development 60

3.6.2. Pharmacokinetic study of UH15_16 with intravenous administration 63

3.6.3. Pharmacokinetic study of UH15_16 with oral administration using oral formulation 1 63

3.6.4. Pharmacokinetic study of UH15_16 with oral administration using oral formulation 2 63

3.6.5. Pharmacokinetic study of UH15_16 with oral administration using oral formulation 3 64

3.7. Toxicity study of UH15_16 and tissue analysis **64**

3.8. *In Vivo* efficacy studies of UH15_16.....**66**

4. RESULTS 67

4.1 tRNA synthetase inhibitor for Cp growth inhibition.....**67**

4.1.1 Results of tRNA synthetase inhibitor screening and SAR studies for *Cp* growth inhibition.....67

4.1.2 SAR analysis of boronic acids for *Cp* Growth inhibition 70

4.2 CpCDPK1 kinase inhibitors for Cp growth inhibition 72

4.2.1 CpCDPK1 kinase and Cp growth inhibition screening results ..72

4.2.2 UH15_16 SAR evaluation for CpCDPK1 and Cp growth inhibition 76

4.2.2.1 UH15_16 scaffold SAR 76

4.2.2.2 Identifying UH15_16 as an optimized *Cp*CDPK1 inhibitor.....78

4.2.2.3 SAR of UH15_16: Modifying R_1.....78

4.2.2.4 SAR of UH15_16: Modifying R_2.....81

4.2.3. Molecular docking of UH15_16 in *Cp*CDPK1.....82

4.2.4. ADME assessment and kinase screening of UH15_16.....83

4.2.4.1. ADME assessment.....83

4.2.4.2. Kinase screening.....83

4.2.4.2.1 KinomeSCAN 83

4.2.4.2.2 Kinase IC_{50} values 84

4.2.5. Formulation experiments and optimizations.....84

4.2.5.1. Ligand-ligand docking.....85

4.2.5.2. Formulation optimization 86

4.2.5.3. Determining formulations 87

4.2.6. Pharmacokinetic studies.....89

4.2.6.1. Intravenous pharmacokinetic study.....89

4.2.6.2. Oral pharmacokinetic study with formulation 1 90

4.2.6.3. Oral pharmacokinetic study with formulation 2 92

4.2.6.4. Oral pharmacokinetic study with oral formulation 3 93

4.2.7. *In Vivo* efficacy 94

4.2.7.1. Efficacy evaluation of UH15_16 using oral formulation 1 94

4.2.7.2. Efficacy evaluation of UH15_16 using oral formulation 2 95

4.2.7.3. Efficacy evaluation of UH15_16 using oral formulation 3 95

5. DISCUSSION 97

6. SUMMARY AND CONCLUSION 104

7. REFERENCES 106

8. APPENDICES 119

8.1. NMR Data 119

8.2. High-resolution mass-spectroscopy data 139

8.3. UV plate reader data 145

8.4 HPLC Data 148

ABSTRACT

Cryptosporidium parvum, Cp, is a protozoan parasite that can cause life-threatening diarrhea. Given that only one drug is currently FDA approved for the treatment of cryptosporidiosis but with only limited efficacy, new medications are needed. In this dissertation compounds directed towards tRNA synthetase and calcium dependent protein kinase 1 (CDPK1), two promising molecular targets in the field, were assessed.

In the case of tRNA synthetase, a collection of previously identified eukaryotic and prokaryotic tRNA synthetase inhibitors were screened for Cp growth inhibition in HCT-8 host cells. Three compounds, halofuginone, borrelidin and AN3661, were found to potently block Cp growth. A limited structure-activity relationship (SAR) analysis of AN3361 found that the propionic acid moiety present in the compound is critical for potent anti-*Cryptosporidium* activity.

In the case of *Cp*CDPK1, a diversified set of known protein kinases inhibitors were similarly assessed for *Cp* growth inhibition. This exercise identified pyridopyrimidones as a new chemotype of potent Cp growth inhibitors that were confirmed to block *Cp*CDPK1 kinase activity. SAR analysis provided further insights into two structural features for achieving potent CpCDPK1 kinase and Cp growth inhibition, namely appropriate occupancy of the ATP binding pocket near the αC-helix and the presence of a hydrogen bond acceptor in the solvent exposed portion of the inhibitor. A promising derivative, UH15_16, potently inhibited *Cp* growth (EC_{50} = 14 nM) and *Cp*CDPK1 kinase (IC_{50} = 5.4 nM) activities, as well as displayed moderate selectivity based on kinase profiling. UH15_16 formulated as a 2:1 mixture with Captisol® in water demonstrated limited systemic exposure following oral administration, was well tolerated at 50 mg/kg once per day dosing for 5 days in mice and resulted in a 75% reduced burden of the

gut pathogen at 50 mg/kg once per day dosing for 7 days in an acute mouse model of cryptosporidiosis. The third formulation (5x Captisol with 2% Tween 80 at double the volume in water), dosed 25 mg/kg BID, resulted in a safe toxicity profile and a 74% reduction of the gut pathogen when dosed for 7 days in the same model

LIST OF TABLES

Table 1. LCMS - LC Method

Table 2. LCMS – MS Method

Table 3: *Cp* Growth Inhibition

Table 4. Screening Boronic Acid Compounds

Table 5. Kinase Screen

Table 6. UH15 Scaffold SAR with *Cp*CDPK1 and *Cp* growth inhibition vs. Src Kinase

Table 7. UH15_16 Modifications to R_1 with *Cp*CDPK1 and *Cp* growth inhibition vs. Src Kinase

Table 8. UH15_16 Modifications to R_2 with *Cp*CDPK1 and *Cp* growth inhibition vs. Src Kinase

Table 9. ADME Assessment of UH15_16

Table 10. Kinase IC_{50} values

Table 11. UH15_16 Pharmacokinetic Profile Following IV Administration

Table 12. UH15_16 Pharmacokinetic Profile Following Oral Administration with Formulation 1

LIST OF FIGURES

Figure 1. *Cryptosporidium* Life Cycle, (CDC & Global Health, 2019)

Figure 2. Mupirocin Structure (Bactroban, 1987)

Figure 3. Tavaborole Structure, (Kerydin, 2014)

Figure 4. Structures of phenyl-alanyl synthetase inhibitor scaffold (Vinayak et al., 2020).

Figure 5. Structures of Lysyl-tRNA synthetase inhibitors (Baragaña et al., 2019).

Figure 6. Structures of prolyl-tRNA synthetase inhibitors (Herman et al., 2015).

Figure 7. Structures of methionyl-tRNA synthetase inhibitors (Buckner et al., 2019).

Figure 8. Structures of Leucyl-tRNA synthetase inhibitors (Plaencia et al., 2016)

Figure 9. Src Kinase in the inactive position with critical elements labeled

Figure 10. CpCDPK1 inhibitors

Figure 11. General Synthesis Scheme

Figure 12. Alternative Synthesis of Heterocycle

Figure 13. Synthesis of Acid Labile Amides

Figure 14. Structures of UH Scaffolds

Figure 15. UH15_16 Docked into CpCPKD1 (PDB: 3NCG)

Figure 16. Docked images of UH15_16 into β-cyclodextrin.

Figure 17. Examples of UV Plate Reader Results.

Figure 18. Blood Concentrations from IV Administration of 1 mg/kg UH15_16

Figure 19. Blood Concentrations from Oral Administration of 5 mg/kg UH15_16 in oral formulation 1

Figure 20. Blood Concentrations from Oral Administration of 5 mg/kg UH15_16 in oral formulation 2

Figure 21. Blood Concentrations from Oral Administration of 5 mg/kg UH15_16 in oral formulation 3

Figure 22. Efficacy of 50 mg/kg UH15_16 in oral formulation 1

Figure 23. Efficacy of 50 mg/kg UH15_16 in oral formulation 2

Figure 24. Efficacy of 25 mg/kg BID UH15_16 in oral formulation 3

1. INTRODUCTION

Cryptosporidium is not a commonly reported pathogen in the US, however on occasion, it often occurs in outbreaks, rather than an isolated incident (Hlavsa et al., 2021). *Cryptosporidium* is the most common infection from treated water in the US (Hlavsa et al., 2021). Internationally, *Cryptosporidium* is seen as an endemic problem. *Cryptosporidium* is responsible for nearly 50,000 children's deaths and morbidly of nearly 5 million (Khalil et al., 2018). These infections often occur due to infected drinking water, rather than infected recreational water (Khalil et al., 2018). This is due to *Cryptosporidium* being highly contagious and highly resistant to water treatment (Kosek et al., 2001). In 1993, *Cryptosporidium* got into Milwaukee's water supply, raising concern about bioterrorism. Due to the infectious nature, a small amount of the pathogen is required to infect, it was estimated only a sip of water of trace oocytes infected people (Kenzie et al., 1994). While public health officials, infectious disease doctors, and the scientific community would like to view these waterborne outbreaks as a thing of the past, recent events have shown how susceptible our water supply is to infectious contamination. In both 2020 and 2021, Texas had children die of *Naegleria fowleri,* "the brain eating amoeba" due to underchlorinated water (AP News, 2021), indicating how susceptible these areas are potential *Cryptosporidium* outbreaks in their water supply. While nitazoxanide, the only recommended treatment for *Cryptosporidium,* is available, it is not a very effective agent (CDC, NCEZID, and DFWED, 2019). Therefore, developing new agents is of high importance, for children here in the US and those abroad.

Two types of inhibitors were investigated for this purpose: tRNA synthetase inhibitors and CpCDPK1 inhibitors. These two classes of inhibitors have shown promise in similar pathogens. For example, tRNA synthetase inhibitors have already been approved in other

eukaryotes for fungal infections (Kerydin, 2014). And other classes of CDPK1 inhibitors have been advanced (Castellanos-Gonzalez et al., 2016; Arnold et al., 2017). Simply put, tRNA synthetase inhibitors prevent the correct amino acid from being loaded onto the tRNA, so in the ribosome the correct protein cannot be synthesized (Pham et al., 2014). This is a rather recycled mechanism - Mupirocin was one of the first to utilize this mechanism (Bactroban, 1987). It has been heavily researched since. Newer agents, namely tavaborole, have since been developed for fungal infections (Kerydin, 2014). CDPK1 plays a role with invasion of host cells, egress, and motility in *Toxoplasma gondii* (Bisio et al., 2019), but believed to act the same way in *Cryptosporidium* (Billker et al., 2009; Kieschnick et al., 2001; Green, 2018). Pharmacologically, CDPK1 plays a role in calcium signaling and vacuole secretion (Billker et al., 2009; Kieschnick et al., 2001; Green, 2018). CDPK1 is a unique protein target because it is a "bump kinase". This means there is a small amino acid where a large amino acid is typically (Wernimont et al., 2010). When developing inhibitors, this slight amino acid change allows for a slightly larger binding pocket which allows for a larger inhibitor (Wernimont et al., 2010). This larger inhibitor should have lower potency at human kinases – therefore it should have higher selectively and a better safety profile (Wernimont et al., 2010). This is what we pursued and found with our CDPK1 inhibitors, but we found the binding pocket larger due to additional factors, not just the bump.

2. REVIEW OF LITERATURE

2.1. *Cryptosporidium*

Cryptosporidiosis, a form of parasitic infectious diarrhea, has only one FDA-approved antimicrobial, nitazoxanide. However, many patients die despite this therapy. In 2016, nearly 50,000 children under the age of five died of cryptosporidiosis, and 4.8 million children suffered long-term consequences of the infection (Khalil et al., 2018). Some of these long-term consequences included poor cognition, physical developmental delays, and disrupted immune system (Khalil et al., 2018).

In the United States, the Centers for Disease Control and Prevention reported approximately 10,000 cases of cryptosporidiosis in 2016 (Painter et al., 2015). In the US, *Cryptosporidium* is infamously spread via swimming pools due to chlorine tolerance, causing strict hyperchlorination guidelines (Murphy et al., 2015). Three-quarters of the outbreaks from public recreational water (i.e. swimming pools, hot-tubs, water playgrounds etc.) were due to *Cryptosporidium* between 2015 and 2019 in the United States (Hlavsa et al., 2021). Compared to the other outbreaks in this class of treated water pathogens, *Cryptosporidium* most often resulted in >100 infections, while other pathogens typically infected <100 (Hlavsa et al., 2021). However, due to the shortage of chlorine in 2021, an increase in *Cryptosporidium* cases is projected (DiLella et al., 2021). Furthermore, *Cryptosporidium sp*. (*Cp*) presents a high risk of outbreak via contaminated water sources due to the low dose required to infect (e.g. only a few oocytes) (Kosek et al., 2001). This low inoculation dose allows it to be so resistant to water-treatment (Kosek et al., 2001).

Low inoculation can pose a more sinister problem as it elicits a risk for bioterrorism through widespread dissemination, as demonstrated in the Milwaukee Incident (Kenzie et al., 1994). In 1993, *Cryptosporidium* infiltrated the city's water supply and was estimated to have infected over 400,000 people (Kenzie et al., 1994). In part to the parasite relatively low virulence factors in healthy adults, over 100 people died as a result (Kenzie et al., 1994). Nevertheless, this incident caused concerns that *Cryptosporidium* could be altered to be more virulent and deadly (Kenzie et al., 1994), thus causing concern that *Cryptosporidium* could itself become a bioterrorism agent.

As mentioned, *Cryptosporidium* is a parasite causing diarrhea, it is spread by water and almost always restricted to the gut. However, there are reports of *Cryptosporidium*-pneumonia, this is rare and believed to be due to aspirating during emesis (Reina et al., 2016). Due to the belief this is a secondary complication and incredibly rare in the HIV/AIDS population, our study is not going to focus on this element of *Cryptosporidium* infections. However, this might be an area for future studies. So, for our purposes, we will be describing *Cryptosporidium* as simply a gut pathogen.

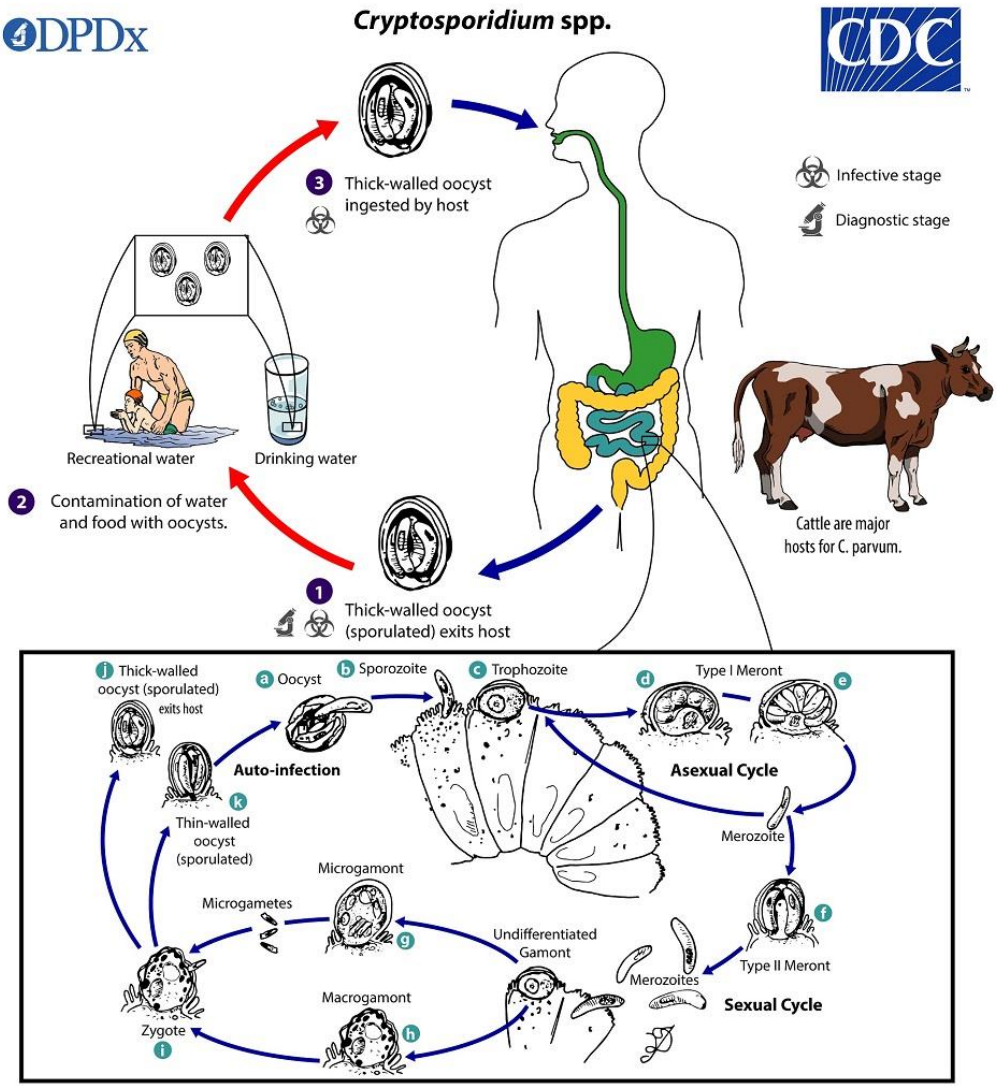

Figure 2. *Cryptosporidium Life Cycle, (CDC & Global Health, 2019).*

Cryptosporidium is an obligate intracellular protozoan pathogen; thus it relies on the host for part of its lifecycle (CDC & Global Health, 2019). *Cryptosporidium*, like other Apicomplexan pathogens, has a complex life cycle (Figure 1) that requires a host for both asexual and sexual reproduction (CDC & Global Health, 2019). As shown in the infographic by the CDC, a typical *Cryptosporidium* infection is restricted to the enterocytes of the gut (CDC & Global Health, 2019). Inside the enterocyte, the pathogen creates a sac in which reproduction occurs to produces either thin-walled oocytes for reinfection of the host or thick-walled oocytes

for extra-host infection (CDC & Global Health, 2019). Cryptosporidiosis typically clears in about a week. However, immunodeficient patients may experience longer infections (CDC, NCEZID, and DFWED, 2019).

2.2. Approaches to *Cryptosporidium* inhibition

2.2.1. Current therapy for treating cryptosporidiosis

As mentioned, healthy adults are at relatively low risk, but immunocompromised patients and malnourished children are at increased risk of death and recurrent cryptosporidiosis, even with therapy (Amadi et al., 2002). Therefore, new treatment options, especially for patients with deficient immune systems, are urgently needed.

As mentioned above nitazoxanide is the only currently approved treatment for *Cryptosporidium*. However, this is not a highly effective agent. The CDC warns it can take as long as 5 days to resolve patients, if it works (CDC, NCEZID, and DFWED, 2019). While nitazoxanide is approved for those from the age one and above, the efficacy in healthy patients is limited to approximately 75% (CDC, NCEZID, and DFWED, 2019). The mechanism of action is ill-defined, although a published report claims it is an inhibitor of pyruvate:ferredoxin oxidoreductase (PFOR), allowing it to interfere with anaerobic metabolism (Alinia et al., 2005).

Paromomycin, while not recommended by infectious disease guidelines, as mentioned below, nor FDA approved, is still used off-label due to the lack of alternatives to nitazoxanide (Panel on Guidelines, 2020). Paromomycin is an orally dosed aminoglycoside (Humatin, 2001). As per the package insert, paromomycin has such poor absorption it is nearly entirely recovered in the stool yet remains water-soluble. While paromomycin did not show much success in a major clinical trial in 2000 (Hewitt et al., 2000), it was promptly debated in the infectious disease

community (White et al., 2001). Some of White et al. concerns were centered around statistical analysis interpretation, sample size, confounders, among other concerns. Nevertheless, no further clinical trials have been completed since 2001, nor has it been registered with the FDA.

2.2.1.1. Special populations

The HIV/AIDS population is among those that typically suffers the most with cryptosporidiosis. Most severe cases of cryptosporidiosis occur in the HIV population when the CD4 T lymphocyte cell (CD4) count is <100 cells/mm^3 (Panel on Guidelines, 2020). For reference, AIDS is defined as a CD4 count <200 cells/mm^3. Unfortunately, in the HIV population nitazoxanide is even less effective, such that it is not recommended in the "Guidelines for the Prevention and Treatment of Opportunistic Infections in Adults and Adolescents with HIV" (Panel on Guidelines, 2020). Rather, they recommend optimizing or initiating antiretroviral therapy to manage the HIV and increase the CD4 count, such that patients are no longer immunocompromised (Panel on Guidelines, 2020). Symptomatic treatment may also be considered, like antidiarrheals (Panel on Guidelines, 2020). Supportive care, including rehydration and electrolytes, are also strongly encouraged (Panel on Guidelines, 2020). Spiramycin has also been investigated for potential use in HIV patients with cryptosporidiosis. Unfortunately, it fares no better than nitazoxanide (Panel on Guidelines, 2020). Thus, this population may benefit for an improved agent as an adjunct to antiretroviral therapy.

Another population that nitazoxanide shows reduced efficacy is in malnourished children (Amadi, 2002). This population is not only more likely to fail treatment, but more prone to life-long complications of the infection, like poor cognition (Ashigbie et al., 2021). In malnourished and underweight children, nitazoxanide worked approximately half the time (Amadi et al., 2002). When HIV is a comorbidity efficacy dropped to 8% and 16% as assessed by clinical and

parasitic cures, respectively (Amadi et al., 2002). However, this was a relatively small study with n = 25 in the treatment group and n = 22 and 24 in placebo groups (Amadi et al., 2002). A mouse experiment demonstrated how the comorbidity of cryptosporidiosis with malnutrition may be so detrimental (Costa et al., 2011). Costa et al. showed malnourished mice with cryptosporidiosis weight loss was exacerbated. Additionally, the parasite burden was over 5-fold greater in the malnourished model and damage to the intestinal lining was noted (Costa et al., 2011). While this experiment did not fully investigate the difference in treatment in malnourished vs nourished mice, it did shed light on why this population may be so hard to treat (Costa et al., 2011). Nevertheless, this is another population that could benefit from more potent and effective anti-*Cryptosporidium* agents.

2.2.2. Novel approaches for treating cryptosporidiosis

Cryptosporidium is infamous for scavenging pathways, allowing it to circumvent numerous metabolic inhibitors. Statins, or HMG-CoA reductase inhibitors, which inhibit cholesterol synthesis in humans, were briefly investigated as a potential *Cryptosporidium* inhibitor when a screen found them to be active (Bessoff et al., 2013). However, this was not the first study to target the cholesterol pathway (Ehrenman et al, 2013). Unfortunately, it has since been discovered that *Cryptosporidium* may have upwards of four pathways to obtain critical cholesterol (Ehrenman et al., 2013). Given these pathways, Bessoff *et al*. theorized cholesterol itself may not have been the critical step. They suggested another potential downstream target of HMG-CoA. Nevertheless, finding a target that *Cryptosporidium* cannot circumvent is of utmost importance on a pharmacological level.

2.3. t-RNA synthetase inhibitors for *Cryptosporidium* inhibition

2.3.1. t-RNA synthetases

Aminoacryl t-RNA synthetase inhibitors block the process of protein synthesis by preventing the addition of the next amino acid in the growing peptide chain (Pham et al., 2014). In many cases, the inhibitor competes for binding with the amino acid (Pham et al., 2014). This causes dysfunction in protein synthesis, ideally completely halting protein synthesis once that amino acid is coded (Pham et al., 2014). The resulting erroneous proteins can accumulate and harm or kill the pathogen (Pham et al., 2014). This class of targets is not a new concept - Bactroban, or mupirocin, is an antibiotic that targets bacterial isoleucyl t-RNA synthetase (Bactroban, 1987). More recently, Kerydin (a.k.a. tavaborole), another t-RNA synthetase inhibitor for fungal infections, has also been approved (Kerydin, 2014), validating t-RNA synthetase inhibitors as plausible treatments for eukaryotic infections. Below are the chemical structures along with the year of FDA approval of mupirocin, (Bactroban, 1987) and tavaborole (Kerydin, 2014), in Figures 2 and 3, respectively.

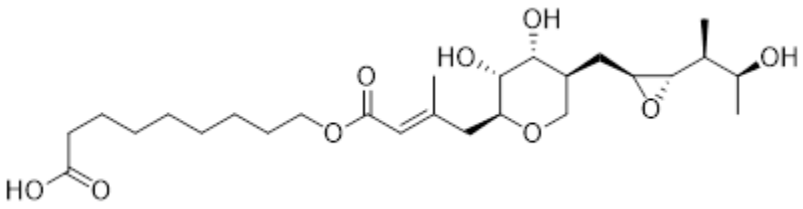

Figure 2. *Mupirocin Structure (Bactroban, 1987)*

***Figure 3**. Tavaborole Structure, (Kerydin, 2014)*

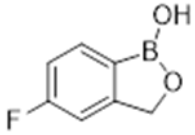

2.3.2. Amino acid inhibitors for *Cryptosporidium* inhibition

Tryptophanyl-tRNA synthetase (TrpRS) attaches a tryptophan to its respective tRNA (Merritt et al., 2011). *Cryptosporidium* only has one TrpRS in its genome, limiting its ability to scavenge or circumvent a TrpRS inhibitor (Merritt et al., 2011). Merritt *et al*. also found this to apply to *Trypanosoma brucei* and *Entamoeba histolytica* based on genomic analysis. It is not uncommon for eukaryotes, like *Cryptosporidium*, to have more than one copy of some t-RNA synthetases (Merritt et al., 2011). However, to avoid a scavenge pathway potentially rendering the inhibitor useless, targeting t-RNAs that only have a single copy would be ideal. As far as selectivity, a potential inhibitor would need to preferentially bind to specifically the *Cryptosporidium* or general pathogenic TrpRS over the human TrpRS (Merritt et al., 2011).

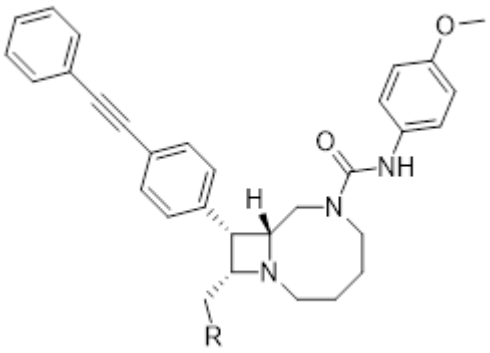

***Figure 4**. Structures of phenyl-alanyl synthetase inhibitor scaffold (Vinayak et al., 2020).*

Phenyl-alanyl-tRNA synthetase (PheRS) inhibitors (Figure 4) block the attachment of phenylalanine to its respective tRNA. (Vinayak et al., 2020). A series of PheRS inhibitors developed by Vinayak *et al*., demonstrated antimicrobial activity against *Plasmodium falciparum*. Compounds

have advanced into testing in *in vivo* malaria models. These same compounds were optimized for *Cryptosporidium parvum* and *hominis,* and a structure-activity relationship was determined (Vinayak et al., 2020). The top compounds had potencies in the nanomolar range *in vitro,* and selectivity in select human cell lines was just under 1,000-fold to nearly 10,000-fold (Vinayak et al., 2020). A few of these compounds were tested *in vivo*. Vinayak *et al*. found that the compounds with poor bioavailability had the best reduction of oocytes in an immunocompromised model. The lead compound also showed success in an acute infection model in IFN-γ KO mice (Vinayak et al., 2020). Thus Vinayak *et al*. have determined that PheRS could be a very promising target in *Cryptosporidium* and potentially other Apicomplexan pathogens.

Lysyl-tRNA synthetase inhibitors (Figure 5) prevent lysine from being attached to lysyl-tRNA synthetase. Hoepfner *et al*. identified the natural product cladosporin as a modestly potent inhibitor (IC_{50} of 40-90 nM) of *Plasmodium falciparum* (Hoepfner et al., 2012). Baragaña *et al*. made cladosporin derivatives to further improve potency against *Plasmodium falciparum* and *Cryptosporidium* (Baragaña et al., 2019). Cladosporin had IC_{50} values of 38 nM and 4 nM against *Cryptosporidium* and *Plasmodium falciparum* lysyl-tRNA synthetases, respectively (Baragaña et al., 2019). Baragaña *et al*. identified a similar compound by replacing the lactone and added an amide, improving Cp lysyl-tRNA synthase potency to 22 nM, However, this compound had metabolic

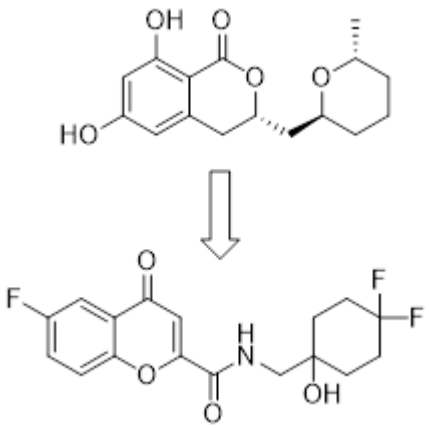

Figure 5*. Structures of Lysyl-tRNA synthetase inhibitors, cladosporin (top) and the optimized lead (bottom) (Baragaña et al., 2019).*

stability issues. So, they improved stability by fluorinating the compound in a couple of places as well as hydroxylating the compound (Baragaña et al., 2019). The resulting compound demonstrated IC_{50} values of 13 nM and 15 nM against *Cryptosporidium* and *Plasmodium falciparum* lysyl-tRNA synthetases, respectively (Baragaña et al., 2019). In an acute cryptosporidiosis model using INF-γ KO mice, the lead compound, dosed at 20 mg/kg, was able to reduce the infection burden over 90% by day 8 (Baragaña et al., 2019). This indicated that lysyl-tRNA synthetase could be a promising target for *Cryptosporidium*.

Halofuginone initiated the t-RNA synthetase investigation. Halofuginone is a semisynthetic derivative of febrifuge (Figure 6). While halofuginone offers an improvement in selectively, it is not enough to be deemed safe for mammals, including humans (Pines and Spector, 2015). Nevertheless, halofuginone is used for veterinary purposes, often for poultry, namely chicken, to treat cryptosporidiosis and coccidiosis (Pines and Spector, 2015). Febrifugine has been used in Chinese medicine for many years, but again has failed for cryptosporidiosis and other indications due to lack of selectivity causing toxicity (Herman et al., 2015). Nevertheless, halofuginone and febrifugine have provided propyl-tRNA synthetase inhibitors, which inspired various derivatives to be made (Pines and Spector, 2015). Halofuginone and febrifugine derivatives have been tested against *Plasmodium falciparum*. While some derivatives did show modest improvement, halofuginol was deemed the lead (Herman et al., 2015). *In vivo*, halofuginol showed efficacy without

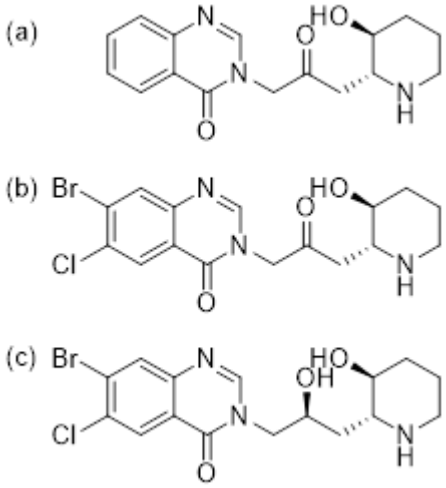

Figure 6*. Structures of prolyl-tRNA synthetase inhibitors (a) febrifugine (b) halofuginone and (c) halofuginol (Herman et al., 2015).*

noted toxicity. When halofuginone was put in the same malaria model, toxicity was noticed in all the animals with one animal dying (Herman et al., 2015). Thus Herman *et al*. indicated halofuginol may have reduced toxicity over halofuginone and that prolyl-tRNA synthetase could be used in *Plasmodium spp*. Whether this compound can be applied to additional Apicomplexan pathogens remains an open question.

Methionyl tRNA synthetase inhibitors (Figure 7) also showed promise against *Cryptosporidium*. (Buckner, 2019). *Cryptosporidium parvum* and *hominis* have a single gene for methionyl tRNA synthetase (Buckner et al., 2019). It is worth noting that most methionyl tRNA synthetases are classified as either class I or class II (Buckner et al., 2019). This classification was named by Eriani *et al*., based on conserved sequences – most tRNA synthetases fit in class I (Eriani et al., 1990). *Cryptosporidium* produces only a class I methionyl tRNA synthetase, which allows it to be vulnerable to inhibitors that block other pathogenic methionyl tRNA synthetases, like in *Trypanosoma brucei* and potentially some bacteria (Buckner et al., 2019). However, humans also produce type I methionyl tRNA synthetases. While the human versions vary more, selectivity is critical for these inhibitors (Buckner et al., 2019). Buckner *et al*. explored a variety of type I methionyl tRNA synthetases inhibitors against *Cryptosporidium parvum.* They found that a number of these compounds had sub-nanomolar potency against the synthetase, and a couple compounds had single digit

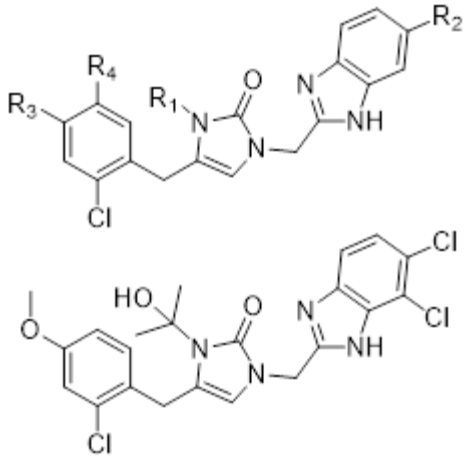

Figure 7*. Structures of methionyl-tRNA synthetase inhibitors – the hit and the optimized compound (top and bottom, respectively), (Buckner et al., 2019).*

micromolar activity in cell-based assays (Buckner et al., 2019). Upon optimization, they were able to achieve nanomolar potency of 6-29 nM with their lead, as well as success in two *in vivo* mice models (Buckner et al., 2019). They also showed that other methionyl tRNA synthetase inhibitors could target *Cryptosporidium*.

Leucyl-tRNA synthetase inhibitors (Figure 8) were particularly interesting given their unique chemical structure. This series of benzoxaboroles mimicked tavaborole (see Figure 3), as a boron-based t-RNA synthetase inhibitor (Palencia et al., 2016). However, this series was slightly less potent (e.g. 2.2 and 6.86 µM) than nitazoxanide, which as 1.9 µM (Palencia et al., 2016). Of note, this reported used a different cell line than most others (Palencia et al., 2016), but nitazoxanide is not an ideal inhibitor nor particularly potent.

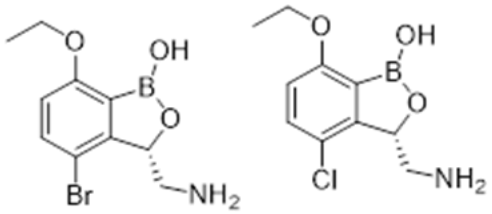

Figure 8*. Structures of Leucyl-tRNA synthetase inhibitors AN8432 (left) and AN6426 (right) (Plaencia et al., 2016)*

2.4. Calcium-dependent protein kinase-1 (CDPK1) inhibitors for *Cryptosporidium*

2.4.1. Protein kinases

Protein kinases are ubiquitous in a variety of organisms. Humans have over 500 protein kinases. They are also found in other eukaryotes as well as pathogenic microorganisms. Protein kinases catalyze the transfer of a phosphate from ATP to protein substrates. The residue of the substrate is often a serine, threonine, or tyrosine. This process is critical in many cellular functions.

2.4.2. Structure of protein kinases

Most protein kinases have a rather conserved structure, particularly in the catalytic site. This includes the ATP-binding region (Figure 9) which is comprised of a gatekeeper residue, the hinge, a DFG (aspartic acid [D], phenylalanine [F], and glycine [G]) motif, and an αC helix (Roskoski et al., 2016). The gatekeeper controls access to the inner portion of the ATP binding pocket (Roskoski et al., 2016). This inner binding pocket is typically hydrophobic, and the end, or inner most region, is signified by the αC helix (Roskoski et al., 2016). The hinge provides one of the most important interactions with type I-II inhibitors (Roskoski et al., 2016).

If an inhibitor interacts in the ATP pocket, it must make strong hydrogen bond interactions with the hinge, at least this is true for all approved kinase inhibitors of the class as

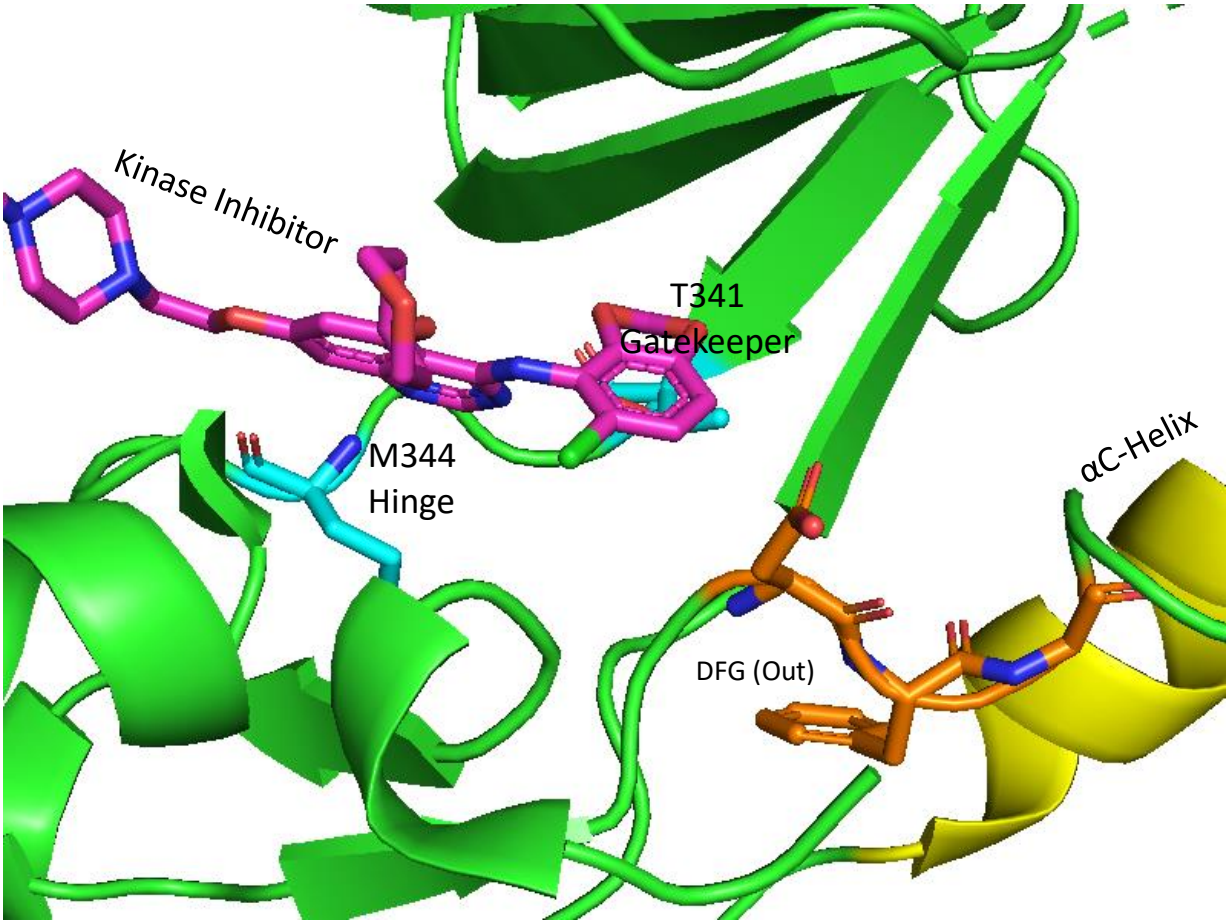

Figure 9. *Src Kinase in the inactive position with critical elements labeled*

well as with ATP (Roskoski et al., 2016). The DGF on the other hand helps determine kinase activity and the type of inhibitor – if the aspartic acid (D) points away from the binding pocket, it is in the DFG out conformation, which is catalytically inactive (Roskoski et al., 2016). The position of the DFG can also exist in intermediate conformations, which are also catalytically inactive. If the aspartic acid is pointed into the pocket, the opposite is true – the kinase is likely active (Roskoski et al., 2016). To determine if the kinase is likely active, the αC-helix must also be considered, as this region can also move (Roskoski et al., 2016). If the kinase is in the active state, the αC-helix will form an interaction with the catalytic lysine, referred to as the "αC-helix in" state (Roskoski et al., 2016). However, if the αC-helix moves too much the kinase will be inactive regardless of the position of the DFG (Roskoski et al., 2016).

2.4.3. Types of protein kinase inhibitors

The types of protein kinase inhibitors correspond to the states mentioned above. A type I inhibitor corresponds to an inhibitor binding to the active state, DFG in and αC helix in (Roskoski et al., 2016). A type I ½ inhibitor corresponds to the intermediate state, typically where the DFG or αC helix has moved (Roskoski et al., 2016). A type II inhibitor binds to the inactive conformation, typically both DFG out and αC helix out, but the DFG out is often viewed as the more critical of the two (Roskoski et al., 2016). As mentioned above, type I, I ½, and 2 inhibitors interact via hydrogen bonds to the hinge region (Roskoski et al., 2016). Type III and type IV are both allosteric inhibitors (Roskoski et al., 2016). Type III inhibitors binds adjacent to the ATP binding location, near where type I and II inhibitors bind (Roskoski et al., 2016). Of note, type III inhibitors do not compete with ATP such that ATP can still bind at the same time. Thus, type III inhibitors do not make hydrogen bonds with the hinge (Roskoski et al., 2016). Type IV inhibitors, contrary to the type III, do not have to have proximity to the ATP binding

site – these may bind on the opposite end of the kinase relative to the binding site (Roskoski et al., 2016). Type V inhibitors are bivalent inhibitors, meaning they bind or interact with two locations on the kinase (Roskoski et al., 2016). To date, there are no FDA approved type IV or type V inhibitors. Lastly type VI inhibitors are simply defined as covalently bound inhibitors (Roskoski et al., 2016). These do not have a defined binding location (Roskoski et al, 2016). However, the currently approved type VI inhibitors interact in the ATP binding site and form a covalent bond with a cysteine within the pocket (Roskoski et al., 2016).

One concern with type I, I ½, and II inhibitors is lack of selectivity, since all protein kinases are so similar that achieving selectivity can be a challenge (Wu et al., 2015). However, targeting the ATP binding site with type I-II inhibitors over allosteric inhibitors often allows for a high degree of potency (Wu et al., 2015). Unfortunately, finding potent allosteric sites are notoriously problematic, which is partly why type I-II have reigned over alternative inhibitor types. However, such selectivity challenges might be mitigated for kinase with more unique ATP binding sites.

2.4.4. *Cryptosporidium* calcium-dependent protein kinase-1 (CDPK1) inhibitors

Fortunately, *Cryptosporidium* and other pathogens in the Apicomplexa family have a structurally distinct protein kinase family called calcium-dependent protein kinase, CDPK1 (Wernimont et al., 2010). *Cryptosporidium [parvum]* CDPK1 (CpCDPK1) has a glycine in the critical gatekeeper position of the ATP-binding site (Wernimont et al., 2010). Contrarily, human protein kinases typically have a bulkier amino acid, like threonine or methionine, in this position (Wernimont et al., 2010). This difference allows for the design of potentially selective inhibitors targeting the parasite kinase. Additionally, CDPKs play an important role in calcium signaling, motility, and vacuole secretion (Billker et al., 2009; Kieschnick et al., 2001; Green, 2018).

Studies have shown that when *Cp*CDPK1 is silenced, the infection is significantly reduced in an *in vitro* model (Castellanos-Gonzalez et al., 2015). In addition, several *Cp*CDPK1 inhibitors (Figure 10) have proven efficacious in *in vitro* and *in vivo* animal models of cryptosporidiosis (Castellanos-Gonzalez et al., 2016; Arnold et al., 2017). Unfortunately, some of these *Cp*CDPK1 inhibitors have off-target toxicity, including cardiotoxicity (Van Voorhis et al., 2017), necessitating the need to identify improved inhibitor chemotypes.

Most *Cp*CDPK1 inhibitors reported to date are pyrazolopyrimidines (Larson et al., 2012) (Figure 10) (Larson et al., 2012; Haung et al., 2015; Zhang et al., 2012). This class of inhibitors often demonstrates potent *Cp*CDPK1 kinase inhibition. However, many series fail to show efficacy in cell-based assays or invasion models (Kuhlenschmidt et al., 2015; Arnold et al., 2017). Thus, they exhibit poor correlation between the CpCDPK1 enzyme activity and *in vitro* activity against the organism. The difference between the biochemical assay and *in vitro* model inhibition can be 100-1000-fold (Kuhlenschmidt et al., 2015). Additionally, compounds from the pyrazolopyrimidines class have been affiliated with cardiotoxicity (Van Voorhis et al., 2017).

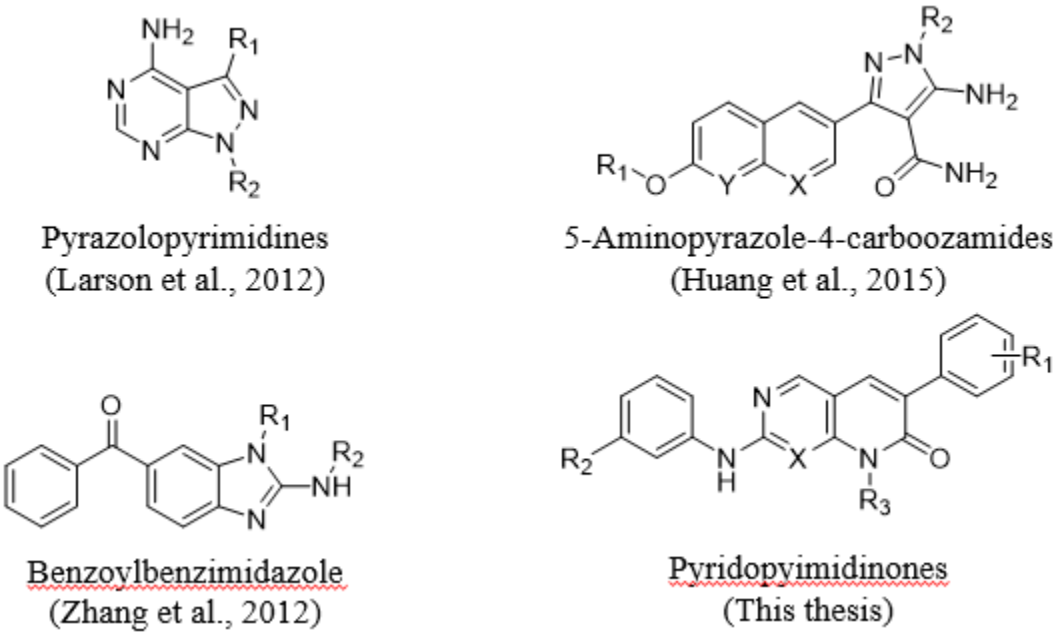

Figure 10*. CpCDPK1 Inhibitors*

There are several other classes of CpCDPK1 inhibitors, but they also have significant limitations (Huang et al., 2017; Zhang et al., 2012). For example, benzoylbenzimidazoles are only modestly potent against CpCDPK1 and have not been validated in cell-based *Cryptosporidium* growth assays (Zhang et al., 2012). The most potent compound of the benzoylbenzimidazoles has an IC_{50} value of 26 nM (Zhang et al., 2012). While this is encouraging, without confirmation that these compounds have similar activity in the invasion or cell-based model, their viability as lead compounds remains unknown, since it is not uncommon for compounds to have 100-fold loss in activity moving from the kinase assay to the *in vitro* invasion assay, (i.e. 2 nM activity in the kinase, but only 0.2 µM activity in the invasion model) (Kuhlenschmidt et al., 2015). Another series, 5-aminopyrazole-4-carboxamides, showed similar issues as pyrazolopyrimidines – poor correlation between CpCDPK1 enzyme inhibition and *in vitro* activity, 175-30,000-fold variation between the CpCDPK1 assay and invasion model (Huang et al., 2017). The most potent 5-aminopyrazole-4-carboxamide compound had IC_{50}

values as low as 0.03 nM against the enzyme. However, most active compounds in the series had IC_{50} values closer to 2 nM against the enzyme (Huang et al., 2017). When tested against Cp *in vitro*, the compounds were drastically less potent (Huang et al., 2017). The most potent compound against the enzyme had an EC_{50} of only 1.03 µM in the invasion model, a difference of over 30,000 (Huang et al., 2017). Most of the compounds remained in the µM range, despite potent enzyme activity (Huang et al, 2017). The real detriment of these compounds was the degree of hERG channel inhibition. Huang *et al*. reported EC_{50} values around 30 µM for some compounds, which corresponds to only about 30-fold selective, raising cardiotoxicity as a concern given the limited *in vitro* potency (Huang et al., 2017). Thus, a new series of CpCDPK1 inhibitors is needed as well as further understanding of the structure-activity relationship for achieving potent Cp growth inhibition.

3. MATERIALS AND METHODS

3.1. Assessing t-RNA inhibitors for *Cryptosporidium* inhibition

3.1.1. Screening library composition

A variety of reported t-RNA synthetases inhibitors were screened for *Cryptosporidium* growth inhibition. The tRNA synthetase inhibitors were: GSK2251052 / AN3365 (hydrochloride), borrelidin, ochratoxin A, AN2690 / tavaborole, cispentacin, methyl ester cispentacin, thialysine, REP3123, and mupirocin. An additional tRNA synthetase compound (referred to as ELI) was synthesized for screening. The synthesis of this compound follows a published method (Shibata et al., 2012). Other than ELI, the other compounds were commercially available.

3.1.2. *Cryptosporidium* cellular assay and screening

Since Cp is an intracellular pathogen, standard anti-microbial activity assessments, like broth microdilution, cannot be used. Additionally, Cp cannot be cultured for continuous passage, meaning Cp must be acquired from a natural host and cannot be entirely lab grown (Vinayak et al, 2015). Oocysts are obtained from the hosts' fecal material and purified; it is also at this time that oocysts can be genetically modified to ease the counting process (Vinayak et al., 2015). At this point cell-based invasion assays can be used in place of broth microdilution or other anti-microbial testing methods (Sun et al., 2010). This assay utilizes human colon ileocecal cells (HCT-8 cells) as host cells to mimic infection. The HCT-8 cells are infected with *Cp* (Sun et al., 2010). In the method used by Dr. Mead's laboratory, purified *Cryptosporidium parvum* oocysts (IOWA isolate) are first washed free of 2.5% aqueous potassium dichromate ($K_2Cr_2O_7$, a storage buffer) with phosphate-based saline (PBS) (Mead and McNair, 2006). The washed oocytes were resuspended Dulbecco's modified Eagle's medium (DMEM) base with 0.75% sodium

taurocholate and incubated for 30-45 min at 37 °C (Mead and McNair, 2006). The excystation mixture was diluted with Ultraculture™ medium (BioWhittaker Inc., Walkersville, MD) and c. 1 × 10^5 oocysts and sporozoites were dispensed in 24 well plates containing confluent HCT-8 cells (Mead and McNair, 2006). Cells were incubated for 3 hours (Mead and McNair, 2006). The cells were washed with PBS and replaced with fresh Ultraculture™ medium with or without test compounds for 48 h (i.e. tRNA synthase inhibitors, nitazoxanide, kinase inhibitors, etc.) (Mead and McNair, 2006). Cells were washed with PBS, and fixed with Bouin's solution (Mead and McNair, 2006). Once fixed, Bouin's solution is removed, and ethanol is applied to decolorize (Mead and McNair, 2006). An anti-*Cryptosporidium. parvum* fluorescein-labeled monoclonal antibody (C3C3-FITC) is applied and incubated to label the *Cryptosporidium parvum* cells (Mead and McNair, 2006). The numbers of parasites were counted per well. At least 25 images were obtained per field. Dose–effect curves and the median effective concentration (EC_{50}) of each compound was determined. The EC_{50} was defined as the concentration required for reducing the number of parasites by 50% compared with the untreated control. Statistical analyses included calculation of mean, standard deviation, and ANOVA. This experimentation was repeated at least twice, and performed as per protocol by Dr. Jan Mead's laboratory at Emory University and Atlanta's Veteran's Affairs.

Some compounds were also tested by Dr. Wesley Van Voorhis' laboratory at the University of Washington. This assay also uses HCT-s cells which are infected with Cp at a 1:1 ratio (Murphy et al., 2010). The sporozoites are activated by acid water then 0.8% taurocholate-PBS (Murphy et al., 2010). The infected HCT-8 cells were infected and cultured in a 24-well plate and subjected to varying concentrations of inhibitor (Murphy et al., 2010). Positive controls were diluent and negative controls were heat -killed parasite or no parasite (Murphy et al., 2010).

Cells were left to incubate for 24 hours then RNA was isolated using a QiagenRNeasy plus kit and quantified using a reverse transcription real time PCR (Murphy et al., 2010). Primers from parasite ribosomes were used as described by Castellanos-Gonzalez et al. (Castellanos-Gonzalez et al., 2008). A standard curve was prepared, each concentration was repeated, and a duplicated PCR was performed – then an EC_{50} could be determined (Murphy et al., 2010). One duplicate was performed per each tested concentration (Murphy et al., 2010).

3.1.3. Structure-activity relationship study of boron derivatives

To further investigate boron derivatives related to tRNA synthetase inhibitors from the screening library described in section 3.1.1, a chemical substructure search was performed to find related commercially available compounds to test for Cp growth inhibition. This search identified the following compounds: 2-(hydroxymethyl)-6-methoxyphenylboronic acid dehydrate, 7-(hydroxymethyl) benzo[c] [1,2] oxaborol-1(3H)-ol, 2-(hydroxymethyl) phenylboronic acid, 2-(1-hydroxy1,3- dihydro-2,1-benzoxaborol-7-yl) acetic acid, and AN3365. Code names were given to these compounds as a blinding measure (also as an abbreviation compared to the chemical name) – these code names are used as compound names as shown in the result section. Structures are also shown in the results section.

3.2. Assessing kinase inhibitors for CpCDPK1 and *Cryptosporidium* inhibition

3.2.1. Kinase screening library composition for CpCDPK1 and Cp growth inhibition

A set of protein kinase inhibitors were assembled to assess and identify novel CDPK1 inhibitors. A variety of commercially available kinases inhibitors were purchased, included: CS0709, Imatinib, Ponatinib, Rebastinib, PF 431396, Doramapimod, Nilutinib, Bosutinib, R406, Dasatinib, Tozasertib, and Sorafonib. UH15_15, a previously optimized receptor-interacting

protein kinase 2 (RIPK2) inhibitor (Nikhar et al., 2016), was also included in this cohort for assessment against CpCDPK1 and for Cp growth inhibition. Compounds were initially prepared for testing as 10 mM DMSO stock solutions.

3.2.2. CDPK1 and Src enzymatic assays

To determine inhibitor activity against CpCDPK1 an established biochemical assay in Dr. Van Voorhis' laboratory was used. Recombinant CpCDPK1 was used in a published Kinaseglo luciferase assay (Ojo et al., 2010). Kinase phosphorylation occurred in 25 µL buffered solution of 20 mM HEPES (pH=7.5), 0.1% BSA, 10 mM $MgCl_2$, 1 mM EGTA, 2 mM $CaCl_2$, 40 µM peptide substrate (Murphy et al., 2010). 1.3 nM of CpCDPK1 protein were used and 3 to 0.00137 µM inhibitor were used in 3-fold serial dilutions (Murphy et al., 2010). Phosphorylation reactions were initiated by the addition of µM Na_2ATP (Murphy et al., 2010). The reaction was incubated for 90 minutes at 30 ºC. 5 mM of EGTA was added to terminate the reaction (Murphy et al., 2010). The Kinaseglo luciferase reagent and luminescence was used to determine the change in ATP concentrations (Murphy et al., 2010). Luminescence was measured by the Chameleon 425-104 multi-label plate scintillation counter (Murphy et al., 2010).To determine inhibitors activity against the catalytic domain of the wild-type Src kinase compounds were tested at 20 µM and diluted down again in 3-fold serial dilutions (Murphy et al., 2010). A buffering solution of 33.5 mM HEPES (pH = 7.5), 6.7 mM $MgCl_2$, 1.7 mM EGTA, 67 mM NaCl, 2 mM Na_3VO_4, 0.08 mg/mL BSA, 3 µM ATP, and an optimized Src peptide substrate was used (Murphy et al., 2010). The final volume was 30 µL (Murphy et al., 2010). The reaction was allowed to run at room temperature for 30 minutes before passing 4.5 µL of the reaction mixture through a phosphocellulose membrane (Murphy et al., 2010). Membranes were then washed 4 times with 0.5% phosphoric acid then once with acetone (10 minutes each wash) (Murphy et al.,

2010). The membrane was dried and then radioactivity was measured by phosphorimaging with a Storm 840 phosphor scanner and quantified with ImageQuant and converted to percent inhibition (Murphy et al., 2010). IC_{50} values for CpCDPK1 and Src were determined by Prism Graphpad software using non-linear regression analysis (Murphy et al., 2010).

3.2.3. Preliminary structure-activity relationship analysis

Once UH15_15 was identified as a promising hit, other compounds in the UH15 series that challenged various structural elements were tested. Compounds composed of the same scaffold included UH15_8, UH15_16, UH15_22, and UH15_30. Compounds with varied scaffolds that were also tested included UH_PN1, UH_PN2, UH_LPSN, UH15_37, UH15_38, and UH15_31. Compounds structures are shown in the results section 4.2. All compounds were initially made as DMSO stock solutions (10 mM). Additional compounds to expand the structure-activity relationship analysis were synthesized as described in section 3.2.5.

3.2.4. Molecular docking studies

Molecular docking is a type of computation study that is used to indicate how and how well a protein or molecule binds to another protein or molecules. The docking software can determine which poses are most thermodynamically favored based on the delta G (Gibbs free energy), which is dependent on delta H (enthalpy) and delta S (entropy). Docking poses are determined based on the sum of interactions. This produces 5-10 final poses of theoretical binding arrangements. Based on these 3D poses critical interactions can be determined (i.e. which amino acids form hydrogen bonds with which functional groups or where pi-pi interactions are formed with aromatic regions, etc.). For these studies, UH15_16 was docked using the MOE software. Discovery Studio and Pymol were used to process and visualize docked structures. The resulting poses of MOE docking require additional processing in which

the original structures are deleted, as MOE will “twist” the structures in flexible fit docking and therefore duplicate both the defined “ligand” and “receptor” (in rigid fit only the defined “ligand” will be duplicated).

To prepare proteins, MOE was used. Protein data bank (PDB) file 3NCG was the main CpCDPK1 protein structure used to generate data presented in the results section. Originally, proteins and ligands were prepared using the method recommended in the manual (upload, protonate, etc.). However, once QuickPrep became available with an update to MOE, it was used to obtain data shown in the results section.

Chemical structures were drawn in the 2D platform, cleaned up and their 3D structure optimized (energy minimization) using ChemSketch. Compounds were saved as a “.mol” file and imported into the MOE software. These could then undergo energy minimization again within MOE.

Compounds were docked into the ATP binding pocket. Ligands can be docked using a variety of placement methods. The triangle method was used by default and resulted in most acquired data. This determines how the ligands are angled to fit into the pocket. The second option is the refinement. Both rigid fit and induced fit have been used. For consistency, induced fit was used, because it gives a more accurate picture. In induced fit modeling, amino acids can twist to or away from the ligand – which is more indicative of physical binding.

3.2.5. Expansion of structure-activity relationship analysis

The expanded SAR study used additional compounds generated as part of the RIPK2 optimization program (Nikhar et al., 2016) or synthesized as described below.

3.2.5.1. General experimental conditions

All reactions were set up, monitored and purified under similar conditions, unless otherwise stated. All reactions were set up under dry conditions – meaning round bottom flasks (RBFs) were purged with argon. Argon purging can be performed by either vacuuming out the oxygen and then adding argon each for 5 seconds and repeating 3 times. Alternatively, one can flush the sealed RBF with argon with inlet and outlet needles for 5 minutes. All commercially available starting materials, reactants, solvents, etc. were used "as is" unless otherwise mentioned. To monitor reactions for completion, thin-layer chromatography (TLC) was utilized. When silica TLC plates were used, Baker-flex® Precoated Flexible TLC Sheets, by J.T. Baker® were used. These silica plates have with F254 for a fluorescence indicator and Gypsum for a binder. When alumina was used, Aluminum Oxide F254 Plates with F254 fluorescence indicator and 60Å pore size. Reaction material was "worked up" prior to spotting on TLC plates if a non-volatile solvent, acid, base, or a reagent requiring water to quench the reaction was used. TLC plates were run/processed in mixtures of ethyl acetate (EA) or methanol (MeOH) and dichloromethane (DCM) or hexane (Hex). TLC plates were not regularly dyed/stained. However, a UV-light (254 and 365 nm) was used as a visualizing process. Purification was performed using flash chromatography using a Teledyne ISCO CombiFlash® Rf machine. Silica or alumina gel were regularly used to purify compounds (silica > alumina). The same solvents and mixtures of solvents were used as with TLC (EA, MeOH, DCM, Hex). NMR spectra were acquired using a JOEL 600 MHz NMR instrument. $CDCl_3$, chloroform-D, was most frequently used as the solvent for acquiring NMR spectra, however CH_3OD, or methanol-D, and DMSO-*d*6 were also used. High-resolution mass spectroscopy (HRMS) was performed by the University of Texas Department of Chemistry on an Agilent 6530 Q-TOF instrument. The ionization source was

electronspray. The *m/z* was reported for the compound's molecular (M) and ionization species (M±1). This was performed for final compounds assessed for biological activities. Purity was assessed by high performance liquid chromatography (HPLC) analysis. For numerous compounds, preparative HPLC purification was used to purify compounds using a Waters Acuity HPLC. The HPLC uses a XSelect CSH^{TM} Prep with C18 at 5 µm OBD diameter 19x100 mm Column and Waters 2489 UV/Visible Detector. The HPLC uses a WFCIII auto collector and manual injector. A general method was used for a preliminary analysis, however for each compound a method was developed for analysis of purity. This general method was 2% acetonitrile (ACN) and 98% water (with 0.1% formic acid) to 98% in 30 minutes followed by an 8-minute column wash. The compound-specific methods were developed. For instance, if the product peak comes at 50% ACN/Water the method would focus at 45-55%. This method would be 0% acetonitrile (ACN) to 2% in 2 minutes then 45% at 4 minutes. At 30 minutes the column would be at 55% followed by the column wash. The column wash was 98% ACN to 2% then 0% over 10 minutes. The UV detector was set to 254 nm; however, this could be modified as necessary. Each analytical HPLC used an injection volume of 10 µL and a flow rate of 1.2 mL/min. This analytical flow rate corresponded to the preparatory flow rate of 20 mL/min, using the corresponding flow rate allowed a similar retention time across analytical and preparatory columns as they were the same length.

3.2.5.2. Synthesis of UH15_16 and other analogs

The general synthesis scheme was as follows:

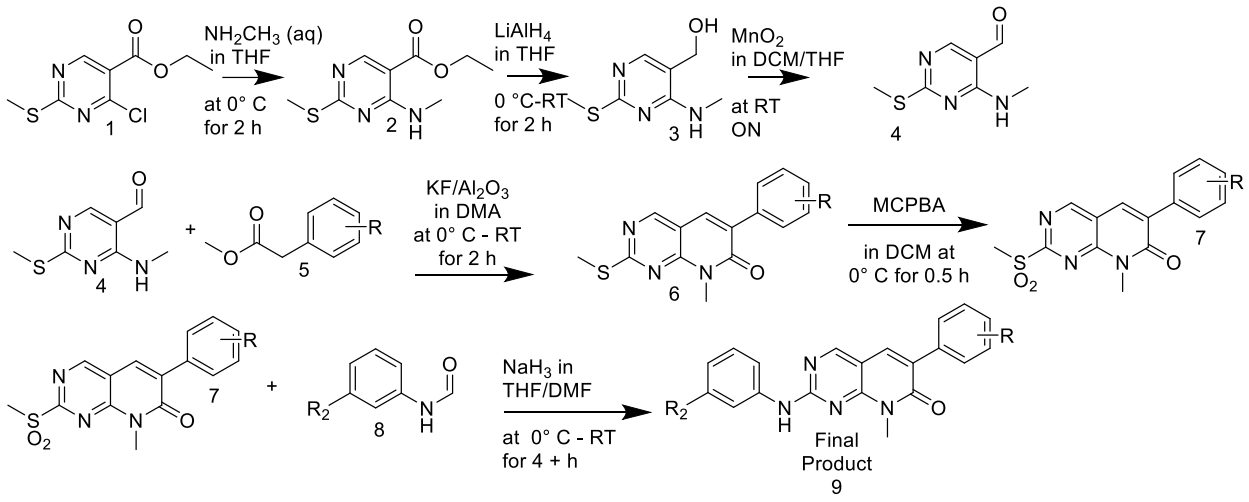

Figure 11. *General Synthesis Scheme*

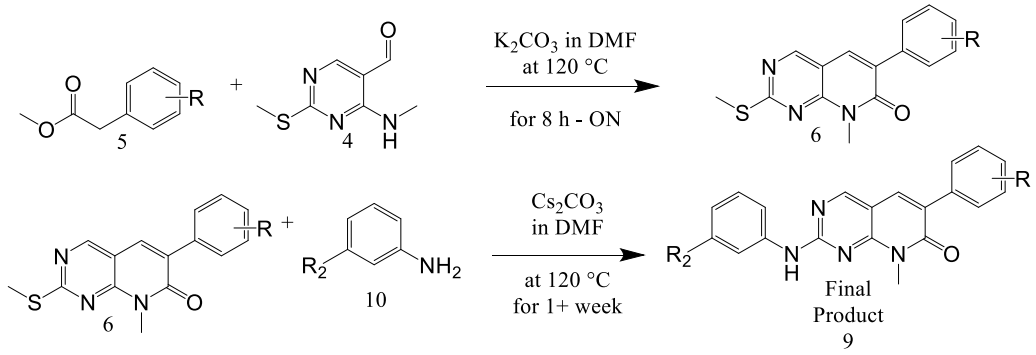

Figure 12. *Alternative Synthesis of Heterocycle*

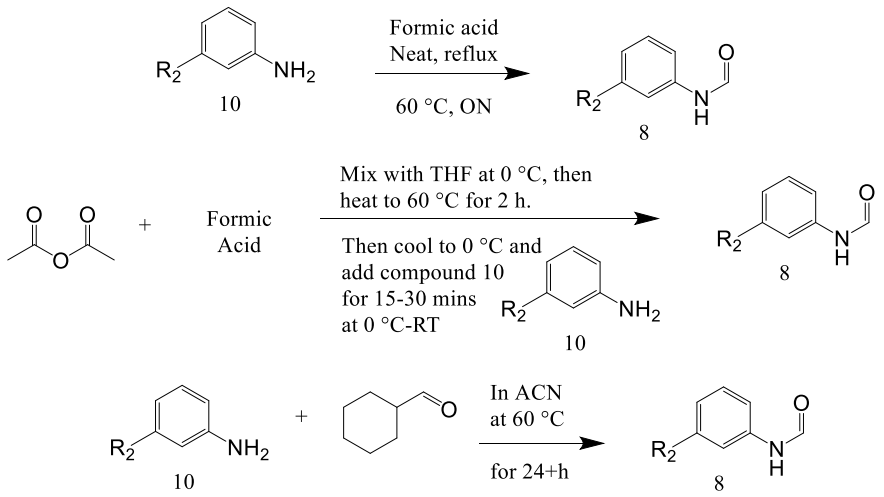

Figure 13. *Synthesis of Acid Labile Amides*

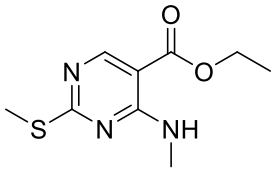

Synthesis of 2. To a solution of ethyl 4-chloro-2-(methylthio) pyrimidine-5-carboxylate, **1,** (6 g, 0.0273 mol) in THF (26 mL) at 0 °C was added 40% aqueous methylamine (6 mL). Additional solvent may be required depending upon the manufacturer of compound **1**. The specific ratio of methylamine to THF did not appear to affect the outcome or yield as long as compound **1** was fully solubilized. The reaction mixture was stirred at 0 °C for 2 hours and then concentrated. To the residue was added NaCl and methanol. The mixture was stirred and then extracted with ethyl acetate. The organic layer was dried with anhydrous Na_2SO_4, filtered and concentrated. The crude product was prepared by column chromatography on silica gel using 0-5% EA/Hex as eluent to give **2** (60-95% yield) as a white solid. ^{1}H-NMR ($CDCl_3$, 600 MHz) δ 8.53 (s, 1H), 8.1 (s, 1H), 4.24-4.25 (q, 2H), 3.00 (s, 3H), 2.47 (s, 3H), 1.30 (t, J = 13.8 Hz, 3H). ^{13}C-NMR ($CDCl_3$, 600 MHz) 176.0, 167.0, 160.6, 158.1, 100.9, 60.7, 27.2, 14.2, 14.1.

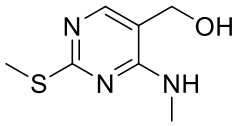

Synthesis of Compound 3. To a solution of compound **2** (5 g, 23 mmol) in anhydrous THF (36 mL) at 0 °C was slowly added $LiAlH_4$ (1.33 g, 35 mmol or 1.5 equiv)– noxious gas may be released. To allow the gas to be safely released, a needle was placed in the stopped. The reaction mixture turned from white to olive to grey throughout the addition of $LiAlH_4$. The reaction mixture was allowed to warm to room temperature and stirred for 4 hours. The reaction was cooled to 0 °C and cold water (6 mL) was added dropwise to quench. The needle was added

again to release the noxious gas, then the reaction mixture was stirred at 0 °C for at least 20 minutes. The reaction material was vacuum-filtered through a small amount of celite-545 and washed with EA, MeOH, and DCM until the solute was no longer UV active. Typically, over a liter of solvents was necessary to get adequate yield. The solution was concentrated, and the crude product was prepared by column chromatography on silica gel using 0-5% MeOH/DCM as eluent to give **3** (80% yield) as a white solid. ^{1}H-NMR ($CDCl_3$, 600 MHz) δ 7.71 (s, 1H), 5.88 (s, 1H), 4.52 (s, 2H), 3.04-3.05 (d, J = 4.2 Hz, 3H), 2.53 (s, 3H). ^{13}C-NMR ($CDCl_3$, 600 MHz) 171.6, 161.6, 152.3. 111. 1, 61.2, 27.7, 14.2.

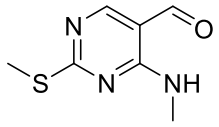

Synthesis of compound 4. To a solution of compound **3** (2.5 g, 13.6 mmol) dissolved in DCM/THF at a 5:1 ratio, MnO_2 (10 g, 0.122 mol, 9 eq.) was added. The reaction was stirred overnight at room temperature. A second method was developed with reduced amounts of MnO_2 (equal weight of MnO_2 as compound **3,** or ~ 3 eq. or MnO_2 and left for about 3 days). Once the reaction was deemed complete by TLC, the reaction material was vacuum-filtered with sufficient celite-545. The filtrate was washed with EA; DCM and MeOH may also be added. The resulting material concentrated. The crude product was purified by column chromatography on silica gel 0-25% EA/Hex as eluent to give **4** (81% yield, note the MnO_2-sparing method did not affect purity nor yield.) as a white solid. ^{1}H-NMR ($CDCl_3$, 600 MHz) δ 9.70 (s, 1H), 8. 56 (bs, 1H), 8.30 (s 1H), 3.10-3.11 (d, J = 4.8 Hz 3H), 2.55 (s, 3H). ^{13}C-NMR ($CDCl_3$, 600 MHz) 190.5, 177.1, 162.5, 159.1, 109.2, 26.8.

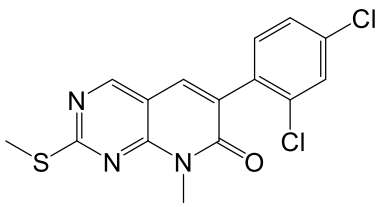

Synthesis of compound 6a. To a solution of compound **4** (200 mg, 1.105 mmol) dissolved in dimethylacetamide (DMA) (3 mL) at 0 °C. KF/Al_2O_3 (200 mg, 1682g/mmol) and commercially available compound **5a** (0.13 mL or 174 mg, 0.995 mmol) were added. If less KF/Al_2O_3 was used, the reaction may be left overnight without a significant increase in impurities. For future renditions of this reaction, compound **5a** was added in slight excess (1.1 equiv.). The reaction was left for at least 2 hours or deemed complete by TLC. Once complete, the reaction was vacuum filtered to remove the KF/Al_2O_3. The reaction material should be extracted and purified quickly as a degree of KF is present in the reaction material. To remove the DMA, extract with EA and water at least 5-10 times. Then wash the EA layer with brine. Dry the organic layer over anhydrous Na_2SO_4, filter and concentrate. The crude product was purified by column chromatography on silica gel 0-25% EA/DCM as eluent to give **6a** as a yellow crystalline powder in 55% yield. ^{1}H-NMR ($CDCl_3$, 600 MHz) δ 8.65 (s, 1H), 7.66 (s, 1H), 7.50 (s, 1H), 7.31 (s, 2H), 3.81 (s, 3H), 2.66 (s, 3H). ^{13}C-NMR ($CDCl_3$, 600 MHz) 173.7, 161.6, 156.5, 154.3, 135.3, 135.1, 134.5, 133.2, 132.3, 130.3, 129.7, 127.2, 109.2, 53.6, 14.6.

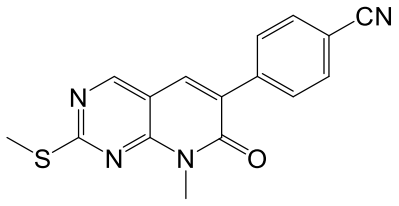

Synthesis of compound 6b. While the aforementioned method could be used for the synthesis of compound **6b**, the yield was about 25%. Therefore, a more rewarding method was devised, as

follows. To a mixture of compound **4** (37.6 mg, 0.21 mmol) in DMF (1.5 mL) was added commercially available compound **5b** (35.9 mg, 0.21 mmol) along with K_2CO_3 (56.7 mg, 0.41 mmol). The reaction was heated to 120 °C overnight. TLC ensured completeness. DMF would be removed via extraction (To remove the DMF, an extraction with EA and water was necessary and repeated at least 5-10 times. Then the organic layer was washed with brine and EA, the resulting organic layer was dried over anhydrous Na_2SO_4, filtered and concentrated) The dried crude product was prepared by column chromatography on silica gel 0-25% EA/DCM as eluent to give **6b.** This resulted in a scarlet/red crystalline powder in 61% yield. ^{1}H-NMR ($CDCl_3$, 600 MHz) δ 8.70 (s, 1H), 7.82-7.73 (m, 5H), 3.84 (s, 3H), 2.67 (s, 3H). ^{13}C-NMR ($CDCl_3$, 600 MHz) 174.1, 161.9, 156.8, 154.2, 154.1, 140.2, 134.0, 132.2, 130.8, 129.6, 118.8, 112.3, 109.6, 28.6, 14.7.

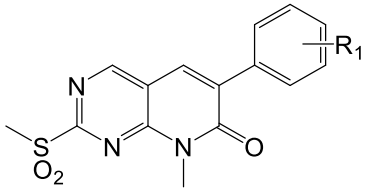

Synthesis of compounds 7a-b. To a solution of compound **6a**/**b** (1.7 g, 5.5 mmol) dissolved in dichloromethane (36 mL) at 0°C, meta-chloroperoxybenzoic acid (2.5 g, 16 mmol) was added. The mixture was stirred at 0 °C for 30 minutes. To ensure completeness, the reaction was monitored by TLC. The completed reaction was quenched by adding water on ice. The organic layer was extracted and washed with brine. The residue was dried over anhydrous Na_2SO_4, filtered and concentrated. The residue was purified by column chromatography on silica using 0-25% EA/DCM.

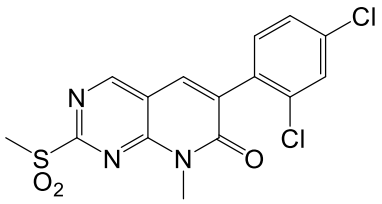

Compound 7a. A white/yellow powder. ^{1}H-NMR ($CDCl_3$, 600 MHz) δ 9.04 (s, 1H), 7.86 (s, 1H), 7.53 (s, 1H), 7.32-7.37 (q, 2H), 3.89 (s, 3H), 3.44 (s, 3H). ^{13}C-NMR ($CDCl_3$, 600 MHz) 164.6, 161.0, 157.5, 155.1, 135.9, 135.3, 135.3, 134.3, 134.1, 132.2, 132.0, 129.9, 127.4, 114.9, 39.3, 29.3.

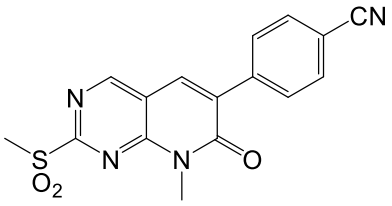

Compound 7b. A reddish/brown crystalline powder, ^{1}H-NMR ($CDCl_3$, 600 MHz) δ 7.99-8.09 (s+d, 3H), 7.93* (s, 1H), 7.78-7.84 (q, 4H), 7.60-7.59 (d, J = 7.8 Hz, 2H), 7.45-7.42 (t, J = 15 Hz, 2H), 392 (s, 3H), 3.45 (s, 3H).

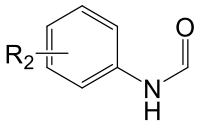

Synthesis of compound 8a-b. A solution of acetic anhydride (0.22 mL), formic acid (0.1 mL), and tetrahydrofuran, THF (8.4 mL) was heated at 60 °C for 2 hours. The reaction material was then allowed to cool to 0°. The commercially available amine **10b** (100 mg, 0.5 mmol), was added at 0 °C. The ice bath was removed and the reaction was maintained at room temperature (or when R_2 contains an amine or sulfonamide at 0°C) for at least 30 minutes and monitored by TLC. However, to produce **8c** and **8d**, quenching was done sooner to avoid impurities. It is also recommended to leave the reaction at 0 °C to limit byproducts and monitor the reaction closely

by TLC. Once complete, the reaction mixture was cooled to 0 °C, and quench by adding freshly (3-4 mL) prepared 2N NaOH (1.6 g NaOH in 20 mL water). The mixture was stirred for 20 minutes at 0 °C to neutralize the acid. Then the organic solvents are removed by rotovap. The NaOH (aq) is extracted by separatory funnel then the organic layer was washed with water, EA, and brine. Then the organic layer was dried over anhydrous Na_2SO_4, filtered and concentrated. The crude product was purified by column chromatography on silica column using 0-5% MeOH/DCM.

Due to potential stability issues with these compounds, they were immediately placed in the freezer. Due to this stability issue, they could not be left in the NMR overnight to get a ^{13}C, so instead, the compound would be validated after the next step, as finalized compounds.

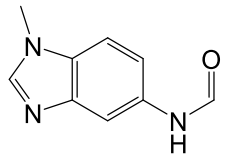

Compound 8a. Pale yellowish crystalline powder, 82.3% yield. ^{1}H-NMR (MeOH, 600 MHz) δ 8.67 (s, 1H), 8.29 (s, 1H), 8.10 (s, 1H), 8.04 (s, 1H), 7.48 (s, 2H), 3.87 (s, 3H).

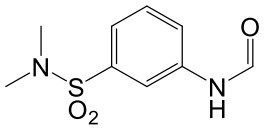

Compounds 8b. Pale yellowish white crystalline powder, 82% yield – this compound was very unstable. Due to stability concerns, characterization was limited. ^{1}H-NMR ($CDCl_3$, 600 MHz) δ 8.32 (s, 1H), 8.12 (s, 1H), 7.71-7.79 (d, J = 8.4 Hz, 1H), 7.61-7.51 (m, 2H), 2.67 (s, 6H).

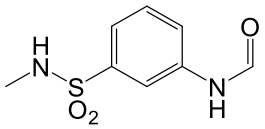

Compound 8c. Pale yellow crystalline power. NMR not included, as compound would degrade and produce inconclusive NMR – however resulting NMR was different from starting material. Compound was confirmed in the next step.

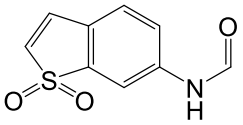

Compounds 8e. Off-white crystalline powder, 81% yield– this compound was very unstable. Due to stability concerns, characterization was limited. ^{1}H-NMR ($CDCl_3$, 600 MHz) δ 8.35 (s, 1H), 7.86 (s, 1H), 7.70-7.75 (dd, 1H), 7.39-7.47 (m, 3H), 6.89-6.93 (dd, 1H).

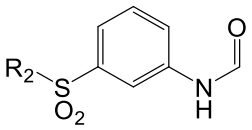

Synthesis of compound 8e-f. The amine (500 mg) was placed in an RBF with formic acid (10 to 25 mL). The formic acid was refluxed at 60 °C overnight. The reaction was allowed to cool and then it was neutralized and extracted with saturated K_2CO_3 and further washed and extracted with EA. The organic layer was dried over anhydrous Na_2SO_4, filtered, and concentrated. The published protocol did not call for purification of this product. However, to limit impurities in the final product, it was purified on alumina with 0-33% EA/hex.

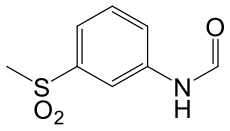

Compound 8f. The material was white to tan crystalline powder, when the purified yield was about 70%, and 75%, respectively. ^{1}H-NMR ($CDCl_3$, 600 MHz) δ 7.30-7.33 (dt, 1.5H), 7.27 (s, 0.5H), 7.22 (s, 2H), 4.07 (bs, 3H).

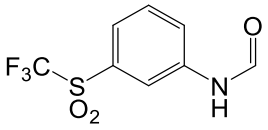

Compound 8g. Pale tan crystalline powder, 72% yield. The original protocol did not call for purification of this compound. The crude compound was taken to the next step. The final compound was used to confirm this step.

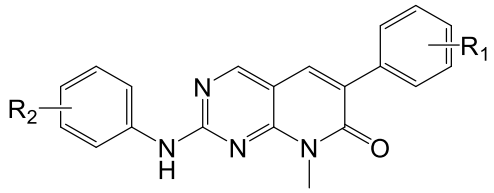

Synthesis of compound 9. A solution of compound **8b** (99 mg, 0.406 mmol) dissolved in a mixture of DMF and THF (approximately 0.5 mL DMF to 5 mL THF was added initially) at 0 °C was added NaH (29 mg, 1.2 mmol, or 3 equiv.). This mixture was stirred at 0 °C for at least 20 minutes. Then compound **7a** (171 mg, 0.446 mmol, or 1.1 equiv.) was added. Additional DMF or THF may be added with the resulting ratio of 1:3-10 of DMF to THF, to achieve complete solubility. For these compounds, 1 mL of DMF was added to 10 mL THF. The reaction was left for 4 hours, and TLC was used to monitor completeness of reaction. Next, water (2 mL) was added to react with the excess NaH and then the mixture was extracted with EA and water to

remove the DMF and THF. The organic layer was washed with water at least 5-10 times to ensure all DMF was removed. The resulting organic layer was dried over anhydrous Na_2SO_4, filtered, and concentrated. The crude material was purified by column chromatography on silica and/or alumina. Typically, 0-35% EA/DCM or 0-10% Me/DCM was used for silica columns while 0-35% EA/Hex was used for alumina.

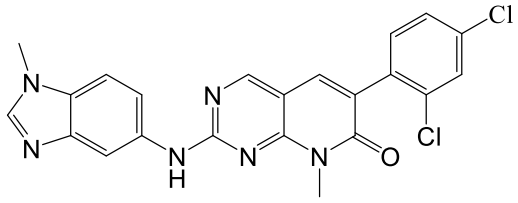

Compound CDPK-7. Bright yellow crystalline powder with an HPLC purity of >95%. ^{1}H-NMR (1:1 MeOD/$CDCl_3$, 600 MHz) δ 8.66 (s, 1H), 8.23 (bs, 1H), 8.01 (s, 1H), 7.70 (s, 1H), 7.66-7.65 (d, J = 7.8 Hz 1H), 7.57 (s, 1H), 7.52 (s, 1H), 7.50-7.48 (d, J = 9 Hz, 1H) 7.33-7.36 (t, 2H), 3.93 (s, 3H), 3.82 (s, 3H). ^{13}C-NMR (1:1 MeOD/$CDCl_3$, 600 MHz) 163.2, 160.1, 159.5, 156.2, 144.8, 143.5, 137.0, 135.3, 135.1, 134.9, 134.4, 133.1, 131.7, 129.9, 127.6, 126.6, 118.4, 110.35, 107.0, 31.5, 28.9.

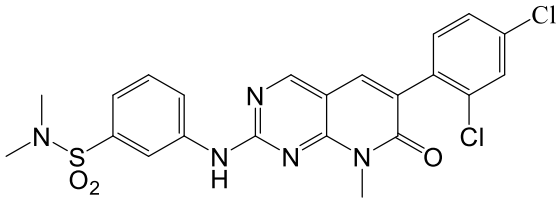

Compound CDPK-6. Off-white powder with an HPLC purity of > 97%. ^{1}H-NMR (DMSO-D_6, 600 MHz) δ 10.62 (s, 1H), 8.90 (s, 1H), 8.62 (bs, 1H), 8.98-9.00 (d, J = 8.4 Hz, 1H), 7.95 (s, 1H), 7.75 (s, 1H), 7.62-7.64 (t, J = 15 Hz, 1H), 7.52-7.53 (d, J = 6.6 Hz, 1H), 7.44-7.46 (d, J = 6 Hz, 1H), 7.38-7.40 (d, J = 7.8 Hz, 1H), 3.70 (s, 3H), 2.64 (s, 6H). ^{13}C-NMR (DMSO-D_6, 600 MHz) 161.5, 159.8, 159.6, 155.6, 141.1, 136.6, 135.6, 135.0, 134.7, 134.0, 133.7, 130.3, 129.3, 127.8, 126.6, 123.8, 121.5, 106.9, 38.2, 28.8.

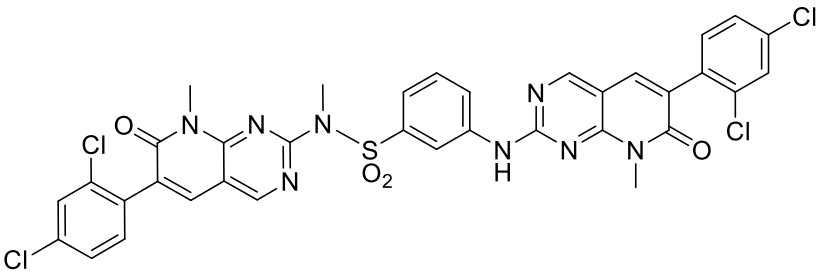

Compound CDPK-8. Off-white powder with an HPLC purity of 97-100% purity, using the HPLC standard method and compound specific methods. Of note, this compound may be unstable on the bench. ^{1}H-NMR (DMSO-D_6, 600 MHz) δ 8.86-8.88 (d, J = 12.6 Hz, 2H), 7.91-7.93 (t, 1H), 7.70 (d, J = 1.2 1H), 7.68 (d, J = 1.8 1H), 7.63-7.64 (d, J = 9.8 Hz, 1H), 7.54-7.56 (t, 1H), 7.45-7.49 (m, 2H), 7.40-7.41 (d, J = 8.4 Hz, 1H), 7.34-7.35 (d, J = 8.4 Hz, 1H) 3.73 (s, 3H), 3.64 (s, 3H). ^{13}C-NMR could not be collected due to poor solubility. When high-resolution mass spectrometry was used, it was determined that the intended product, the secondary sulfonamide, was coupling again with the heterocycle.

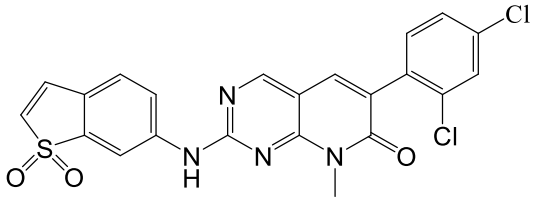

Compound CDPK-9. Sunflower yellow powder with an HPLC purity of >95% purity, using the HPLC standard method and compound specific methods. Of note, this compound may be unstable on the bench. ^{1}H-NMR ($CDCl_3$, 600 MHz) δ 10.14 (s, 1H), 8.70 (s, 1H), 7.70 (s, 1H), 7.66 (s, 3H), 7.540-7.50 (t, 3H), 7.35-7.31 (m, 3H), 6.82-6.83 (d, J = 6.6 Hz, 1H), 3.62 (s, 3H). ^{13}C-NMR (CDCl3, 600 MHz) 162.3, 161.4, 158.1, 157.9, 155.2, 138.2, 137.6, 135.4, 134.6, 134.4, 134.1, 132.7, 132.1, 131.9, 131.7, 131.1, 131.0, 129.8, 127.2, 125.8, 122.6, 110.4, 28.7.

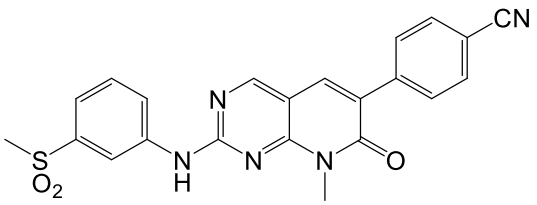

Compound CDPK-2. Pale yellowish powder with an HPLC purity of >95% purity, using the HPLC standard method and compound specific methods. ^{1}H-NMR ($CDCl_3$, 600 MHz) δ 8.74 (s, 1H), 8.69 (s, 1H), 7.81-7.83 (d, J = 7.2 Hz, 2H), 7.73-7.76 (m, 4H), 7.68-7.69 (d, J = 6.6 Hz, 1H), 7.60-7.62 (m, 2H), 3.87 (s, 3H), 3.11 (s, 3H).

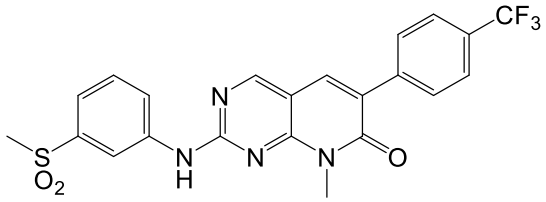

Compound CDPK-4. White crystalline powder with an HPLC purity of > 95%, using the HPLC standard method and compound specific methods. ^{1}H-NMR (DMSO-D_6, 600 MHz) δ 10.65 (s, 1H), 8.93 (s, 1H), 8.79 (bs, 1H), 8.20 (s, 1H), 7.92-7.97 (dd, J = 27 Hz, 3H), 7.81-7.82 (d, J = 8.4 Hz, 2H), 7.62-7.65 (t, 1H), 7.59-7.58 (d, J = 7.8 Hz, 1H), 3.72 (t, 3H), 3.23 (s, 3H). ^{13}C-NMR (DMSO-D_6, 600 MHz) 162.2, 160.1, 159.1, 155.3, 141.9, 141.0, 140.8, 135.8, 130.4, 130.0, 129.7, 128.6, 126.7, 125.5, 125.4, 124.4, 121.0, 117.6, 107.4, 70.2, 44.2, 28.8.

3.3. *In Vitro* pharmacokinetic metrics of UH15_16: Solubility, absorption, distribution, and metabolism

UH15_16 was sent to Eurofins for analysis. Aqueous solubility in PBS buffer was determined at pH 7.4 by the shake-flask method for 24 h at room temperature with compound detection by HPLC-UV/VIS (Lipinski, 1997). Caco-2 cells were used to determine absorption. This was assessed apically to basally and basally to apically. Recovery was calculated for both assessments. Metabolism was assessed using mouse liver microsomes.

3.4. UH15_16 kinase profiling

UH15_16 was screened against 97 kinases at Eurofins using the KinomeSCAN - scanEDGE for kinase profiling. This screen includes AGC, CAMK, CMGC, CK1, HER1, STE, TK, TKL, lipid, and atypical kinase families. The KINOMEscan™ screening method utilizes an active site-directed competition binding assay to quantitatively measuring interactions between test compounds and kinases in a non-ATP concentration depend manner (Fabian, 2005). A concentration of 1 µM of UH15_16 was used for this assessment.

To confirm kinase activity, UH15_16 was tested in biochemical kinase assays by Reaction Biology. Ten concentrations were tested for each kinase (7 kinases were tested, ABL-1, BRAF, c-Kit, c-Src, FGFR2, FMS, PDGFRb) starting at 10 µM to determine IC_{50} values. Staurosporine or GW5074 were used as positive controls, while DMSO was used as a negative control.

3.5. Formulation studies

3.5.1 Development of intravenous formulation.

A variety of formulations were attempted to fully solubilize UH15_16 for intravenous administration. Eventually UH15_16 was formulated in 30% Tween 80, 20% PBS, and 50% ethanol to achieve complete solubility. The formulation consisted of 450 µL Tween 80, 300 µL PBS, 750 µL ethanol, and 1.5 mg UH15_16. resulting mixture of approximately 1.5 mL was sonicated and then passed through a 0.2 µm PTFE membrane filter to remove any particles that may cause venous harm. The resulting concentration of the compound was 0.5 mg/mL.

3.5.2 Development of oral formulation 1.

For the first oral formulation, UH15_16 was suspension with 10% (v/v) polyethylene glycol 400 and 90% (v/v) Ora-Plus. Ora-Plus is a suspending agent with a mixture of commonly used formulating agents and includes methylcellulose. UH15_16 was formulated by placing 3.75 mg of UH15-16 in a vial and adding 30 µL (or 10% of final volume) of polyethylene glycol (PEG) 400, then vortexing the vial. Then 270 µL (or 90% of final volume) Ora-Plus was added to the vial and vortex again. The resulting mixture is a milking suspension.

3.5.3 Development of oral formulation 2.

3.5.3.1 UH15_16 docking with cyclodextrin

Ligand-cyclodextrin docking was performed using MOE, employing methods similar as the ligand-protein docking. The structure of β-cyclodextrin was extracted from PDB 1Z0N. However similar structures were not available for α-cyclodextrin or γ-cyclodextrin. So, such files were created in ChemSketch and Discovery Studio with energy minimization and tautomerization.

A structure file of UH15_16 was prepared as described in section 3.2.4.

Each cyclodextrin file was imported into MOE. Energy minimization was performed again or QuickPrep. The cyclodextrin was selected and labeled as a set. The UH15_16 structure file was then added. Of note, this does cause some twisting of the cyclodextrin tails.

To dock, the receptor and site were changed to the set labeled cyclodextrin. The ligand was set to the desired compound, UH15_16. The triangle method was used as default and induced fit was necessary for the cyclodextrin to respond to UH15_16. Once docked, delta S was used to determine the binding affinity.

Poses were saved and processed in Discovery Studio. Images can be seen in the results section. PyMol was also used to visualize the poses of UH15_16 in various cyclodextrins, but Discovery Studio was the preferred platform.

3.5.3.2 Oral formulation 2

In an initial experiment the molar ratio of Captisol (e.g. sulfobutylether-β-cyclodextrin) to UH15_16 was assessed. UH15_16 (6.25 mg) and 50, 100 or 200 mg Captisol (approximately 2x, 4x, and 8x) were added to 0.5 mL deionized (DI) water. Five additional 0.5 mL aliquots of DI water were added. After the addition of each aliquot, the mixture was vortexed for 2 minutes, observed for 15 minutes and any precipitation was noted. After the 5^{th} DI water aliquot was added, the mixture was left to sit overnight.

A second experiment was conducted with a Captisol to UH15_16 molar ratio of 2:1. For each 6.25 mg of UH15_16, 50 mg of Captisol and 0.5 mL of DI water was used. It is recommended to only sonicate this solution for at least 2 minutes rather than vortexing.

3.5.4. Development of oral formulation 3

3.5.4.1. Simulated gastric fluid

Simulated gastric fluid was made by dissolving 1g NaCl in 483 mL DI water. Then, the solution was pH adjusted to ~1.2 (± 0.1) with HCl.

3.5.4.2. Simulated intestinal fluid

Simulated intestinal fluid was made using a method published by Pan (Pan, 2015). Potassium phosphate monobasic (3.4 g), 1.25 g SDS (or 0.25% sodium dodecyl sulphate) was dissolved in 333 mL DI water. This solution was mixed and pH-adjusted to 6.8 (± 0.1) with freshly prepared 1N NaOH.

3.5.4.3. Fed-state simulated intestinal fluid (FeSSIF)

Fed-state simulated intestinal fluid (FeSSIF) was made using the methods of Galia and Marques (Galia, 1999 and Marques, 2004). NaOH (pellets, 2.02 g), 4.33 g (or mL) glacial acetic acid, and 5.94 g NaCl was added to 500 mL DI water. This solution was then pH adjusted to 5 ± 0.1 using 1N NaOH/HCl as applicable. The pH was confirmed with both pH paper and a pH probe. Next, 100 mL of this blank FeSSIF solution was transferred into a RBF along with 3.3 g of sodium taurocholate [acid]. Separately a 100 mg/mL solution of [soybean] lecithin in dichloromethane (DCM) was prepared using 1.5g of lecithin in 15 mL of anhydrous DCM. 11.8 mL of the lecithin solution was added to the RBF forming a cloudy emulsion. To remove the DCM, the RBF was placed on a rotovap at 40 ℃. Once no DCM could be detected, the solution in the RBF was cooled to room temperature. The approximately 100 mL was volume adjusted to 400 mL with the rest of the blank FeSSIF. The final FeSSIF became translucent but had a distinct yellowish tint.

3.5.4.4. Fasted-state simulated intestinal fluid (FaSSIF)

Fasted-State Simulated Intestinal Fluid (FaSSIF) was made also following protocols from Galia and Marques (Galia, 1999 and Marques, 2004). 0.174 g NaOH pellets, 1.98 g NaH_2PO_4, H_2O, and 3.09 g NaCl were mixed in 500 mL DI water. This solution was then pH adjusted to 6.5 ± 0.1 using 1N NaOH/HCl as applicable. The pH was confirmed with both pH paper and a pH probe. Then 100 mL of this blank FaSSIF solution was transferred into a RBF and then 0.66 g sodium taurocholate [acid] was added. Only 2.36 mL of the lecithin solution previously mentioned in 3.5.4.3 was added to the RBF forming an emulsion. This emulsion also turned slightly cloudy. The RBF was concentrated until DCM could not be detected. FaSSIF was also volume adjusted to 400 mL FaSSIF becoming translucent but lacked the distinct yellow tint.

3.5.4.5. Anti-precipitation assay

The anti-precipitation experiment follows protocols by Yamashita and Klein (Yamashita, 2011 and Klein, 2010; Klein, 2012). A solution of anti-precipitant(s), including Tween 80, methylcellulose, and/or Captisol were dissolved in gastric fluid (20 mg/mL of Captisol = 1x). Then 2.5 mg/mL of UH15_16 was added to the solution. The mixture was vortexed and sonicated for 2 minutes each. Additional anti-precipitants or quantities of Captisol were added (Captisol 0x, 1x, 2x, 3x 4x, 5x, 6x, 7x, 8x +/- methyl cellulose or Tween 80 may have been plated). It is worth noting that over time volume was lost from repeat sampling from the same vial(s). However, in the case of Captisol, that would not significantly affect the concentration as each time 20 mg was added, a portion of the Captisol would get stuck at the end of the weigh paper. It is assumed this would cancel out against the 30 µL removed.

To plate the 96-well plate, 100 µL of DI water in the first row of a 96-well plate was used as a control. Another row is plated with just gastric fluid serving as another negative control.

Then 30 µL of the UH15_16/anti-precipitant solutions were placed into the assigned well. Pure UH15_16, at the correlating dose of 5-50 mg/kg or concentration 0.08-0.79 mM, and pure Captisol, at 20 mg/mL, in gastric fluid was also plated as controls. When Tween 80 or methylcellulose was used, that too was plated as a control at the highest concentration use (3% v/v and 1% w/v respectively. It is worth noting these percentages are not equal to the percentage in the formulation. Instead, the 3% v/v/ or 1% w/v was the amount used as a percentage of the total well, 100 µL. We later used a ratio of excipient to UH15_16 to determine the final formulation). Once the plate is plated with the first round of solutions, it is sealed. The plate is shaken for 5 minutes at 425 rpm then centrifuged at 950g for 5 minutes (the first time the experiment was run, this was not performed, instead it sat for 15 minutes). Then, every place that has gastric fluid (i.e. not the first row), 70 µL of simulated intestinal fluid is added. The plate is then placed in the UV plate reader.

The UV plate reader follows a protocol in which it is heated to 37 ºC and held at this temperature. Then it starts a "kinetic run". In this kinetic run it scans at 450 nm every 5-15 minutes for 4 hours and continuously shakes orbitally at 205 cpm. At the end of the 4 hours the kinetic run ends.

The results of the UV plate reader are graphed as absorbance over time as well as an absorbance level at each time point.

3.5.4.6. Oral formulation 3

The third formulation consisted of a higher concentration of Captisol at 5-fold molar ratio to UH15_16. Additional excipients were investigated, and Tween 80 was added at 2.5% v/v. For each 2.5 mg of UH15_16, 57 mg of Captisol, 20 µL Tween 80 and 0.8 mL of DI water was used. The protocol for making the third formulation is the following for the dose of 25 mg/kg to 3 mice

(assuming 25 g/mouse) with a dosing volume of 200 µL/mouse. First in a vial weigh 57 mg of Captisol and add 721 µL water. Sonicate (if sonication is not available, vortexing is acceptable in its place). Then, add 20 µL Tween 80 and 2.5 mg of UH15-16then sonicate. This should result in 800 µL of a milky suspension.

3.6. *In vivo* pharmacokinetic studies of UH15_16

The pharmacokinetic studies were performed under the direction of Dr. Ming Hu's laboratory. All the described experiments follow the protocol, PROTO201800072, approved by the Institutional Animal Care and Use Committee (IACUC) at University of Houston, which has been accredited by the American Association of Laboratory Animal Care (AALAC). In accordance with the efficacy study, the same mouse strain was used to avoid any potential strain discrepancies. However, due to complications with IL-12 being immunocompromised, wild-type mice were used for pharmacokinetic assessments. Adult male mice, 4-6-week-old, were used, again in accordance with the efficacy experiments. Blood samples were taken via tail vein sampling at set time points – this varied depending upon the formulation.

3.6. Formulation Assessments

3.6.1. Bioanalytical method development

To analyze blood samples from the experiments above an ABSciex 5500 Qtrap mass spectrometer (LCMS/MS) was used to quantify UH15_16 in the blood (and later tissue samples). The method was developed with the assistance of Li Li.

The liquid chromatography utilizes a Waters Acquity UPLC BEH C18 Column with the dimensions 50 mm × 2.1 mm I.D., 1.7 µm. Column temperature was set to 30 ℃, while the

sample temperature was chilled to 10 ℃. Each injection volume was 10 µL. The liquid chromatography gradient was as follows:

Table 1. LCMS - LC Method

Time	**Flow rate (mL/min)**	**Phase A (Water with 0.1% Formic Acid)**	**Phase B (100% Acetonitrile)**
0	0.40	90	10
1.0	0.40	90	10
2.0	0.40	35	65
3.0	0.40	30	70
3.5	0.40	10	90
4.0	0.40	10	90
4.5	0.40	90	10
5.0	0.40	90	10

The mass spectroscopy portion of the method was set to the positive setting. The ion spray voltage was set to 5.5 kV. The ion source temperature was set to 500 ℃. The ion source gas (or gas 1) and turbo gas were both established as nitrogen at 35 psi. The curtain gas was also set as nitrogen but set only to 30 psi. The m/z transitions and compound dependent parameters are defined below (this includes UH15_16, its fragment, and the internal standard Baohuoside or "bao").

Table 2. LCMS – MS Method							
	Q1 Mass	**Q3 Mass**	**Time(msec)**	**ID**	**DP**	**CE**	**CXP**
1	476	362.2	100	UH 15_16 1	56	52	15
2	476	397.2	100	UH 15_16 1	61	50	10
3	515	369	100	Baohuoside	32	13	4

Standard samples were prepared using a stock solution. The stock solution of UH15_16 was solubilized in DMSO at a concentration of 7 mM. This was diluted to 10 µM or 10,000 nM with acetonitrile – this is the first working standard. The working standards were diluted 2x in a descending fashion from 10,000 nM to 4.9 nM across 12 tubes. These working standards were used to prepare 12 standard curve samples in blood, one for each working standard. 10 µL of the working solutions, 10 µL blank rodent (rat was often used as it was more readily available) blood, and 200 µL internal standard (acetonitrile with 0.05 µM baohuoside) were combined for protein precipitation. Protein precipitation constituted vortexing the mixture vigorously for 2 minutes then centrifuging at 15,000 rpm at 4 ℃ for 15 min (if the machine was not cooled prior to use, the additional centrifugation may be used, or centrifugation may be delayed allowing it to cool). Then 176 µL (80% of the tubes volume) of the supernatant was transferred to a new labeled tube and the liquid was evaporated until dry under a stream of air (> 20 minutes). This should result in an opaque residue at the bottom of the tube (it is more visible with higher concentrations of compound). The residue was reconstituted with 100 µL of 50% acetonitrile in Milli-Q water. After centrifuge at 15,000 rpm for 15 min, approximately 80% of the supernatant was transferred to an LCMS tube and capped. The LCMS used 10uL of the tubes' supernatant to be injected for analysis.

For the blood [and tissue] samples taken in the *in vivo* experiments, these samples were used in place of the blank blood, while pure acetonitrile was used in place of the working standard. So, 10 µL the [blood/tissue] sample, 10 µL of pure acetonitrile and 200 µL internal standard (acetonitrile with 0.05 µM baohuoside) were combined and followed the same procedure for sample preparation as mentioned above.

3.6.2. Pharmacokinetic study of UH15_16 with intravenous administration

Seven animals were dosed 1 mg/kg with the intravenous formulation described in section 3.5.1. Each animal received a dose approximately of 60-70 µL via tail vein injection. Again, C57BL/6 mice were used. An additional animal was dosed, but due to dosing complications, only 6 were sampled. Blood samples were also collected by tail vein. Blood samples were taken at 0, 0.25 0.5, 1, 2, 4, 6, 8, and 24 hours and collected into prepared heparin tubes.

3.6.3. Pharmacokinetic study of UH15_16 with oral administration using oral formulation 1

Four animals were dosed 5 mg/kg using oral formulation 1 as described in section 3.5.2 at a concentration at 1 mg/mL. Each animal received a dose approximately of 150-170 µL via oral gavage. C57BL/6 mice were used for all oral formulations. An additional animal was dosed, but, only 3 were sampled. Blood samples were also collected by tail vein. Blood samples were taken at 0, 0.5, 1, 2, 3, 4, 6, 8, and 24 hours. As per protocol, the mice are not fed for the first 4 hours after the dose by oral gavage. This was standard throughout all three oral PK studies.

3.6.4. Pharmacokinetic study of UH15_16 with oral administration using oral formulation 2

Six animals were dosed 5 mg/kg using oral formulation 2 as described in section 3.5.3.2 at a concentration at 1.25 mg/mL. Each animal received a dose approximately of 100-125 µL via

oral gavage. C57BL/6 mice were used for all oral formulations. While all 6 were sampled, only 4 were analyzed. Blood samples were also collected by tail vein. Blood samples were taken at 0, 0.5, 1, 2, 3, 4, 6, 8, 10, and 24 hours.

3.6.5. Pharmacokinetic study of UH15_16 with oral administration using oral formulation 3

Six animals were dosed 5 mg/kg using oral formulation 3 as described in section 3.5.4.6 at a concentration at 0.625 mg/mL. Each animal received a dose approximately of 215-240 µL via oral gavage. All 6 dosed animals were sampled. Blood samples were also collected by tail vein. Blood samples were taken at 0, 1, 2, 3, 4, 5, 6, 8, 10, 12, 14, and 24 hours. Only half the animals had a sample taken at hour 6, and the other half had a sample taken at 14 hours. This was to limit the amount of blood draws.

3.7. Toxicity study of UH15_16 and tissue analysis

Toxicity studies were performed prior to the first efficacy study to ensure the safety of the mice by Dr Jan Mead's laboratory. C57BL/6 mice (n = 5) were dosed daily at 50 mg/kg for 5 days. Daily weights and survival of mice that receive diluents or various doses of inhibitors (5 mice/group) were recorded. Toxicity was assessed by signs of distress (e.g. ruffled fur, hunched shoulders and decreased appetite). If weight loss was > 20% body weight, mice were to be euthanized. A repeat toxicity assessment was performed at 50 mg/kg with each subsequent formulation. The animals in the group were sacrificed and tissues collected.

The tissues collected were the small intestine, colon, liver, fecal material, and plasma. The small intestine and colon were washed with saline at 4 ºC. The cold saline wash removes any compound in the bile. Thus, any detected compound must have penetrated the cells or

otherwise adhered to the cells. The collected tissues were then frozen with liquid nitrogen and shipped to University of Houston. The samples were prompted placed into a -80 ºC freezer until they could be analyzed.

Tissue analysis was performed by taking a portion of the tissue 25-50 mg of the sample and homogenized. To perform this task, sterilized tweezers and scissors are used. Tweezers are used to pull the organ (liver, intestine, etc.) out of the tube it is stored. The scissors cut off a small portion, ideally weighing between 25-50 mg. The portion is weighed on tared clean weigh paper. If it weighs within the goal weight, it is placed in an Eppendorf tube using the sterile tweezers, and the weight recorded. If not, another portion of the organ is removed and added to the weigh paper until the ideal weight is met. Then the tweezers and scissors must be sterilized. This is done by washing in isopropyl alcohol (or similar organic sterilizing agent), clean DI water, and a second solution of clean isopropyl alcohol. The weighing is repeated with the next animal organ. To reduce cross contamination the blank animals are done first. 1000 µL of HBSS buffer is added to the Eppendorf tube. Tissues are then homologized. Between each tube, the homologizer is washed and dried. This is done by dipping and turning on in water, isopropyl alcohol, then a second cleaner water and turning on and wiping until dry. This prevents contamination between samples and dilution from a wet homologizer. The samples are analyzed using the bioanalytical method developed for the PK studies. Each quantity of UH15_16 in the analyzed sample is divided by the weight of added tissue (i.e. if 45 mg of liver is in the tube, the detected amount of UH15_16 would be divided by 45 mg), resulting in amount of UH15_16 per mg of tissue. This accommodates for significantly varied amount of tissue added in each sample. Dr Weiquin Wang supervised the analysis of the tissue samples at the University of Houston.

3.8. *In Vivo* efficacy studies of UH15_16

In vivo efficacy studies were performed by Dr Jan Mead's laboratory as described in (Sun, 2010).

A variety of KO C57BL/6 mice have been used to test anti-Cp agents. However, for these experiments, IL-12 was knocked out C57BL/6 mice were used. Infected IL-12 KO mice were used to imitate an acute infection. The mice were inoculated with 1000 oocysts to illicit the infection. Four hours post-inoculation, the animals are treated with either a vehicle or UH15_16 at 50 mg/kg or, in the case of the 3rd oral formulation, 25 mg/kg BID (n = 10). Animals were dosed by oral gavage using the same formulation as the pharmacokinetic study mentioned above. Treatment continued for 7 days. It is worth mentioning that throughout the study the mice have *ad libitum* feeding, thus they are not in a fasted state. At the end of the treatment course, the parasite load was determined by fluorescence-activated cell sorter assays, (Sonzogni-Desautels, 2020). To stain the *Cryptosporidium* cells, 8% paraformaldehyde and oocyst-specific monoclonal antibodies with fluorescein isothiocyanate were used (Sonzogni-Desautels, 2020). This allowed for cell cytometry counting of cells and a secondary analysis for increased specificity via histology (Sonzogni-Desautels, 2020). The cell counts via cytometry alone can overestimate the oocyte count and thus cell burden by including debris like dead cells. So, the histology was added and for improved specificity. A t-test was performed to determine statistical difference between the treatment and control groups.

4. RESULTS

4.1 tRNA synthetase inhibitor for Cp growth inhibition

4.1.1 Results of tRNA synthetase inhibitor screening and SAR studies for *Cp* growth inhibition

In this screen, a variety of tRNA synthetase inhibitors were assessed for *Cp* growth inhibition. One compound in this series required synthesizing a previously published methionyl tRNA synthetase inhibitor, referred to as ELI (Shibata et al., 2012). Three hits were identified: Halofuginone (EC_{50} = 31 nM), Borrelidin (EC_{50} = 11 nM), and AN3661 (EC_{50} = 0.63 nM). The screening data is shown below:

Table 3: *Cp* Growth Inhibition

Compound	**tRNA Synthetase Type**	**Chemical Structure**	**Cp Growth Inhibition EC_{50} (µM)**
AN2690 / Tavaborole	Leucyl	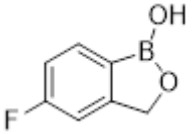	24.6 – 57.7
AN3365 / GSK2251052 (HCl)	Leucyl	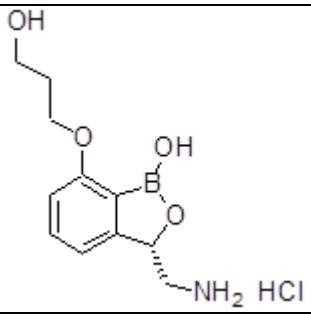	45.6

AN3661	Leucyl	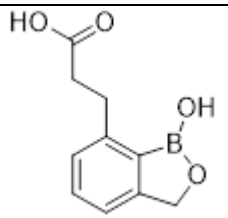	0.000631
Borrelidin	Threonlyl	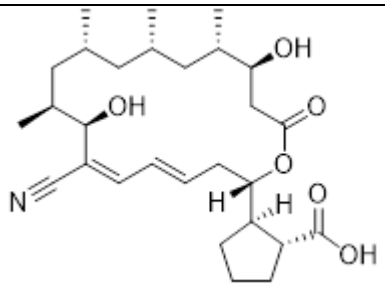	0.011
Cispentacin	Prolyl	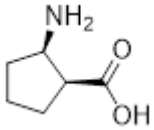	> 100
ELI	Methionyl	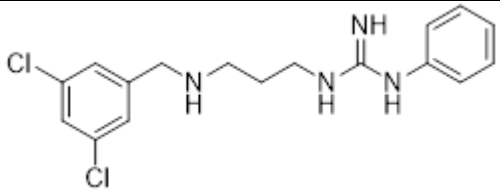	0.874- 19.5
Halofuginone	Prolyl	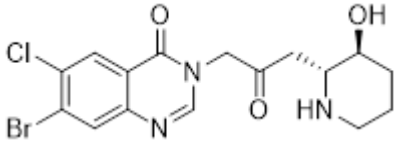	0.0314
Methyl- Cispentacin	Prolyl	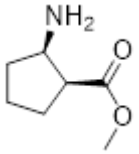	> 100
Mupirocin	Isoleucyl	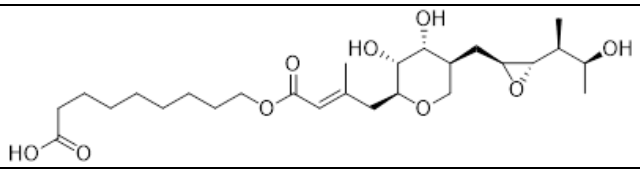	> 100

Ochratoxin A	Phenylalanyl	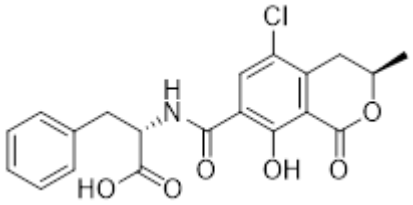	32.2
REP3123	Methionyl	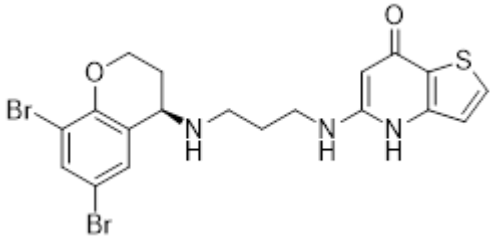	16.1
Thialysine	Lysyl	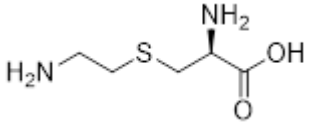	> 100

AN3365, a benzoxaborole bacterial leucyl-tRNA synthetase inhibitor, has been previously tested as a potential treatment in antibiotic resistance in a phase II clinical trial (O'Dwyer et al., 2015). While the clinical trial was not an overwhelming success, the compound was safe. However, AN3365 only demonstrated modest *Cp* growth inhibition activity.

Borrelidin, a well-studied macrolide antibiotic with threonlyl-tRNA synthetase inhibitory activity, showed potent *Cp* growth inhibition (EC_{50} = 0.011 μM).

Ochratoxin A, is a dihydroisocoumarin containing natural product and known toxin with activity for the human phenylalanyl-tRNA synthetase (McMasters et al., 1999), was only a modest inhibitor of *Cp* growth inhibition.

AN2690 or tavaborole is the newest tRNA synthetase approved as an antifungal. However, it was not very potent for inhibiting *Cp* growth. We theorize this has to do with differences between the structures of the *Cryptosporidium* Leucyl-tRNA synthetase and that of *Candida* or fungi in general.

Cispentacin and methyl ester cispentacin were tested as representative propyl-tRNA synthetase inhibitors, but neither showed activity. While cispentacin has reported activity against *Candida albicans* (Oki et al., 1989), it was not very potent against *Candida*.

Thialysine is considered a toxic amino acid by mimicking lysine and disrupting protein synthesis. It is reported to have some antifungal activity in the millimolar range (Gray et al., 1976). However, we found no significant anti-*Cryptosporidium* activity.

REP3123 is a highly potent agent, with sub-nanomolar activity against *Clostridium difficile* (Critchley et al., 2009). However, it is also being developed for a variety of other indications, including malaria, where it has reported sub-micromolar activity (Hussain, 2015). Unfortunately, against *Cryptosporidium*, it was not particularly active.

Mupirocin is one of the few antibiotics available over the counter in the US. It is the first marketed tRNA-synthetase inhibitor. Unfortunately, it appears to be selective for bacteria, and was not active against *Cryptosporidium*.

ELI was reported to be a potent inhibitor of *Trypanosoma brucei* with activity at 20 – 50 nM (Shibata et al., 2012). Unfortunately, this compound was not quite as potent in *Cryptosporidium*.

4.1.2 SAR analysis of boronic acids for *Cp* Growth inhibition

The aforementioned screen indicated that boronic compounds AN3365 and AN2690 showed potential anti-*Cryptosporidium* activity. Palencia *et al.*, also indicated promise with benzoxaborole compounds, like AN6426, against *Cryptosporidium* with single digit micromolar activity (Palencia et al., 2016). Therefore, a focused SAR of this compound class was conducted (Table 4). However, the only other compounds that showed moderate activity against *Cp* was phenyl boronic acid and AN3365. Phenyl boronic acid is a Lewis acid which may cause non-

selective activity against pathogens. However, it also presents with toxicity to humans (Lenga et al., 2020). AN3365 showed some toxicity in HCT-8 cells. At the lowest tested dose of 0.2 µM, there was over a 22% inhibition of HCT-8 cells viability. As the dose increased to 200 µM, so did the percent inhibition which was nearly 40%. This was unexpected since previously reports indicated AN3365 may be a promising lead.

Table 4. Screening Boronic Acid Compounds

Compound	**Chemical Name**	**Chemical Structure**	***Cp* Growth Inhibition EC_{50} (µM)**
AK50285	phenyl boronic acid	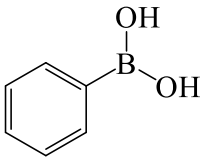	0.332
B20402	7-(hydroxymethyl) benzo[c] [1,2] oxaborol-1 (3H) - ol	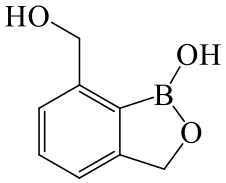	> 100
BB2407	2-(Hydroxymethyl)-6-methoxyphenylboronic acid dehydrate	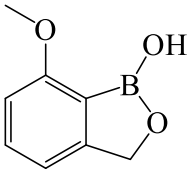	> 100
45288	2-(Hydroxymethyl) phenylboronic acid	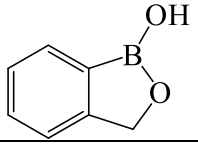	No activity
EN300	2-(1-Hydroxy1,3- dihydro-2,1-benzoxaborol-7-yl) acetic acid	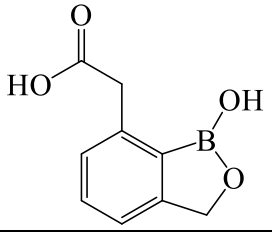	> 100

AN3365	Epetraborole GSK2251052	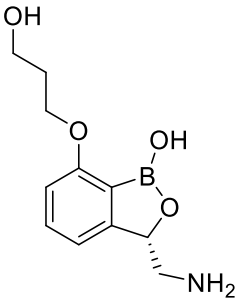	0.265 – 48.5

4.2 CpCDPK1 kinase inhibitors for Cp growth inhibition

4.2.1 CpCDPK1 kinase and Cp growth inhibition screening results

The screening results of protein kinase inhibitors against *Cryptosporidium parvum* CDPK1 is shown in Table 5. Assessment results for *Cp* growth inhibition are also included. Two kinase inhibitors were found to be active – dasatinib, a commercially available type II kinase inhibitor, and UH15_15, a potential type 1½ kinase inhibitor developed in our lab for RIPK2 (Nikhar et al., 2021). Dasatinib was found to have an IC_{50} of 0.2 µM, while UH15_15 has an IC_{50} of 0.015 µM. Other than dasatinib, no other type II inhibitors had significant activity against *Cp*CDPK1 (e.g. IC_{50} <1 µM). Furthermore, dasatinib lacked *Cp* growth inhibition, while UH15_15 demonstrated modest inhibitor in the cell-based Cp growth assay.

Table 5. Kinase Screen

Compound	**Structure**	**Kinase inhibitor type**	***Cp* CDPK1 IC_{50} (µM) ****	***Cp* EC_{50} (µM) ****

CS0709	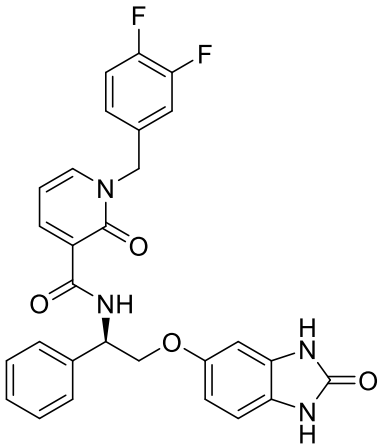	2	NA	NA
Imatinib	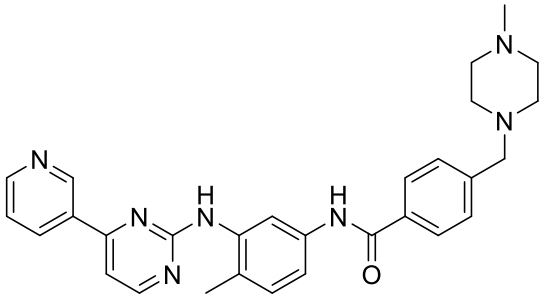	2	NA	2.2
Ponatinib	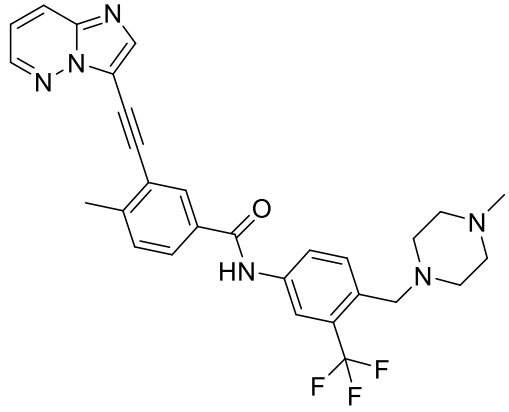	2	>1	3.4
Rebastinib	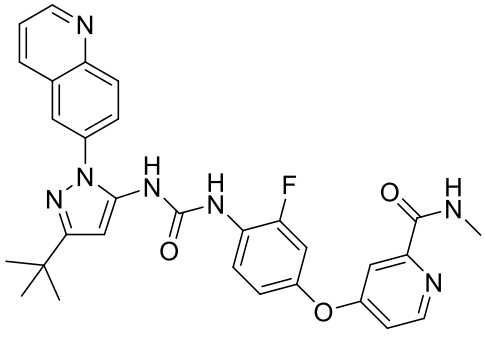	2	NA	9.2

PF 431396	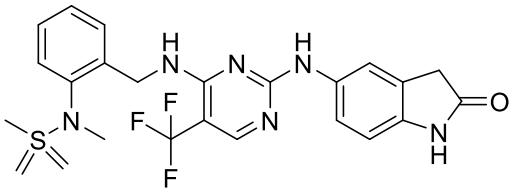	2	NA	>10
Doramapimod	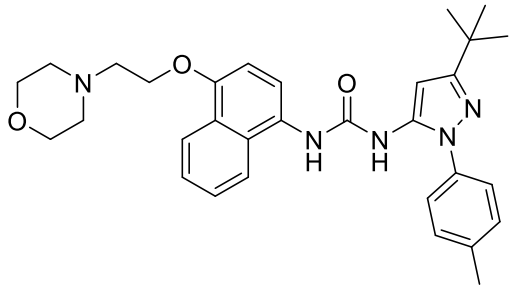	2	NA	5.5
Nilotinib	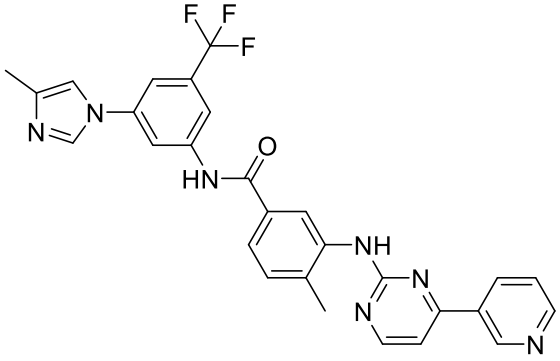	2	NA	9.2
Bosutinib	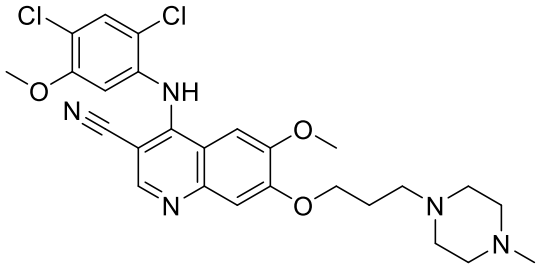	2	NA	>10
R406	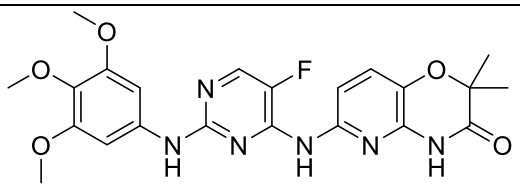	2	NA	8.1

Dasatinib	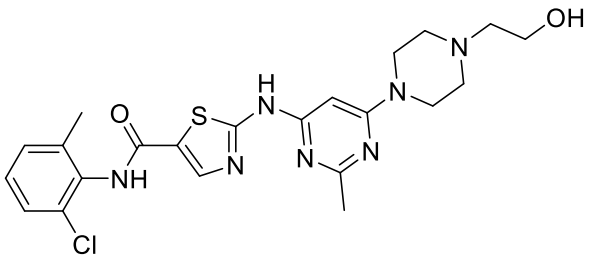	2	0.2197	>10
Tozasertib	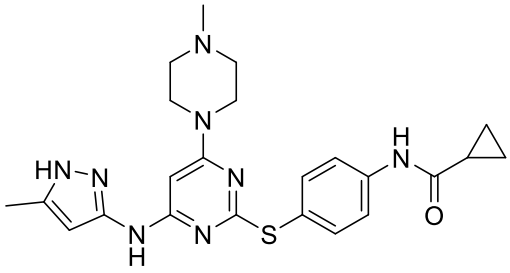	2	NA	>10
Sorafonib	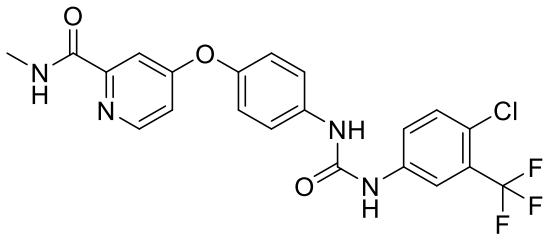	2	NA	3.6
UH15_15	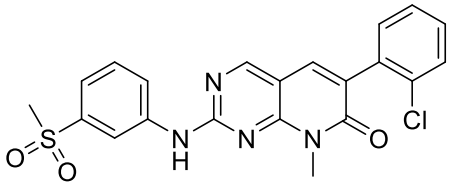	1 ½	0.015	0.78
UH15_22	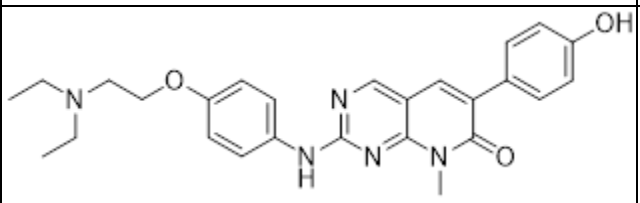	--	0.0028	0.95
UH15_38	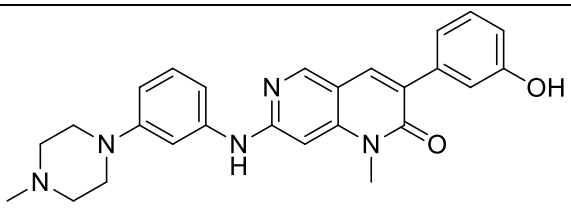	--	0.015	2.2

NA = Not active

** Data from Dr. Van Voorhis' laboratory

4.2.2 UH15_16 SAR evaluation for CpCDPK1 and Cp growth inhibition

4.2.2.1 UH15_16 scaffold SAR

The UH15 scaffold was first identified as a hit. However, to ensure it is the optimal scaffold to pursue, other scaffolds were tested and compared to UH15_15. BKI, a well-established CDPK1 inhibitor was used as a positive control. Only PN1 demonstrated potent CpCDPK1 inhibition. However, it did not retain activity *in vitro* in the *Cp* cell growth

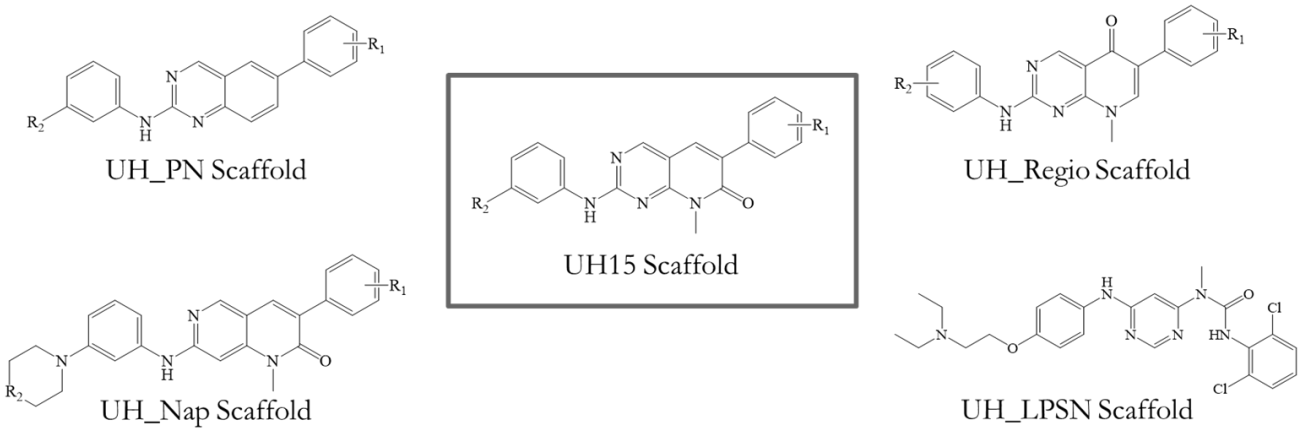

Figure 14. *Structures of UH Scaffolds*

assessment. Thus, the UH15 scaffold was determined to be the lead scaffold.

Table 6. UH15 Scaffold SAR with *Cp*CDPK1 and *Cp* growth inhibition vs. Src Kinase

(1) *Cp* CDPK IC_{50} (µM)

(2) Src IC_{50} (µM)

(3) *Cp* Growth IC_{50} (µM)

(4) Selectivity Src IC_{50}/ *Cp* CDPK1 IC_{50}

Compd.	Scaffold	Structure	(1)	(2)	(3)	(4)

BKI-1294	---	---	0.002	ND	ND	ND
UH15_15	UH15	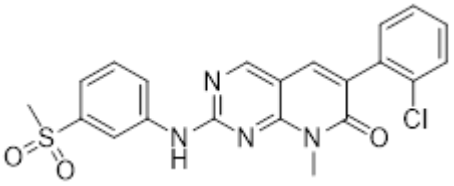	0.015	0.14	0.78	9.6
UH15_8	UH15	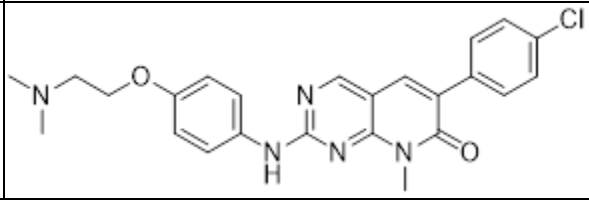	0.012	1.5	>10	124.8
UH15_16	UH15	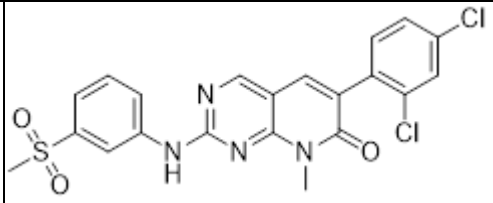	0.0054	0.91	0.014	167.8
UH15_31	Regio	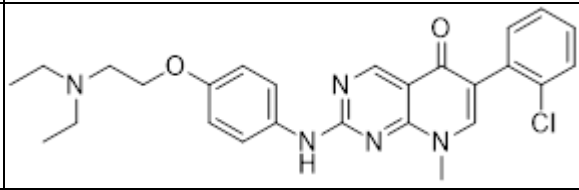	0.99	>5	>10	>5
UH15_37	Nap	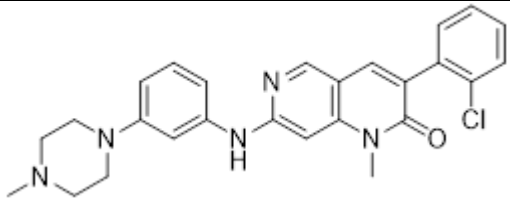	0.047	0.22	1.1	4.6
UH15_38	Nap	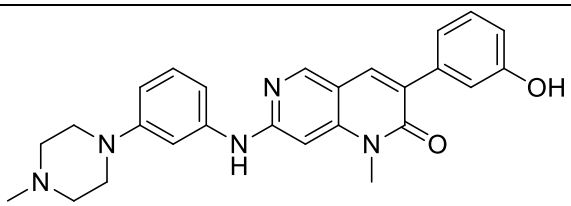	0.015	0.38	2.2	26.1
UH_LPSN	LPSN	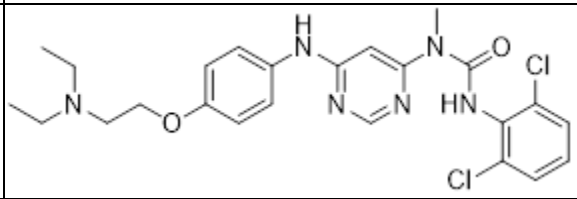	0.31	0.44	NT	1.4
UH_PN1	PN	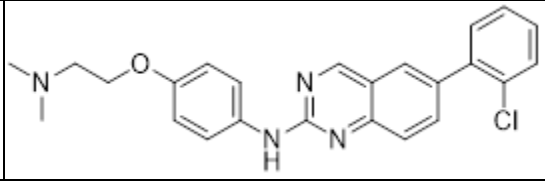	0.0079	0.21	>10	26.9

UH15_PN2	PN	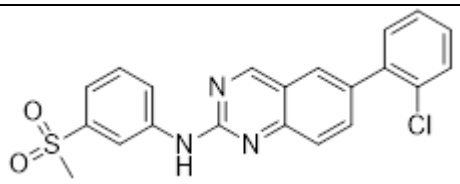	0.23	1.2	3.7	5.5

4.2.2.2 Identifying UH15_16 as an optimized *Cp*CDPK1 inhibitor

Once the UH15 scaffold was identified as the preferred scaffold, an SAR analysis was conducted.

Based on the aforementioned scaffold SAR study, three of the tested UH15 compounds appeared potent against *Cp*CDPK (IC_{50} = 5.4-14.5 nM). However, in the cell-based assay UH15_8 did not block activity (IC_{50} >10 μM). UH15_15 and UH15_16 retained activity in cells (EC_{50} = 0.78 and 0.014 μM, respectively). When investigating kinase selectivity, Src was used as a counter screen. UH15_15 was rather active against Src (EC_{50} = 0.139 μM), while UH15_16 remained relatively inactive (EC_{50} = 0.907 μM). When potency is compared to Src, UH15_16 shows better selectivity. UH15_15 had 9.6-fold selectivity for CpCDPK1 over Src, compared to UH15_16 which had 168-fold selectivity. Since these compounds are originally RIPK2 inhibitors, that data was also included. UH15_16, while active in the RIPK2 kinase assay (IC_{50} = 38 nM), was not significantly active in a cell-based assay of RIPK2 mediated NOD signaling (EC_{50} = 0.705-1.2 μM). Therefore, UH15_16 was deemed the lead compound at this point.

4.2.2.3 SAR of UH15_16: Modifying R_1

Table 7. UH15_16 Modifications to R_1 with *Cp*CDPK1 and *Cp* growth inhibition vs. Src Kinase

(1) LogP Calc.

(2) CpCDPK1 IC_{50} (µM)

(3) Src IC_{50} (µM)

(4) Cp Growth IC_{50} (µM)

(5) Selectivity Src IC_{50}/ *Cp*CDPK1 IC_{50}

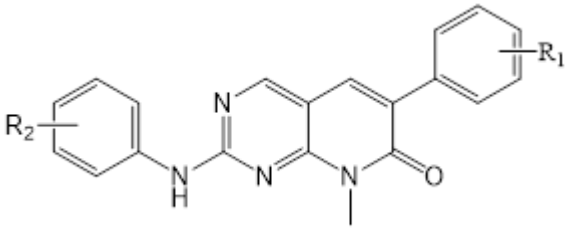

Compd.	**R_1**	**R_2**	**(1)**	**(2)**	**(3)**	**(4)**	**(5)**
UH15_15	2-Cl	3-SO_2CH_3	2.94	0.015	0.14	0.78 ** 0.79 +	9.6
UH15_8×	4-Cl	4-$OCH_2CH_2NEt_2$	4.79	0.012	1.5	>10 ** 1.3 +	124.8
UH15_13	4-Cl	3-SO_2CH_3	2.94	0.18	>10	0.12 +	>56
UH15_16×	2,4- di-Cl	3-SO_2CH_3	3.5	0.0054	0.91	0.14 ** 0.01-0.017 +	167.8
UH15_18	2-Cl, 4-F	3-SO_2CH_3	3.1	0.026	0.20	8.0 – 8.9 +	8
UH15_19	2,5- di-Cl	3-SO_2CH_3	3.5	0.32	0.53	1.6 +	2
UH15_20	2-Cl, 4-Me	3-SO_2CH_3	3.43	0.011	0.65	0.034 – 0.66 +	59
UH15_21	4-OH	3-SO_2CH_3	1.99	0.12	>10	1.1 +	>84
UH15_22	4-OH	4-$OCH_2CH_2NEt_2$	3.84	0.0028	0.09	0.95 ** 0.02 +	31.8

UH15_29	4-OMe	3-SO_2CH_3	2.26	0.026	>10	0.04 -0.009 [+]	>385
UH15_30	4-OMe	4-$OCH_2CH_2NEt_2$	4.1	0.015	2.6	>10 ** 1.8 [+]	175.5
CDPK-2	4-CN	3-SO_2CH_3	2.42	0.068	>10*	0.98 [+]	>147
CDPK-4	4-CF_3	3-SO_2CH_3	3.33	0.74	>10	0.84 [+]	>13

[×] Data also shown in Table 6, but repeated to highlight the modifications to R_1

** Data from Van Voorhis' laboratory

[+] Data from Mead's Laboratory

*CDPK-2 may have hit maximum solubility in the Src assay

SAR analysis of the R1 group indicated that the 2,4-dichloro was still the preferred substitution. The 4-position was briefly investigated, and chlorine atom was the best tolerated. Since most kinases cannot tolerate anything much larger than a hydrogen in this position due to steric hindrance with the αC-helix, utilizing the largest tolerated functional group/halogen in this position optimizes for selectivity. While the 4-hydroxyl in UH15_22 showed astounding potency against the kinase, it lacked significant cellular activity and selectivity. UH15_22 also demonstrated significant cytotoxicity in the absence of *Cp*. A part of the lack of cellular potency may be explained with the R_2 functional group. This lack of cellular potency is also highlighted with UH15_8 and UH15_13, where both have a 4-Cl in the R_1 position, but R_2 varies. UH15_8 has no significant cellular activity, while UH15_13 has an EC_{50} of 120 nM. This indicates the importance of R_2 for cellular potency, and R_1 for *Cp*CDPK potency and selectivity.

4.2.2.4 SAR of UH15_16: Modifying R_2

Table 8. UH15_16 Modifications to R_2 with *Cp*CDPK1 and *Cp* growth inhibition vs. Src Kinase

(1) LogP calc

(2) CpCDPK1 IC_{50} (µM)

(3) Src IC_{50} (µM)

(4) Cp Growth IC_{50} (µM)

(5) Selectivity Src IC_{50}/ *Cp*CDPK1 IC_{50}

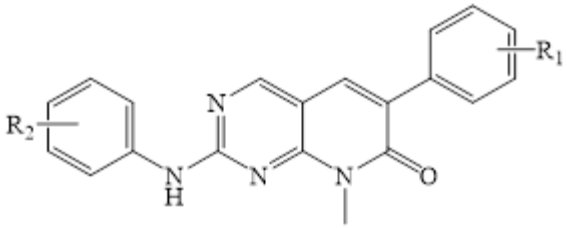

Compd.	R_1	R_2	(1)	(2)	(3)	(4)	(5)
BKI-1294	---	---	---	0.002	ND	ND	ND
UH15_8[×]	4-Cl	4-$OCH_2CH_2NEt_2$	4.79	0.012	1.5	>10 ** 1.3 [+]	124.8
UH15_13	4-Cl	3-SO_2CH_3	2.94	0.18	>10	0.12 [+]	>56
UH15_16[×]	2,4- di-Cl	3-SO_2CH_3	3.5	0.0054	0.91	0.14 ** 0.01 – 0.017 [+]	167.8
CDPK-6	2,4- di-Cl	3-$SO_2N(CH_3)_2$	4.07	0.010	2.7	0.042 [+]	265
CDPK-7	2,4- di-Cl	See image	3.81	0.003	0.047	0.23 [+]	16
CDPK-9	2,4- di-Cl	See image	4.2	0.096	1.8	0.14	19

CDPK-7

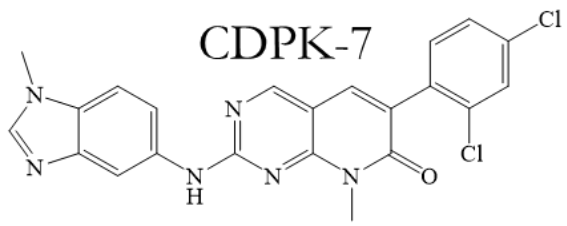

CDPK-9

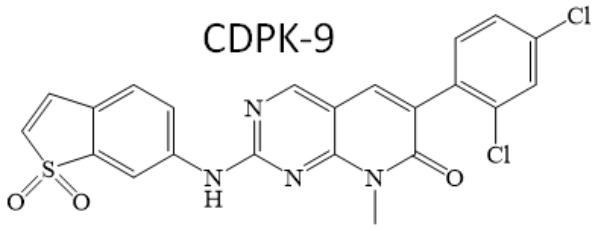

[×] Data also shown in Table 6, but repeated to highlight the modifications to R_1

** Data from Van Voorhis' laboratory

[+] Data from Mead's laboratory

Based on the SAR data, UH15_16 was one of the best compounds to date. While the tertiary sulfonamide CDPK-6 appeared to be decent as well (EC_{50} value of 42 nM), UH15_16 was the most potent (EC_{50} of 14 nM).

4.2.3. Molecular docking of UH15_16 in *Cp*CDPK1

***Figure 15**. UH15_16 Docked into CpCPKD1 (PDB: 3NCG*

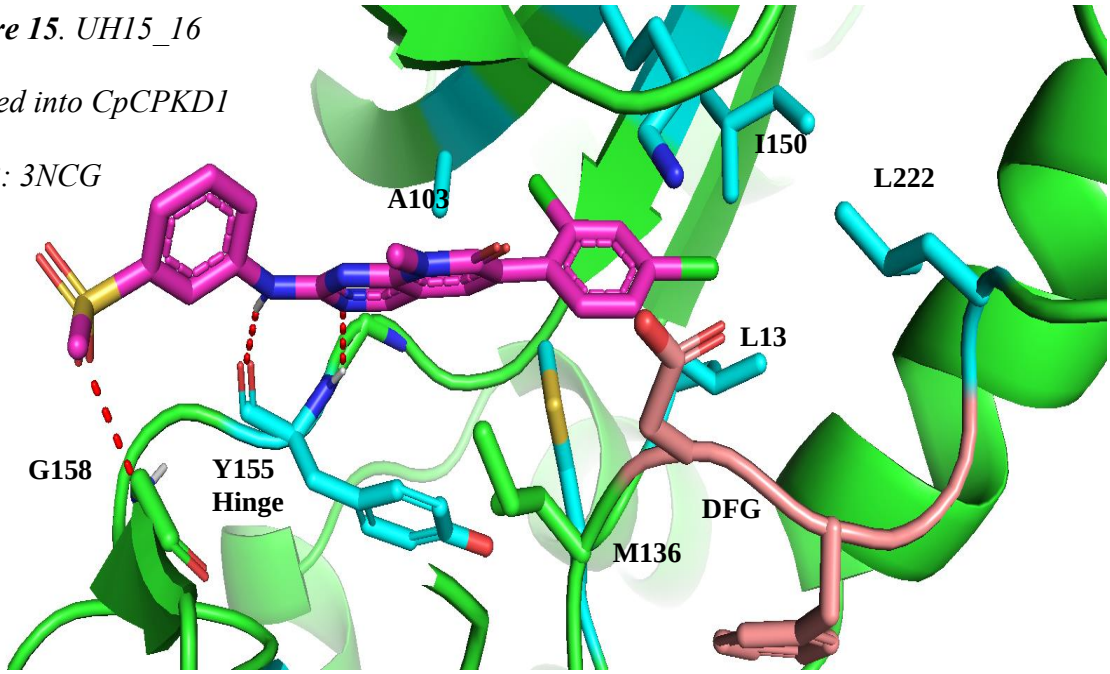

Figure 15 shows the docking results of UH15_16 with CpCDPK1. UH15_16 had several critical interactions. Specifically, UH15_16 interacts via hydrogen bonds with the hinge residue, Y155 (tyrosine, residue number 155). In addition, it has van der Waal interactions with A103, I150, M146, L138, and L122. Lastly, UH15_16 interacts with G158 forming a hydrogen bond.

Most compounds do not form essential interactions in the solvent exposed region, yet this forms a rather important hydrogen bond via the sulfone.

4.2.4. ADME assessment and kinase screening of UH15_16

4.2.4.1. ADME assessment

UH15_16 was assessed in an abbreviated ADME panel of assays by Eurofins.

Table 9. ADME Assessment of UH15_16

Test	Value	Note
Aqueous Solubility	17.4 ± 0.8 µM	Moderate
Microsome stability	$t_{1/2}$ 325 ± 121 min	Stable
Caco-2 Apical-Basal	1.06 x 10^{-6} cm/s	Low recovery (26%)
Caco-2 Basal-Apical	0.42 x 10^{-6} cm/s	Low recovery (14%)

UH15_16 had moderate aqueous solubility. It also demonstrated low cellular permeability. However, compound recovery was low in the experiment. UH15_16 demonstrated good stability in mouse liver microsomes.

4.2.4.2. Kinase screening

The first portion of kinase screening was a high-throughput screen, kinomeSCAN. Hits were then validated and IC_{50}'s were determined.

4.2.4.2.1 KinomeSCAN

The KinomeSCAN scanned 97 kinases, 90 of which were non-mutant kinases. The number of hits compared to number of hits and the degree of hits could be used to produce a selectivity score, which could be compared to other kinase inhibitors. The kinomeSCAN

identified 7 non-mutant kinases (e.g ABL1, BRAF, c-Kit,c-Src, FGFR2, FMS, and PDGFRb) inhibited >90% at 1 μM for a selectivity score (e.g. S(10)) of 0.078, which is comparable to currently marketed drugs erlotinib and sorafenib.

4.2.4.2.2 Kinase IC_{50} values

IC_{50} values for the 7 kinases identified in the KinomeSCAN were determined as shown in Table 10.

Table 10. Kinase IC_{50} values

Kinase	Compound IC_{50} (M)	IC_{50} (M) Control Compound	Control Compound
	UH15-16		
ABL1	< 5.00E-09	2.60E-08	Staurosporine
BRAF	7.39E-08	1.33E-08	GW5074
c-Kit	< 5.00E-09	1.68E-09	Staurosporine
c-Src	< 5.00E-09	1.77E-09	Staurosporine
FGFR2	5.08E-09	1.05E-09	Staurosporine
FMS	8.43E-09	1.09E-09	Staurosporine
PDGFRb	3.20E-08	1.80E-09	Staurosporine

4.2.5. Formulation experiments and optimizations

A variety of formulations were attempted, however, four (one for intravenous and three for oral administration) were used for *in vivo* pharmacokinetic and efficacy evaluations. These formulations were identified via a number of different experiments.

4.2.5.1. Ligand-ligand docking

Based on docking data, UH15_16 had better binding energy with the β-cyclodextrin over other cyclodextrins, such as α-cyclodextrin and γ-cyclodextrin. With α-cyclodextrin the hydrophobic binding cavity was too small and the only docking interaction with UH15_16 occurred in the outer surface. In the case of the γ-cyclodextran the hydrophobic binding cavity was too

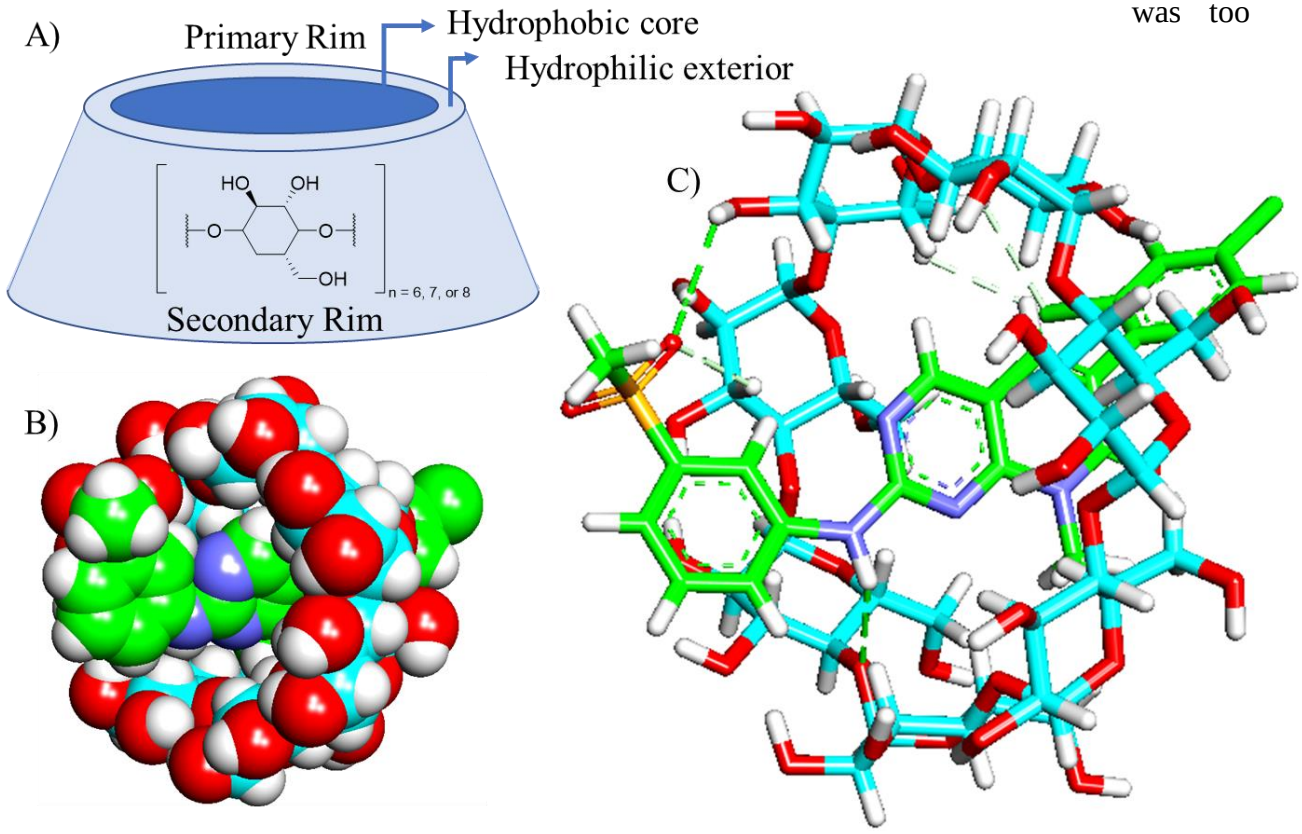

***Figure 16**. Docking of β-Cyclodextrin. A) the conical shape of cyclodextrins allow for a snug fit for compounds, yet still allows for compounds to be released. Think like a belt, each compound has a different sized belt for an optimal fit. B) UH15_16 docked into β-cyclodextrin displayed in a space-filling model, C) UH15_16 docked into β-cyclodextrin displayed as sticks*

large resulting in docking pose and interaction inconsistency. This was also reflected in the binding energies, which were less favorable than with β-cyclodextrin.

Ligand-ligand docking of UH15_16 with β-cyclodextrin produced 4 similar docking poses. In these poses, the sulfone containing phenyl is in the hydrophobic secondary rim with the sulfone projecting towards solvent, while the 2,4-di-chlorophenyl is in the primary rim. While these similar poses may shift up or down, or the β-cyclodextrin "belt" may fit higher up or lower on the UH15_16, the important thing was the interactions with the hydrophilic edge/exterior and hydrophobic core. The one off-pose is flipped, in that the sulfone is towards the primary rim and the 2,4-di-chlorophenyl is in the secondary rim. In all five poses the central heterocycle occupies the hydrophobic core of the β-cyclodextrin.

Given the docking information that β-cyclodextrin was the best size for accommodating UH15_16, three commonly used cyclodextrins are commercially available of this size: β-cyclodextrin, hydroxypropyl-β-cyclodextrin, or Captisol (a sulfated β-cyclodextrin). All three have the same core, thus these interactions would not likely be altered, Captisol is the most water soluble, followed be hydroxypropyl-β-cyclodextrin, and lastly β-cyclodextrin. Given the solubility issues with UH15_16, Captisol was chosen.

4.2.5.2. Formulation optimization

Formulations with Captisol in various molar ratios to UH15_16 (1 to 8-fold) were tested using a UV Plate reader to determine release rate and if/when the formulations precipitate. Once a level of Captisol was determined additional excipients could be added to improve release rates as necessary. Both Tween 80 (Polysorbate 80) and methyl cellulose were tested. After the first experiment, it was decided that only a concentration of 2.5 mg/mL, which would correspond to an in vivo dose of 50 mg/kg, needed to be tested. Unfortunately, all attempts to use methyl cellulose were unsuccessful resulting in rapid precipitation. But Tween 80 was explored further.

The raw UV plate reader results are in the appendix 7.3. Samples from the experiments are shown below.

In determining the ratio of Captisol (4 or 5-fold) to UH15_16 showed the best release rates (Figure 17). Since neither showed much advantage over the other, both were advanced and tested with excipients. The plate reader also compared the original formulation to the proposed formulations. The original Captisol formulation released the compound too quickly. Improvements would be necessary. The 4 or 5x Captisol had a good release as shown below, but excipients were added to potentially improve the formulation.

Since 1% (approx. 0.2 mL/kg) Tween 80 in 5x Captisol had the best release rate of UH15_16, it was repeated and challenged against even higher doses of Tween 80. In the previous plate reader experiment, 1% was the highest tested concentration. Up to 5% Tween 80 in 4x and 5x Captisol were tested. However, 2% and 3% Tween 80 in 5-fold Captisol looked the best with desirable release times (most compound released in 30 minutes and without precipitation). To limit exposure of Tween 80, the 2% Tween 80 was selected for the third oral formulation. This translated to 2.5% *in vivo.*

4.2.5.3. Determining formulations

Intravenous (IV) formulation – For IV formulations, the compound must be made into a solution – not a suspension. Therefore, the compound must be made completely soluble by excipients. For UH15_16, various concentrations of ethanol and Tween 80 in 1x PBS were evaluated. A final solution of 0.5 mg/mL UH15_16 (which would correspond to an *in vivo* dose of 1 mg/kg) in 30% Tween 80, 20% PBS, and 50% ethanol was selected.

Oral formulation 1 – An initial formulation consisting of 1 mg/mL UH15_16 in 90% OraPlus (a commercially available suspending agent) and 10% Polyethylene glycol 400 resulted in a milky white suspension.

Oral formulation 2 – For this formulation, Captisol was selected as the cyclodextrin based in the ligand-ligand docking data to as described above. UH15_16 (1.25 mg/mL) was formulated with Captisol 2x molar ratio and visually compared to each other and oral formulation 1. The formulations were judged on homogeneity, and if/when precipitation occurred.

Oral formulation 3 – UH15_16 (0.625 mg/mL), Captisol (5x molar ratio) and 2% Tween 80 was selected based on time to precipitation as determined by UV Plate reader assessments in 4.2.5.2.

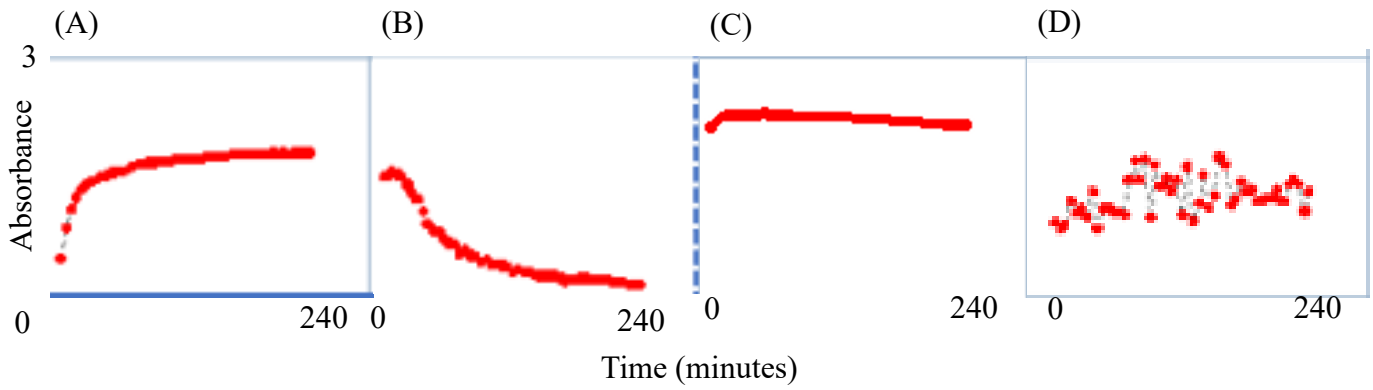

Figure 17. *Examples of UV Plate Reader Results. (A) 5x Captisol, Fasted conditions, 1% (w/v SGF) Tween 80. This exhibits an optimal release of UH15_16, where most of the compound is released in the first 20-30 minutes. (B) 4x Captisol, Fasted conditions, 0.1% (w/v SGF) Tween 80. This also shows an optimal release; however, the absorbance is reduced as the suspension releases compound elsewhere in the well where it is not as easily detected. (C) 8x Captisol and 3% (w/v SGF) Tween 80. This is the manufacturer's recommended dose of Captisol; however, this indicates too slow of disassociation of UH15_16 from the cyclodextrin. (D) 0.1% (w/v) Methylcellulose with 4x Captisol. The result is indicative of rapid precipitation.*

4.2.6. Pharmacokinetic studies

4.2.6.1. Intravenous pharmacokinetic study

UH15_16 was administrated intravenously at 1 mg/kg in the intravenous (IV) formulation to four mice. The pharmacokinetic profile confirms that this compound is not quickly metabolized.

Table 11. UH15_16 Pharmacokinetic Profile Following IV Administration					
T_{max} (h)	C_{max} (ng/mL)	AUC (h*ng/mL)[a]	Cl (mL/h/kg)	V (L/kg)	$t_{½}$ (h)
0.416 ± 0.36	967.1 ± 390.35	4996.22 ± 2061.9	206.57 ± 128.75	2.65 ± 1.21	10.66 ± 5.86

[a] The AUC = 4,943 hr*ng/mL was also estimated per the trapezoid method.

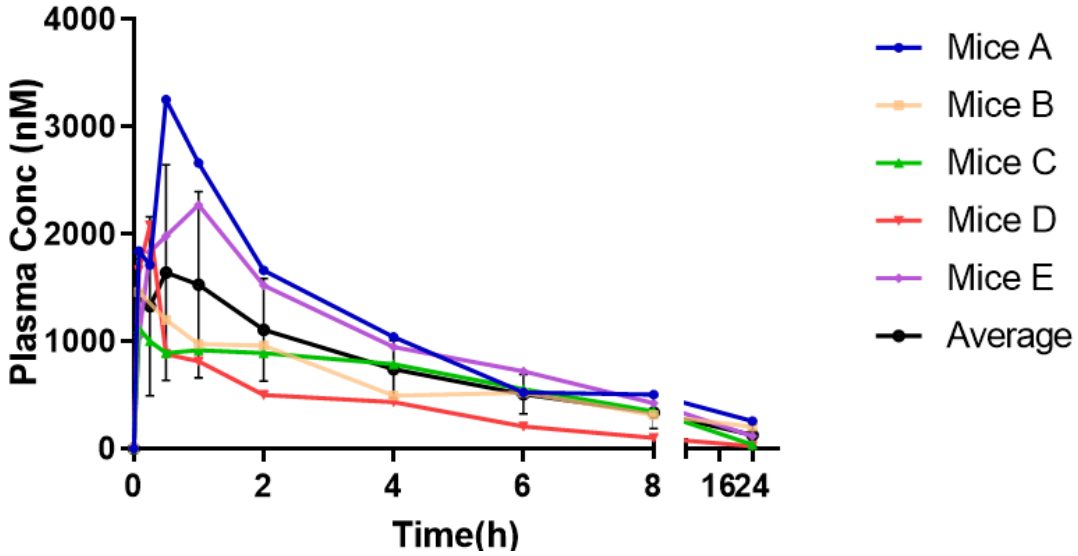

Figure 18. *Blood Concentrations from IV Administration of 1 mg/kg UH15_16*

4.2.6.2. Oral pharmacokinetic study with formulation 1

UH15_16 was administrated orally at 5 mg/kg in oral formulation 1 to three mice. The compound in this formulation shows poor systemic exposure, as evident by the low plasma concentration relative to the IV dosing. The IV dose was a fifth the dose of the oral administration yet resulted in a C_{max} approximately 100-fold greater with the IV dosing. Analysis of the gut organs indicated that UH15_16 remained in the fecal material. The concentration in

the fecal material was 125-409 ng/mg. The second highest concentration was in the small intestine, 3.7-26 ng/mg and colon at 3.2-5.6 ng/mg. The liver samples had between 0.11-2.4 ng/mg.

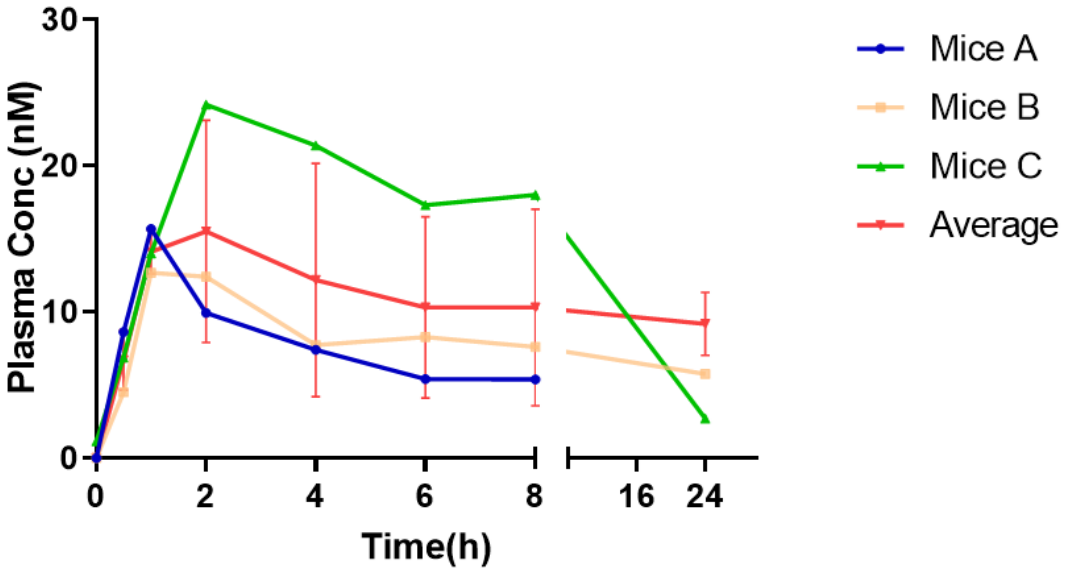

Figure 19. *Blood Concentrations from Oral Administration of 5 mg/kg UH15_16 in oral formulation* 1

Table 12. UH15_16 Pharmacokinetic Profile Following Oral Administration with Formulation 1					
T_{max} (h)	C_{max} (ng/mL)	AUC (h*ng/mL)[a]	Cl (mL/h/kg)	V (L/kg)	$t_{1/2}$ (h)
1.33±0.58	8.32±2.83	87.13±59.27	48340.26±37867.14	780.42±441.82	14.58±18.99

[a]The AUC = 98.45 h*ng/mL was estimated per the trapezoid method.**4.2.6.3. Oral pharmacokinetic study with formulation 2**

At UH15_16 was administrated orally at 5 mg/kg in oral formulation 2 to three mice. This formulation does show higher exposure; C_{max} is about double the value from oral formulation 1. But the exposure is still low for a 5 mg/kg dose. This is still about 1/50th of the IV exposure, and the oral formulations were dosed 5 times the IV dose. T_{max} is also delayed – the previous T_{max} was at 2 h for oral formulation 1. Oral formulation 2 delays the T_{max} to 4 h and 10 h. C_{max} is at 36.3 and 44.9 nM at 4 h and 10 h respectively. The AUC = 324.0 h*ng/mL, was estimated per the trapezoid method.

Figure 20. *Blood Concentrations from Oral Administration of 5 mg/kg UH15_16 in Oral Formulation 2*

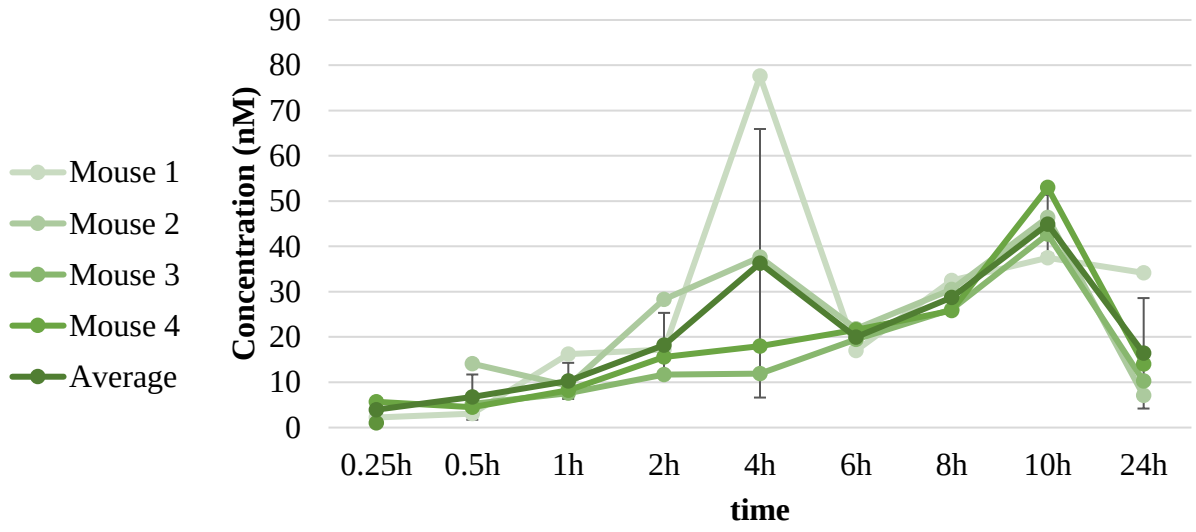

4.2.6.4. Oral pharmacokinetic study with oral formulation 3

Figure 21. Blood Concentrations from Oral Administration of 5 mg/kg UH15_16 in Oral Formulation 3

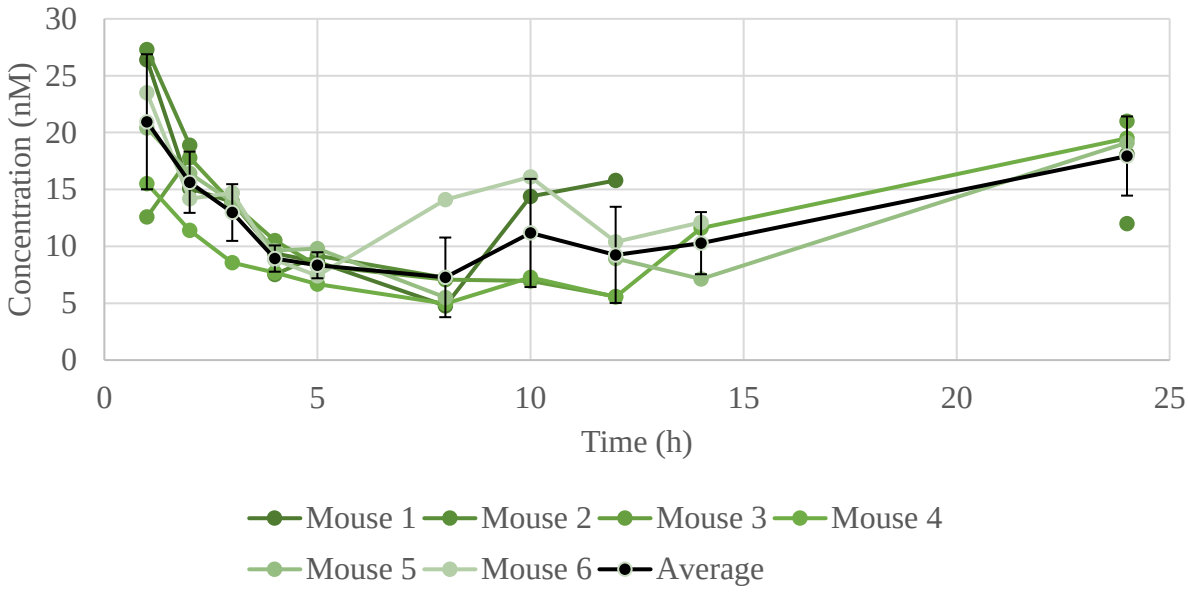

In the third formulation's PK analysis, there was again a low systemic exposure, however the first peak occurred sooner at around 1hour instead of around the 4 hour time point. There was still a second peak at around 10 hour times and potentially a third peak that was not recorded after the 14 hour time point. There does appear to be slow absorption, nevertheless. The AUC = 130.7 h*ng/mL was estimated per the trapezoid method.

4.2.7. Toxicity

Once per day oral administration of UH15_16 at 50 mg/kg in formulations 1, and 2 did not result in any observable adverse events. This included signs of distress (e.g. ruffled fur, hunched shoulders and decreased appetite), Also no weight loss (> 20% body weight), was reported. For the third formulation, the blank formulation and the 25 mg/kg BID dose were tested and again did not produce any noted adverse events.

So, given the AUC calculations of the three oral formulations, the second formulation had the highest plasma exposure, but the compound is not treating an infection in the systemic circulation.

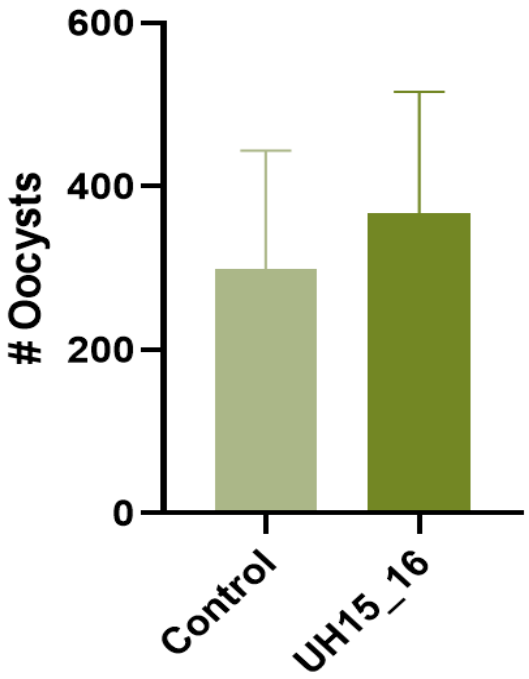

***Figure 22**. Efficacy of 50 mg/kg UH15_16 in oral formulation 1*

4.2.7. *In Vivo* efficacy

4.2.7.1. Efficacy evaluation of UH15_16 using oral formulation 1

When UH15_16 was tested *in vivo* in IL-12 KO mice infected with Cp at 50 mg/kg po qd, it showed no efficacy (Figure 22). Fecal oocyte counts were very similar to that of the untreated group.

4.2.7.2. Efficacy evaluation of UH15_16 using oral formulation 2

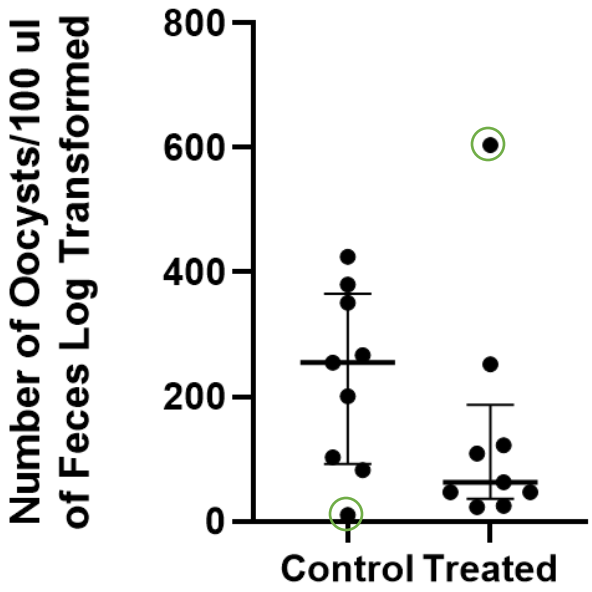

Figure 23. *Efficacy of 50 mg/kg UH15_16 in oral formulation 2*

When UH15_16 was tested in vivo in IL-12 KO mice infected with Cp at 50 mg/kg po qd, a 38% reduction of fecal oocytes were obsserved, (p = 0.285) base on a comparison of the mean number of oocysts per 100 μL of feces (Figure 23). Removal of outliers (as shown in the circles) were excluded from the control and treated group, there was a 68% reduction (p = 0.0051). Further analysis of the data using the median number of oocysts per 100 μL of feces without that better accounts for outliers (or skewed daat) indicated a 75% reduction (p=0.0039).

4.2.7.3. Efficacy evaluation of UH15_16 using oral formulation 3

When the efficacy study was repeated using oral formulation 3 and compound administration of 25 mg/kg BID, there was a slight improvement in oocyte reduction. of 74%. This was statistically significant with a p value of 0.0005 (Mann Whitney test). Overall, there was better inter-animal consistency in the treated group in this experiment and no animals from the control or treatment groups were excluded.

Figure 24. *Efficacy of 25 mg/kg BID UH15_16 in oral formulation 3*

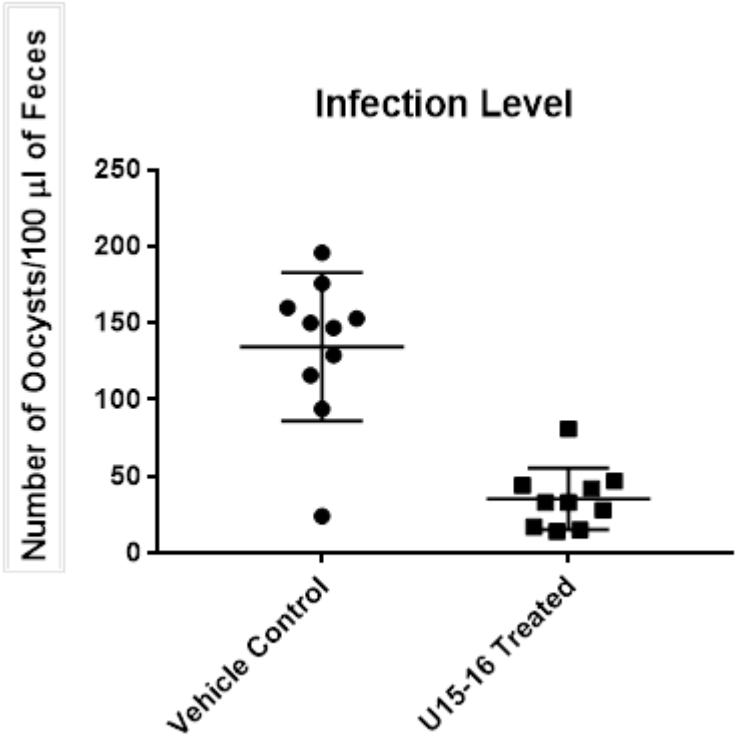

5. DISCUSSION

Cryptosporidium lacks a good treatment option, especially for malnourished children and in the HIV/AIDS population. While there is one agent FDA-approved drug, it is often too slow to work when it does work, so additional therapies are necessary for clinicians to add to their toolbox when treating *Cryptosporidium*. In this project we targeted *Cryptosporidium* via 2 different pathways: tRNA synthetase and kinase inhibition.

We first investigated tRNA synthetase inhibition for potential leads for blocking Cp growth. tRNA synthetase inhibitors work by disrupting protein synthetase. Specifically, by disrupting the amino acid loading of the tRNA synthetase, causing errors in protein synthesis. There are currently 2 FDA approved inhibitors of this class, mupirocin and tavoborole (a.k.a. AN2690), which inhibits a eukaryotic pathogen. Due to the recent approval of tavaborole, there has been renewed interest in trying to make this target viable for anti-infectants, including *Cryptosporidium*.

Screening a focus library of known tRNA synthetase inhibitions identified halofuginone, borrelidin and AN3661 as inhibitors of Cp growth. Halofuginone, a semi-synthetic natural product propyl-tRNA synthetase inhibitor, initiated our search and proved itself potent against Cp with an EC_{50} of 0.0314 mM. Borrelidin, a well-studied macrolide antibiotic with threonlyl-tRNA synthetase inhibitory activity, showed potent Cp growth inhibition (EC_{50} = 0.011 μM). The most notable hit found in this screen was the boronic compound AN3661, which demonstrated very potent inhibition of Cp growth. However, in late 2019 other researchers also identified AN3661 as a potent inhibitor of Cp growth. Furthermore, they have attributed the anti-*Cryptosporidium* activity to inhibition of the parasitic cleavage and polyadenylation specificity factor 3 (CPSF3) and not a tRNA synthetase (Swale, et al. 2019). Our limited SAR analysis of

AN3361 found that only phenyl boronic acid and AN3365 had modest activity, indicating that the propionic acid moiety present in AN3361 appears critical for potent anti-*Cryptosporidium* activity.

Despite our hits, literature about these inhibitors began to tarnish our optimism. While AN3365 was in clinic trials there were reports of rapid resistance, causing the study to be terminated prematurely (O'Dwyer et al., 2015). While the cause of resistance could stem from a variety of sources and mutations, O'Dwyer et al. found in most of these cases, the resistance came from a single mutation in the Leu-tRNA synthetase resulting in high levels of resistance (O'Dwyer et al. 2014). Given how *Cryptosporidium* cannot be cultured, ruling out the plausibility for such mutation with a Leu-tRNA synthetase inhibitor against Cp or any other inhibitor would be difficult. While this may be limited to only Leu-tRNA synthetase or just AN3365, it added some cynicism to the project. Secondly, in late 2019 a paper came out demonstrating that our tRNA synthetase inhibitor lead AN3661, may not be acting as a tRNA-synthetase inhibitor (Swale et al., 2019). Swale et al., established how AN3661 was a potent inhibitor of *Cryptosporidium*, but inhibited a different target, the cleavage and polyadenylation specificity factor 3 (CPSF3). Given the medicinal chemical similarities to tavaborole and Palencia et al. potent benzoxaborole compounds, like AN6426, it had been assumed to be a tRNA synthetase inhibitor. However, AN3661 had a completely different mechanism, which may have explained why it was significantly more potent than the other tRNA synthetase inhibitors of that sub-class. Fortunately, our kinase screens were more promising and were pursed instead.

The second approach taken was to screen a library of known protein kinase inhibitors for CpCDPK1 and Cp growth inhibition. CpCDPK1 has emerged as a compelling molecular target

for *Cryptosporidium* since the kinase had been identified and targeted in *Toxoplasma gondii* (Van Voorhis et al., 2017). Due to similarities between Toxoplasma gondii and other Apicomplexa pathogens, similar compounds showed early success in Cp (Van Voorhis et al., 2017).

The screening library used included commercially available compounds as well as compounds synthesized in our laboratory for other purposes, namely the UH15 series initially pursued for inhibition of RIPK2 and NOD cell signaling (Nikhar, 2021). A number of these kinase inhibitors only had modest activity against *Cryptosporidium*. For example, imatinib, ponatinib, rebastinib, doramapimod, nilotinib, R406, sorafonib, and UH15_38 all had micromolar activity against *Cryptosporidium*. However, two compounds had sub-micromolar activity, UH15_15 and UH15_22.

Intial SAR analysis of the UH15 series for CpCDPK1 and Cp growth inhibition focused on examination of the central heterocycle scaffold comprising the UH15 series. This included a regioisomer, replacement of N-8 with a carbon, a pseudoring derivative and modifications to the amide functional group. However, the UH15 scaffold proved most promising, with UH15_16 emerging as the most selective and potent derivative.

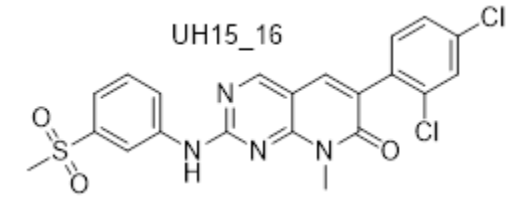

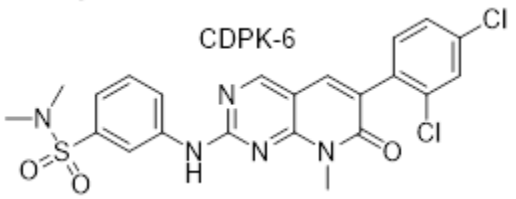

Further modifications were made to UH15_16. However, this compound remained best regarding enzyme potency, ability to block Cp growth and selectivity. The 2,4-dichlorophenyl appeared to provide enhanced potency and selectivity. Of note, the sulfone in the solvent exposed region appeared to play a critical role in providing good

cellular activity. However, CDPK-6 also is a promising compound indicating that the dimethyl sulfonamide may be able to make similar hydrogen bonds as a sulfone.

Molecular docking was utilized using UH15_16 and CpCDPK1 (PDB: 3NCG) to assess potential binding modes of the inhibitor in the enzyme. The ATP binding site was selected for the search grid and only poses that maintained hydrogen bonding interactions between the central heterocycle and the hinge region were considered, since similar poses were observed between UH15_15 and RIPK2 (Nikhar, 2021). The docking results of UH15_16 shows that the sulfone in the 3-position of the phenyl in the solvent exposed region potentially plays a critical role by forming a hydrogen bond with the glycine-158. This critical interaction may also be present with CDPK-6. The second region critical for binding and selectivity was the hydrophobic binding pocket. In the case of UH15_16, this is where the 2,4-dichlorophenyl interacts. In particular, the presence of the 4-chloro may reduce inhibition of human kinases like Src activity by projecting towards the αC-helix. Docking indicates that this substituent is well tolerated in CpCDPK1.

UH15_16 was assessed in several ADME assays. The compound demonstrated moderate aqueous solubility and good stability in human liver microsomes. However, the compound had poor permeability in Caco-2 cell, although poor compound recovery was noted. Since *Cryptosporidium* is an intracellular pathogen targeting enterocytes, the permeability needs of a compound to be locally effective in the gastrointestinal track are not know.

The kinase screening determined UH15_16 has reasonable selectivity, comparable with numerous marketed compounds, namely erlotinib and sorafenib, and superior to other kinase inhibitors. Nevertheless, several kinases were inhibited in the KinomeSCAN and subsequent IC_{50} determinations.

ABL1 plays a most notable role in DNA repair and apoptosis and necrosis and therefore may play a role in antitumor regulation (Dasgupta et al., 2016). Since anti-cryptosporidiosis agents should not be used long term, the benefit of anti-parasite activity would likely outweigh inhibition of ABL1. BRAF is an oncogene in the BRAF-CRAS-CRAF and MERK-ERK pathway (Heidorn, et al., 2010). The oncogene c-Kit may play a role in stem cell differentiation and vast array of critical functions when function of c-Kit was lost (Abbaspour Babaei et al., 2016). Although c-Src, a regulatory kinase playing a role in cellular reproduction amongst other roles (Bjorge et al., 2000), was inhibited in the profile, it was used as a counter-screen by Dr. van Voohoris' laboratory using a biochemical assay. These divergent results may reflect differences in the type of assays used. FGFR2, or fibroblast growth factor receptor 2, plays a role in carcinogenesis, cancer progression, and bone development (Ishiwata, 2018). FMS also plays a critical role in cancers, as well as osteolysis and inflammatory conditions (El-Gamal et at., 2013). PDGFRb, or platelet-derived growth factor receptor beta, plays a role in cancer, but its most notable role is in genetic conditions (Cen et al., 2020). Most of the cancerous activity comes from gain-of-function kinase, so kinase inhibition is used as a therapeutic agent in oncology. Much of the issues with loss of function is seen in early development or with life-long complications. Nevertheless, additional toxicity assessments based on potential off-target kinase inhibition would be needed in future studies for UH15_16.

To assess UH15_16 in *in vivo* pharmacokinetic, toxicity and efficacy models, viable formulations had to be devised with the goal of achieving solutions or homogeneous suspensions. Four formulations were devised. An intravenous formulation that consisted of UH15_16 dissolved in 30% Tween 80, 20% PBS, and 50% ethanol was established. Oral formulation 1 was a robust suspension, using suspending agents. It consisted of 1 mg/mL

UH15_16 in 90% OraPlus and 10% Polyethylene glycol 400 resulted in a milky white suspension. Oral formulation 2 utilized Captisol, a derivatized hydroxypropyl-beta-cyclodextrin, with a composition of 6.25 mg of UH15_16, 50 mg of Captisol and 0.5 mL of DI water. Oral formulation 3 used both Captisol and Tween 80 to achieve a superior suspension deemed the most stable (e.g. slowest release of UH15_16 from Captisol). Its composition is 5-fold Captisol to UH15_16 in 2.5% v/v Tween 80.

The *in vivo* PK assessment of UH15_16 with intravenous administration showed T_{max} = 0.41 h, C_{max} = 967 ng/mL, AUC = 4996 h*ng/mL, Cl = 206 mL/h/kg and $t_{1/2}$ = 10.7 h. Since *Cryptosporidium* is notably an intracellular pathogen of the enterocytes, or at least localized to the gut, achieving high levels of circulating UH15_16, is not particularly beneficial. Therefore, *in vivo* PK assessments using oral administration with three formulations were conducted. With oral formulation 1, the PK study revealed that the absorption was poor. So, the formulation was modified to improve absorption and efficacy. With oral formulation 2, the PK study revealed a modest improvement in systemic exposure, however absorption was delayed. The delayed absorption and poor systemic absorption may not be an issue for the treatment of cryptosporidiosis since it resides primarily in the gastrointestinal tract. The efficacy showed statistically significant reduction in infection burden with the second formulation. With oral formulation 3, the PK study revealed again delayed absorption, but some systemic absorption occurred within the first hour.

Acute in vivo toxicity studies were conducted at 50 mg/kg UH15_16 using the three oral formulations with once per day dosing for five days for oral formulations 1 and 2 and split dosing of oral formulation 3 (e.g. 25 mg/kg, bid). In each experiment the compound was well tolerated with no signs of toxicity.

Finally, the UH15_16 was assessed for efficacy in an acute IL-12 KO mouse model of cryptosporidiosis. In the case of oral formulation 1, 50 mg/kg oral dosing once per day did not show efficacy. However, with oral formulation 2, 50 mg/kg oral dosing once per day demonstrated a 38-68% reduction of fecal oocytes depending on the use of mean verses median values or the removal of outliers. With oral formulation 3, 25 mg/kg dosing twice per day demonstrated a 74% reduction in fecal oocytes with improved consistency in the treatment group. In the efficacy experiment with oral formulation 3 inter-animal variability was noticeably improved. There was also an improvement in inter-animal variation in the PK study of oral formulation 3, which may allow the compound to reach the site in the gastrointestinal tract where infection occurs. The third formulation also appeared more resilient to changing pH's, such as in fed versus fasted states, which might also contribute to a more consistent effect in animals. Collectively, it appears that formulation 3 may be more effective in advancing UH15_16 and other pyridopyrimidinone-based *Cp*CDPK1 inhibitors.

6. SUMMARY AND CONCLUSION

In conclusion, a new class of *Cp*CDPK1 inhibitors was identified. SAR analysis provided insights into two structural features for achieving potent Cp growth inhibition, namely a 4-chloro on the phenyl group that projects into the ATP binding pocket towards the αC-helix and the presence of a hydrogen bond accepting sulfone (or tertiary sulfonamide) in the solvent exposed portion of the inhibitor. An exemplary derivative UH15_16 was successful at inhibiting *Cryptosporidium parvum in vitro* and *in vivo*. This compound was one the most potent compounds tested, with an EC_{50} of about 14 nM for blocking Cp growth in host cells. Although this compound has modest solubility that might limit systemic exposure, its absorption properties may be adequate to achieve sufficient concentration in the gastrointestinal tract where acute *Cryptosporidium* infection resides. Formulation of UH15_16 with 5-fold Captisol and 2.5% Tween 80 enhanced *in vivo* efficacy likely by improving solubility and/or providing delayed compound release increasing gastrointestinal tract concentration. Expanded SAR analysis and optimization of this compound series combined with enterocyte absorption studies and additional compound formulation strategies will likely further improve this class of molecules for the treatment of cryptosporidiosis.

Future studies of pyridopyrimidones, such as UH15_16, can be explored in a variety of ways. For example, examining the question why the sulfone in the solvent exposed region of the inhibitor is critical for achieving potent Cp growth inhibition could provide additional insights into the SAR of this compound series. These efforts would be enhanced via co-crystallization studies of inhibitors with *Cp*CDPK1 that are currently underway. Further optimization of the compound series for improving kinase selectivity, as well as physiochemical and ADME properties could be pursued. Additional optimization of formulations, *in vivo* toxicity

assessments, more advanced animal models, such as using calf and premature pig models, and assessments in chronic models of cryptosporidiosis could also be done. Finally, the compounds could be examined in other Apicomplexa parasites, such as *Toxoplasma gondii*, which have similar CDPK1 kinases.

7. REFERENCES

Abbaspour Babaei M, Kamalidehghan B, Saleem M, Huri HZ, Ahmadipour F. Receptor tyrosine kinase (c-Kit) inhibitors: a potential therapeutic target in cancer cells. Drug Des Devel Ther. 2016;10:2443-2459. Published 2016 Aug 1. doi:10.2147/DDDT.S89114

Alinia®. Package insert. Romark Pharmaceuticals Inc; 2005.

Amadi B, Mwiya M, Musuku J, et al. Effect of nitazoxanide on morbidity and mortality in Zambian children with cryptosporidiosis: a randomised controlled trial. *Lancet*. 2002 ;360(9343):1375-1380. doi:10.1016/S0140-6736(02)11401-2.

Arnold, Samuel L. M., Ryan Choi, Matthew A. Hulverson, Deborah A. Schaefer, Sumiti Vinayak, Rama S. R. Vidadala, Molly C. Mccloskey, et al. "Necessity of Bumped Kinase Inhibitor Gastrointestinal Exposure in Treating *Cryptosporidium* Infection." The Journal of Infectious Diseases 216, no. 1 (May 24, 2017): 55–63. https://doi.org/10.1093/infdis/jix247.

Ashigbie PG, Shepherd S, Steiner KL, et al. Use-case scenarios for an anti-*Cryptosporidium* therapeutic. PLoS Negl Trop Dis. 2021;15(3):e0009057. Published 2021 Mar 11. doi:10.1371/journal.pntd.0009057

Bactroban. Package Insert. GlaxoSmithKline Ltd. 1987.

Baragaña, Beatriz, Barbara Forte, Ryan Choi, Stephen Nakazawa Hewitt, Juan A Bueren-Calabuig, João Pedro Pisco, Caroline Peet, et al. "Lysyl-tRNA Synthetase as a Drug Target in Malaria and Cryptosporidiosis." *Proceedings of the National Academy of Sciences - PNAS* 116, no. 14 (2019): 7015–20. https://doi.org/10.1073/pnas.1814685116.

Bessoff K, Sateriale A, Lee KK, Huston CD. Drug repurposing screen reveals FDA-approved inhibitors of human HMG-CoA reductase and isoprenoid synthesis that block *Cryptosporidium parvum* growth. Antimicrob Agents Chemother. 2013;57(4):1804-1814. doi:10.1128/AAC.02460-12

Billker, Oliver, Sebastian Lourido, and L. David Sibley. "Calcium-Dependent Signaling and Kinases in Apicomplexan Parasites." Cell Host & Microbe 5, no. 6 (June 18, 2009): 612–22. https://doi.org/10.1016/j.chom.2009.05.017.

Bisio, Hugo, and Dominique Soldati-Favre. "Signaling Cascades Governing Entry into and Exit from Host Cells by Toxoplasma Gondii." Annual Review of Microbiology 73, no. 1 (August 2019): 579–99. https://doi.org/10.1146/annurev-micro-020518-120235.

Bjorge, J., Jakymiw, A. & Fujita, D. Selected glimpses into the activation and function of Src kinase. Oncogene 19, 5620–5635 (2000). https://doi.org/10.1038/sj.onc.1203923

Buckner, Frederick S, Ranae M Ranade, J Robert Gillespie, Sayaka Shibata, Matthew A Hulverson, Zhongsheng Zhang, Wenlin Huang, et al. "Optimization of Methionyl tRNA-Synthetase Inhibitors for Treatment of *Cryptosporidium* Infection." Antimicrobial Agents and Chemotherapy 63, no. 4 (2019). https://doi.org/10.1128/AAC.02061-18.

Castellanos-Gonzalez, Alejandro, Hayley Sparks, Samantha Nava, Wenlin Huang, Zhongsheng Zhang, Kasey Rivas, Matthew A. Hulverson, et al. "A Novel Calcium-Dependent Kinase Inhibitor, Bumped Kinase Inhibitor 1517, Cures Cryptosporidiosis in Immunosuppressed Mice." Journal of Infectious Diseases 214, no. 12 (December 15, 2016): 1850–55. https://doi.org/10.1093/infdis/jiw481.

Castellanos-Gonzalez, Alejandro, Nicolas Perry, Samantha Nava, and A. Clinton White. "Preassembled Single-Stranded RNA–Argonaute Complexes: A Novel Method to Silence Genes In *Cryptosporidium*." Journal of Infectious Diseases 213, no. 8 (December 11, 2015): 1307–14. https://doi.org/10.1093/infdis/jiv588.

Castellanos-Gonzalez A, Yancey LS, Wang HC, et al. Cryptosporidium infection of human intestinal epithelial cells increases expression of osteoprotegerin: a novel mechanism for evasion of host defenses. J Infect Dis. 2008;197(6):916-923. doi:10.1086/528374

CDC, Global Health, Division of Parasitic Diseases and Malaria. (2019, May 20). *CDC - DPDx - Cryptosporidiosis*. Centers for Disease Control and Prevention. https://www.cdc.gov/dpdx/cryptosporidiosis/index.html.

CDC, National Center for Emerging and Zoonotic Infectious Diseases (NCEZID), & Division of Foodborne, Waterborne, and Environmental Diseases (DFWED). (2021, February 3). Nitazoxanide. Centers for Disease Control and Prevention. https://www.cdc.gov/parasites/crypto/nitazoxanide.html.

Cen Z, Chen Y, Chen S, et al. Biallelic loss-of-function mutations in JAM2 cause primary familial brain calcification. Brain. 2020;143(2):491-502. doi:10.1093/brain/awz392

Clinton, A, White, Jr., Stanley G. Cron, Cynthia L. Chappell, Paromomycin in Cryptosporidiosis, Clinical Infectious Diseases, Volume 32, Issue 10, 15 May 2001, Pages 1516–1517, https://doi.org/10.1086/320171

Critchley IA, Green LS, Young CL, et al. Spectrum of activity and mode of action of REP3123, a new antibiotic to treat Clostridium difficile infections. J Antimicrob Chemother. 2009;63(5):954-963. doi:10.1093/jac/dkp041

Dasgupta Y, Koptyra M, Hoser G, et al. Normal ABL1 is a tumor suppressor and therapeutic target in human and mouse leukemias expressing oncogenic ABL1 kinases. Blood. 2016;127(17):2131-2143. doi:10.1182/blood-2015-11-681171

DiLella, C., Mody, S., & Parisi, R. (2021, April 30). *A major chlorine shortage is set to spoil summertime fun in the swimming poolChri*. CNBC. https://www.cnbc.com/2021/04/30/a-major-chlorine-shortage-is-set-to-spoil-swimming-pool-fun-this-summer.html.

Ehrenman K, Wanyiri JW, Bhat N, Ward HD, Coppens I. *Cryptosporidium parvum* scavenges LDL-derived cholesterol and micellar cholesterol internalized into enterocytes. Cell Microbiol. 2013;15(7):1182-1197. doi:10.1111/cmi.12107

El-Gamal MI, Anbar HS, Yoo KH, Oh CH. FMS Kinase Inhibitors: Current Status and Future Prospects. Med Res Rev. 2013;33(3):599-636. doi:10.1002/med.21258

Eriani G, Delarue M, Poch O, Gangloff J, Moras D. Partition of tRNA synthetases into two classes based on mutually exclusive sets of sequence motifs. Nature. 1990;347(6289):203-206. doi:10.1038/347203a0.

Fabian, M.A. et al. A small molecule-kinase interaction map for clinical kinase inhibitors. Nat. Biotechnol. 23, 329-336 (2005).

Galia E. Physiologically based dissolution tests. Doctoral thesis, Johann Wolfgang Goethe University, Frankfurt; 1999.

Green, Judith L., Roxanne R. Rees-Channer, Stephen A. Howell, Stephen R. Martin, Ellen Knuepfer, Helen M. Taylor, Munira Grainger, and Anthony A. Holder. “The Motor

Complex Of Plasmodium Falciparum." Journal of Biological Chemistry 283, no. 45 (August 3, 2008): 30980–89. https://doi.org/10.1074/jbc.m803129200.

Heidorn SJ, Milagre C, Whittaker S, et al. Kinase-dead BRAF and oncogenic RAS cooperate to drive tumor progression through CRAF. Cell. 2010;140(2):209-221. doi:10.1016/j.cell.2009.12.040

Herman, Jonathan D, Lauren R Pepper, Joseph F Cortese, Guillermina Estiu, Kevin Galinsky, Vanessa Zuzarte-Luis, Emily R Derbyshire, et al. "The Cytoplasmic Prolyl-tRNA Synthetase of the Malaria Parasite Is a Dual-Stage Target of Febrifugine and Its Analogs." Science Translational Medicine 7, no. 288 (2015): 288ra77–288ra77. https://doi.org/10.1126/scitranslmed.aaa3575.

Hewitt RG, Yiannoutsos CT, Higgs ES, et al. Paromomycin: no more effective than placebo for treatment of cryptosporidiosis in patients with advanced human immunodeficiency virus infection. AIDS Clinical Trial Group. *Clin Infect Dis*. 2000;31(4):1084-1092. doi:10.1086/318155.

Hlavsa MC, Aluko SK, Miller AD, et al. Outbreaks associated with treated recreational water — United States, 2015–2019. *American Journal of Transplantation*. 2021;21(7):2605-2609. doi:10.1111/ajt.16037

Hoepfner D, McNamara CW, Lim CS, et al. Selective and specific inhibition of the plasmodium falciparum lysyl-tRNA synthetase by the fungal secondary metabolite cladosporin. Cell Host Microbe. 2012;11(6):654-663. doi:10.1016/j.chom.2012.04.015

Huang, Wenlin, Kayode K. Ojo, Zhongsheng Zhang, Kasey Rivas, Rama Subba Rao Vidadala, Suzanne Scheele, Amy E. Derocher, et al. "SAR Studies of 5-Aminopyrazole-4-Carboxamide Analogues as Potent and Selective Inhibitors of Toxoplasma Gondii CDPK1." ACS Medicinal Chemistry Letters 6, no. 12 (October 26, 2015): 1184–89. https://doi.org/10.1021/acsmedchemlett.5b00319.

Huang, Wenlin A., Ryan C. Choi, Matthew A. Hulverson, Zhongsheng R. Zhang, Molly K. Mccloskey, Deborah Subba Rao Schaefer, Grant W. Whitman, et al. "5-Aminopyrazole-4-Carboxamide-Based Compounds Prevent the Growth of *Cryptosporidium Parvum*." Antimicrobial Agents and Chemotherapy 61, no. 8 (May 22, 2017). https://doi.org/10.1128/aac.00020-17.

Humatin®. Package insert. Monarch Pharmaceuticals Inc; 2001.

Hussain, Tahir, Manickam Yogavel, and Amit Sharma. "Inhibition of Protein Synthesis and Malaria Parasite Development by Drug Targeting of Methionyl-tRNA Synthetases." Antimicrobial Agents and Chemotherapy 59, no. 4 (2015): 1856–67. https://doi.org/10.1128/AAC.02220-13.

Ishiwata T. Role of fibroblast growth factor receptor-2 splicing in normal and cancer cells. Front Biosci (Landmark Ed). 2018;23:626-639. Published 2018 Jan 1. doi:10.2741/4609

Kenzie, William R. Mac, Neil J. Hoxie, Mary E. Proctor, M. Stephen Gradus, Kathleen A. Blair, Dan E. Peterson, James J. Kazmierczak, et al. "A Massive Outbreak in Milwaukee of *Cryptosporidium* Infection Transmitted through the Public Water Supply." New England Journal of Medicine 331, no. 3 (1994): 161–67. https://doi.org/10.1056/nejm199407213310304.

Kerydin. Package Insert. Anacor Pharmaceuticals, Inc. 2014.

Khalil, Ibrahim A, Christopher Troeger, Puja C Rao, Brigette F Blacker, Alexandria Brown, Thomas G Brewer, Danny V Colombara, et al. "Morbidity, Mortality, and Long-Term Consequences Associated with Diarrhoea from *Cryptosporidium* Infection in Children Younger than 5 Years: a Meta-Analyses Study." The Lancet Global Health 6, no. 7 (July 1, 2018). https://doi.org/10.1016/s2214-109x(18)30283-3.

Kieschnick, Heidi, Therese Wakefield, Carl Anthony Narducci, and Con Beckers. "Toxoplasma Gondii Attachment to Host Cells Is Regulated by a Calmodulin-like Domain Protein Kinase." Journal of Biological Chemistry 276, no. 15 (November 2001): 12369–77. https://doi.org/10.1074/jbc.m011045200.

Klein S. The use of biorelevant dissolution media to forecast the in vivo performance of a drug. AAPS J. 2010;12(3):397-406. doi:10.1208/s12248-010-9203-3.

Klein S, Buchanan NL, Buchanan CM. Miniaturized transfer models to predict the precipitation of poorly soluble weak bases upon entry into the small intestine. AAPS PharmSciTech. 2012;13(4):1230-1235. doi:10.1208/s12249-012-9851-y

Kosek, Margaret, Cirle Alcantara, Aldo Am Lima, and Richard L Guerrant. "Cryptosporidiosis: an Update." The Lancet Infectious Diseases 1, no. 4 (November 1, 2001): 262–69. https://doi.org/10.1016/s1473-3099(01)00121-9.

Kuhlenschmidt, Theresa B., Florentine U. Rutaganira, Shaojun Long, Keliang Tang, Kevan M. Shokat, Mark S. Kuhlenschmidt, and L. David Sibley. "Inhibition of Calcium-Dependent Protein Kinase 1 (CDPK1) In Vitro by Pyrazolopyrimidine Derivatives Does Not Correlate with Sensitivity of *Cryptosporidium Parvum* Growth in Cell Culture."

Antimicrobial Agents and Chemotherapy 60, no. 1 (November 9, 2015): 570–79. https://doi.org/10.1128/aac.01915-15.

Larson, Eric T., Kayode K. Ojo, Ryan C. Murphy, Steven M. Johnson, Zhongsheng Zhang, Jessica E. Kim, David J. Leibly, et al. "Multiple Determinants for Selective Inhibition of Apicomplexan Calcium-Dependent Protein Kinase CDPK1." Journal of Medicinal Chemistry 55, no. 6 (March 13, 2012): 2803–10. https://doi.org/10.1021/jm201725v.

[edited by] Robert E. Lenga. The Sigma-Aldrich Library of Chemical Safety Data. Phenylboronic acid. [Milwaukee, Wis., USA] :Sigma-Aldrich Corp., 2020.

Lipinski CA, Lombardo F, Dominy BW, Feeney PJ. Experimental and computational approaches to estimate solubility and permeability in drug discovery and development settings. Adv Drug Deliv Rev. 2001;46(1-3):3-26. doi:10.1016/s0169-409x(00)00129-0.

Marques M. Dissolution media simulating fasted and fed states. Dissolution Technologies. 2004;11(2):16.

McMasters DR, Vedani A. Ochratoxin binding to phenylalanyl-tRNA synthetase: computational approach to the mechanism of ochratoxicosis and its antagonism. J Med Chem. 1999;42(16):3075-3086. doi:10.1021/jm991040k

Mead J, McNair N. Antiparasitic activity of flavonoids and isoflavones against Cryptosporidium parvum and Encephalitozoon intestinalis. FEMS Microbiol Lett. 2006;259(1):153-157. doi:10.1111/j.1574-6968.2006.00263.x

Merritt, Ethan A, Tracy L Arakaki, Robert Gillespie, Alberto J Napuli, Jessica E Kim, Frederick S Buckner, Wesley C Van Voorhis, et al. "Crystal Structures of Three Protozoan

Homologs of Tryptophanyl-tRNA Synthetase." Molecular and Biochemical Parasitology 177, no. 1 (2011): 20–28. https://doi.org/10.1016/j.molbiopara.2011.01.003.

Murphy RC, Ojo KK, Larson ET, et al. Discovery of Potent and Selective Inhibitors of Calcium-Dependent Protein Kinase 1 (CDPK1) from C. parvum and T. gondii. ACS Med Chem Lett. 2010;1(7):331-335. doi:10.1021/ml100096t

Murphy JL, Arrowood MJ, Lu X, Hlavsa MC, Beach MJ, Hill VR. Effect of cyanuric acid on the inactivation of Cryptosporidium parvum under hyperchlorination conditions. Environ Sci Technol. 2015;49(12):7348-7355. doi:10.1021/acs.est.5b00962

Nikhar S, Siokas I, Schlicher L, et al. Design of pyrido[2,3-d]pyrimidin-7-one inhibitors of receptor interacting protein kinase-2 (RIPK2) and nucleotide-binding oligomerization domain (NOD) cell signaling. Eur J Med Chem. 2021;215:113252. doi:10.1016/j.ejmech.2021.113252

O'Dwyer, Karen, Aaron T Spivak, Karen Ingraham, Sharon Min, David J Holmes, Charles Jakielaszek, Stephen Rittenhouse, et al. "Bacterial Resistance to Leucyl-tRNA Synthetase Inhibitor GSK2251052 Develops During Treatment of Complicated Urinary Tract Infections." Antimicrobial Agents and Chemotherapy 59, no. 1 (2015): 289–98. https://doi.org/10.1128/AAC.03774-14.

Oki T, Hirano M, Tomatsu K, Numata K, Kamei H. Cispentacin, a new antifungal antibiotic. II. In vitro and in vivo antifungal activities. J Antibiot (Tokyo). 1989;42(12):1756-1762. doi:10.7164/antibiotics.42.1756

Painter, Julia E, Michele C Hlavsa, Sarah A Collier, Lihua Xiao, and Jonathan S Yoder. "Cryptosporidiosis Surveillance — United States, 2011–2012." Morbidity and Mortality Weekly Report (MMWR) 64(SS03) (May 1, 2015): 1–14.

Palencia, Andrés, Ru-Juan Liu, Maria Lukarska, Jiri Gut, Alexandre Bougdour, Bastien Touquet, En-Duo Wang, et al. "*Cryptosporidium* and *Toxoplasma* Parasites Are Inhibited by a Benzoxaborole Targeting Leucyl-tRNA Synthetase." Antimicrobial Agents and Chemotherapy 60, no. 10 (2016): 5817–27. https://doi.org/10.1128/AAC.00873-16.

Pan XM, Li J, Gan R, Hu XN. Preparation and in vitro evaluation of enteric-coated tablets of rosiglitazone sodium. Saudi Pharm J. 2015;23(5):581-586. doi:10.1016/j.jsps.2015.02.018

Panel on Guidelines for the Prevention and Treatment of Opportunistic Infections in Adults and Adolescents with HIV. Guidelines for the Prevention and Treatment of Opportunistic Infections in HIV-infected Adults and Adolescents: Recommendations from the Centers for Disease Control and Prevention, the National Institutes of Health, and the HIV Medicine Association of the Infectious Diseases Society of America. Available at https://clinicalinfo.hiv.gov/sites/default/files/inline-files/adult_oi.pdf. Accessed (6/17/2021) [87-93, Cryptosporidiosis].

Parents sue in boy's death from brain-eating amoeba in Texas. AP NEWS. https://apnews.com/article/fort-worth-texas-lawsuits-352fa75f51211e1f5a7a51a776b73eee. Published October 5, 2021. Accessed October 19, 2021.

Pham, James S, Karen L Dawson, Katherine E Jackson, Erin E Lim, Charisse Flerida A Pasaje, Kelsey E.C Turner, and Stuart A Ralph. “Aminoacyl-tRNA Synthetases as Drug Targets in Eukaryotic Parasites.” International Journal for Parasitology -- Drugs and Drug Resistance 4, no. 1 (2014): 1–13. https://doi.org/10.1016/j.ijpddr.2013.10.001.

Pines, Mark, and Itai Spector. “Halofuginone - the Multifaceted Molecule.” Molecules (Basel, Switzerland) 20, no. 1 (2015): 573–94. https://doi.org/10.3390/molecules20010573.

Reina FT, Ribeiro CA, Araújo RS, et al. INTESTINAL AND PULMONARY INFECTION BY *Cryptosporidium parvum* IN TWO PATIENTS WITH HIV/AIDS. Rev Inst Med Trop Sao Paulo. 2016;58:21. doi:10.1590/S1678-9946201658021

Roskoski, Robert. “Classification of Small Molecule Protein Kinase Inhibitors Based Upon the Structures of Their Drug-Enzyme Complexes.” Pharmacological Research 103 (2016): 26–48. https://doi.org/10.1016/j.phrs.2015.10.021.

Shibata S, Gillespie JR, Ranade RM, et al. Urea-based inhibitors of Trypanosoma brucei methionyl-tRNA synthetase: selectivity and in vivo characterization. J Med Chem. 2012;55(14):6342-6351. doi:10.1021/jm300303e

Sonzogni-Desautels K, Mead JR, Ndao M. Mouse Models for Use in Cryptosporidium Infection Studies and Quantification of Parasite Burden Using Flow Cytometry, qPCR, and Histopathology. Methods Mol Biol. 2020;2052:229-251. doi:10.1007/978-1-4939-9748-0_14

Vinayak, Sumiti, Rajiv S Jumani, Peter Miller, Muhammad M Hasan, Briana I McLeod, Jayesh Tandel, Erin E Stebbins, et al. “Bicyclic Azetidines Kill the Diarrheal Pathogen

Cryptosporidium in Mice by Inhibiting Parasite Phenylalanyl-tRNA Synthetase." Science Translational Medicine 12, no. 563 (2020). https://doi.org/10.1126/scitranslmed.aba8412.

Voorhis, Wesley C. Van, J. Stone Doggett, Marilyn Parsons, Matthew A. Hulverson, Ryan Choi, Samuel L.m. Arnold, Michael W. Riggs, et al. "Extended-Spectrum Antiprotozoal Bumped Kinase Inhibitors: A Review." Experimental Parasitology 180 (January 5, 2017): 71–83. https://doi.org/10.1016/j.exppara.2017.01.001.

Wernimont, Amy K, Jennifer D Artz, Patrick Finerty, Yu-Hui Lin, Mehrnaz Amani, Abdellah Allali-Hassani, Guillermo Senisterra, et al. "Structures of Apicomplexan Calcium-Dependent Protein Kinases Reveal Mechanism of Activation by Calcium." Nature Structural & Molecular Biology 17, no. 5 (May 2010): 596–601. https://doi.org/10.1038/nsmb.1795.

Wu, Peng, Thomas E Nielsen, and Mads H Clausen. "FDA-Approved Small-Molecule Kinase Inhibitors." Trends in Pharmacological Sciences (Regular Ed.) 36, no. 7 (2015): 422–39. https://doi.org/10.1016/j.tips.2015.04.005.

Yamashita T, Ozaki S, Kushida I. Solvent shift method for anti-precipitant screening of poorly soluble drugs using biorelevant medium and dimethyl sulfoxide. Int J Pharm. 2011;419(1-2):170-174. doi:10.1016/j.ijpharm.2011.07.045.

Zhang, Zhongsheng, Kayode K. Ojo, Steven M. Johnson, Eric T. Larson, Penqing He, Jennifer A. Geiger, Alejandro Castellanos-Gonzalez, et al. "Benzoylbenzimidazole-Based Selective Inhibitors Targeting *Cryptosporidium Parvum* and Toxoplasma Gondii

Calcium-Dependent Protein Kinase-1." Bioorganic & Medicinal Chemistry Letters 22, no. 16 (August 15, 2012): 5264–67. https://doi.org/10.1016/j.bmcl.2012.06.050.

8. APPENDICES

8.1. NMR Data

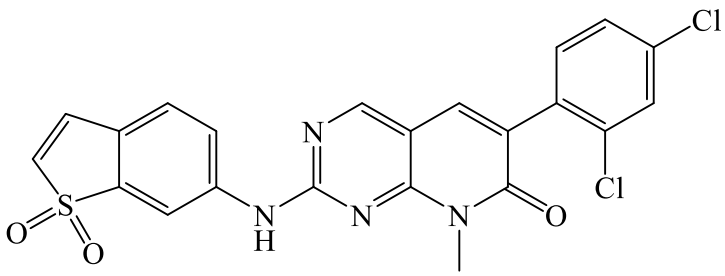

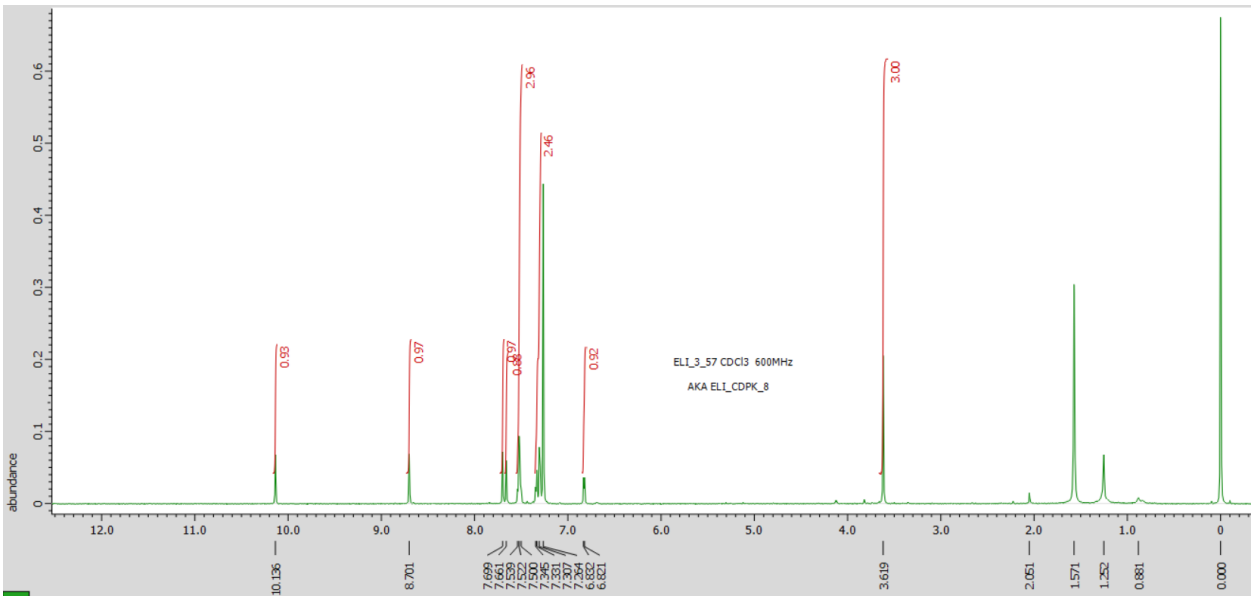

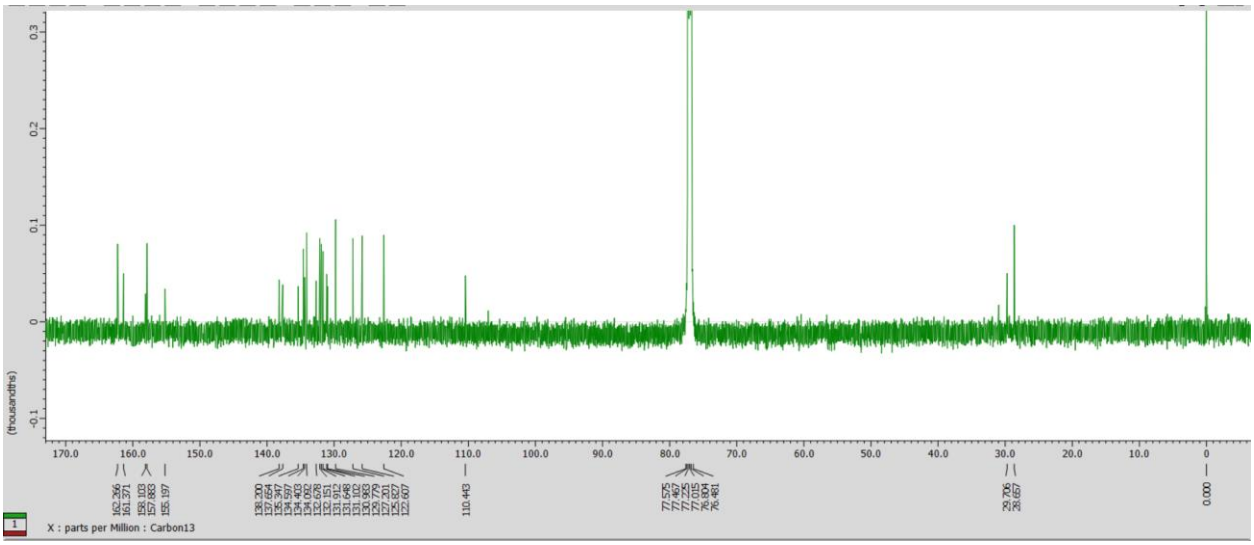

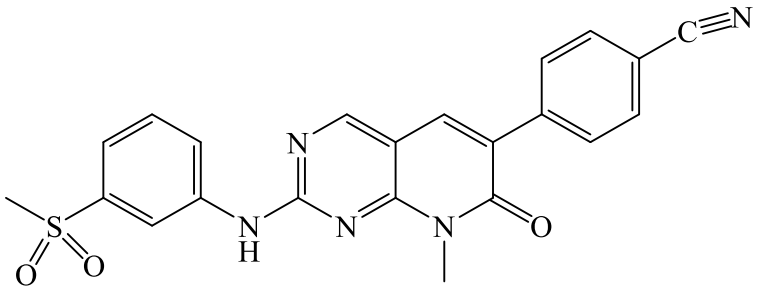
C≡N
N
N
N
O
S
O
O
H

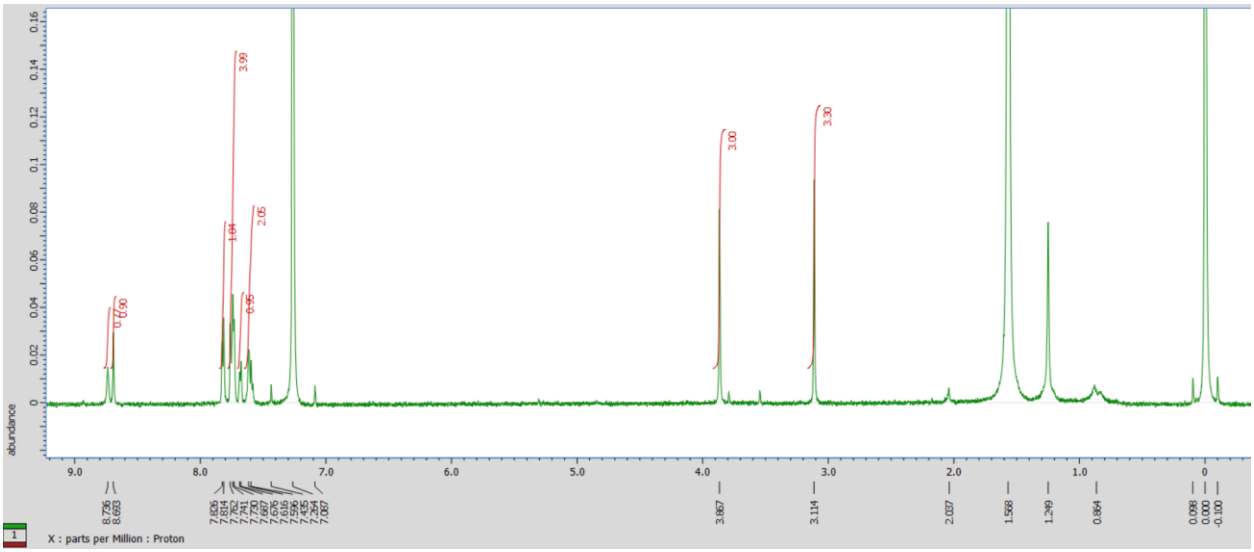
abundance
X : parts per Million : Proton
3.99
3.00
3.30
2.05
1.04
0.90
0.95

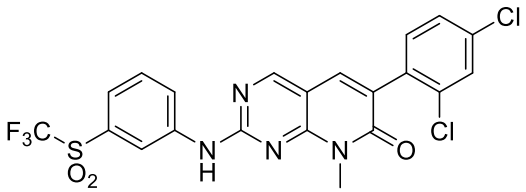
Cl
F3C
S
O2
N
H
N
N
N
O
Cl

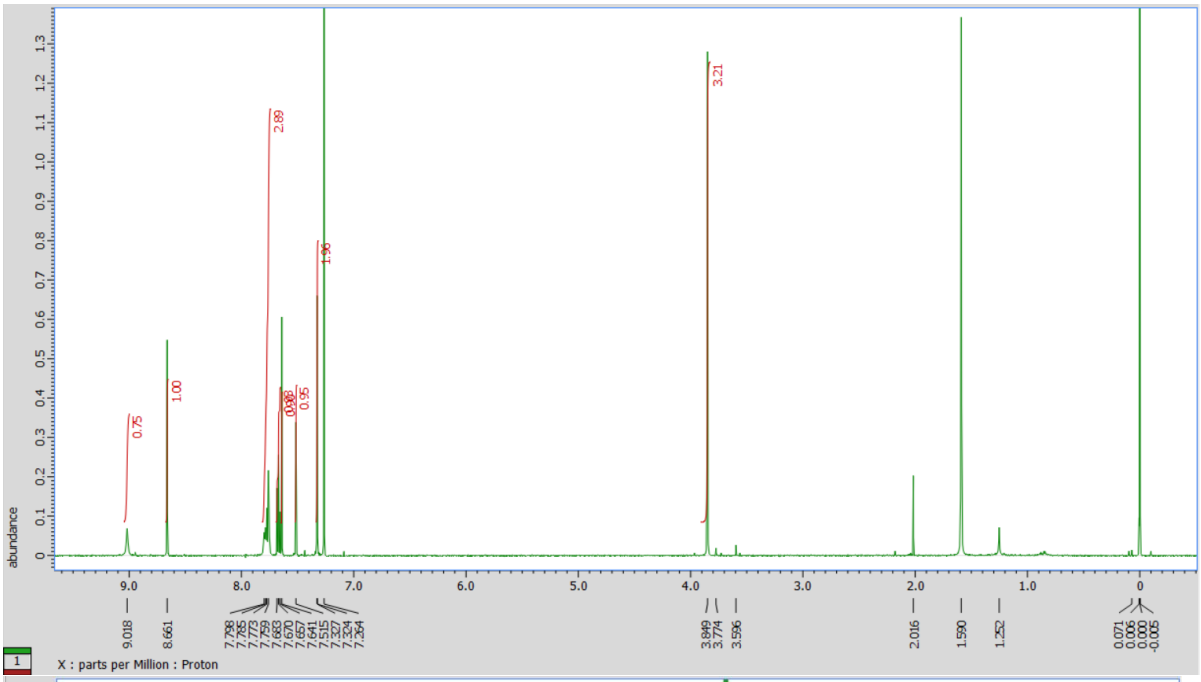
abundance
X : parts per Million : Proton

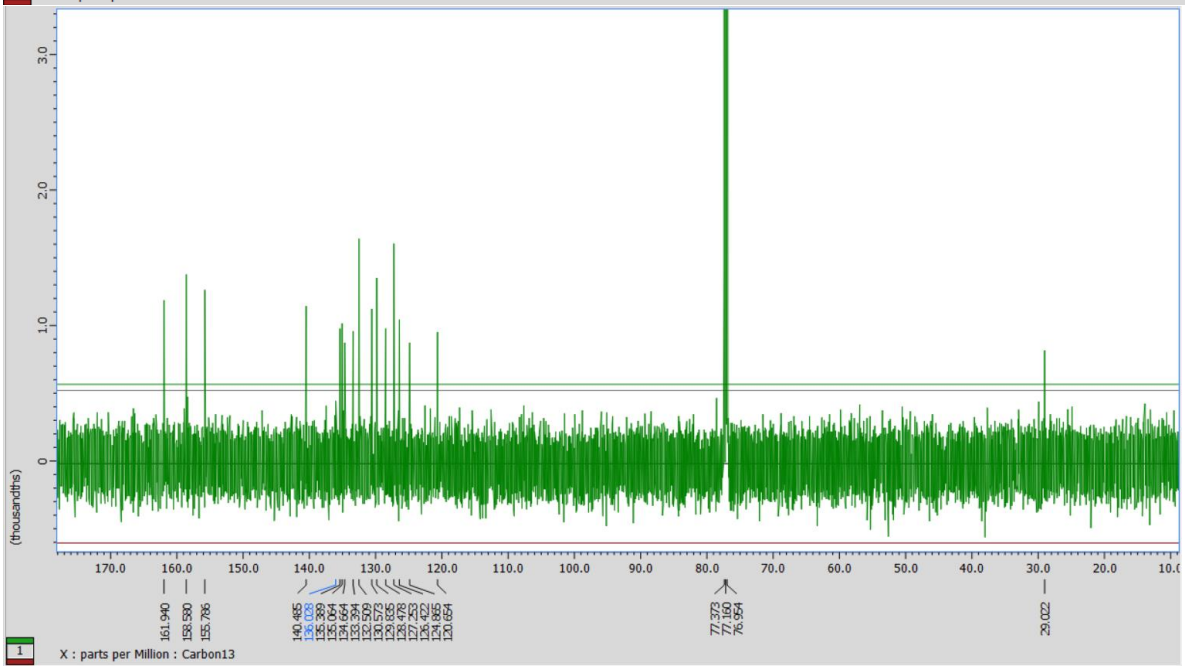
(thousandths)
X : parts per Million : Carbon13

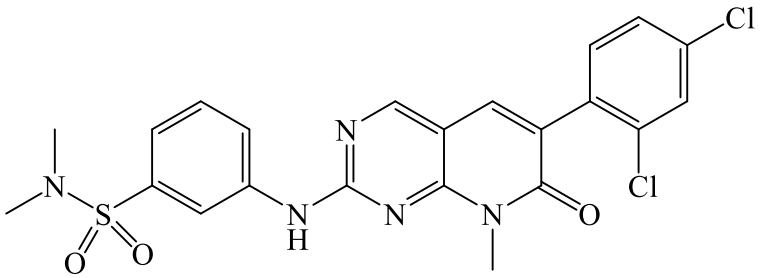
Cl
Cl
N
S
O
O
N
H
N
N
N
O

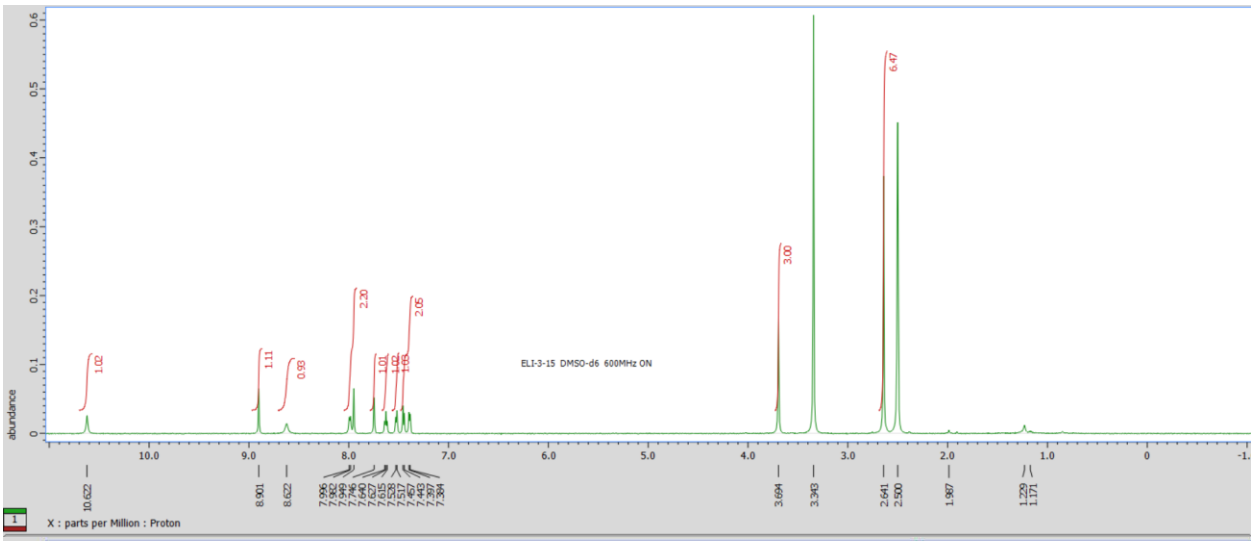
ELI-3-15 DMSO-d6 600MHz ON
abundance
X : parts per Million : Proton

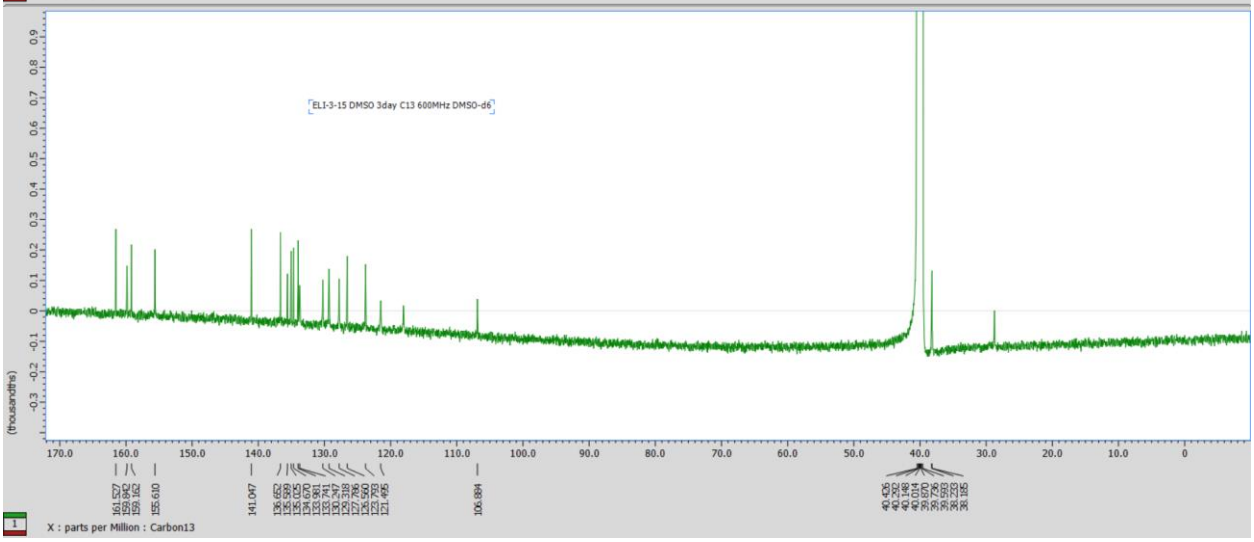
ELI-3-15 DMSO 3day C13 600MHz DMSO-d6
(thousandths)
X : parts per Million : Carbon13

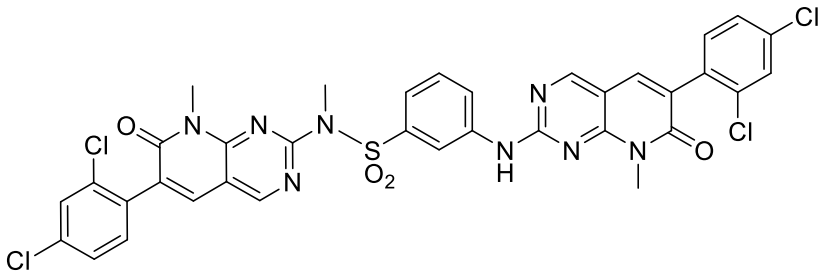
Cl
O
N
N
N
S
O2
N
H
N
N
N
O
Cl
Cl
Cl

ELI_CDPK_8

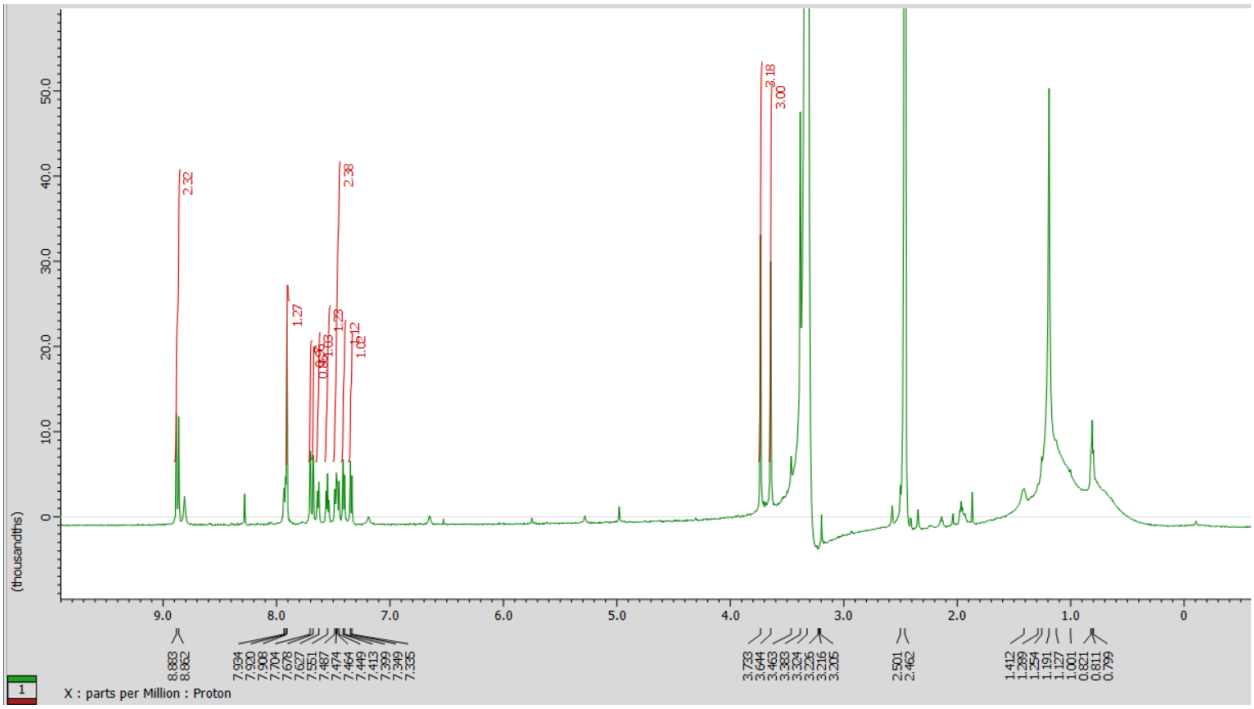
(thousandths)
50.0
40.0
30.0
20.0
10.0
0
9.0
8.0
7.0
6.0
5.0
4.0
3.0
2.0
1.0
0
2.32
1.27
2.38
3.18
3.00
1.23
1.12
1.02
X : parts per Million : Proton

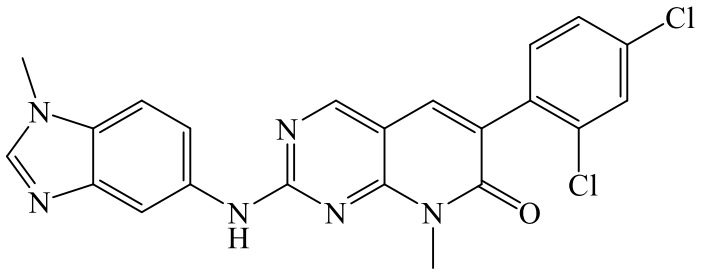
Cl
N
N
N
H
N
N
N
O
Cl

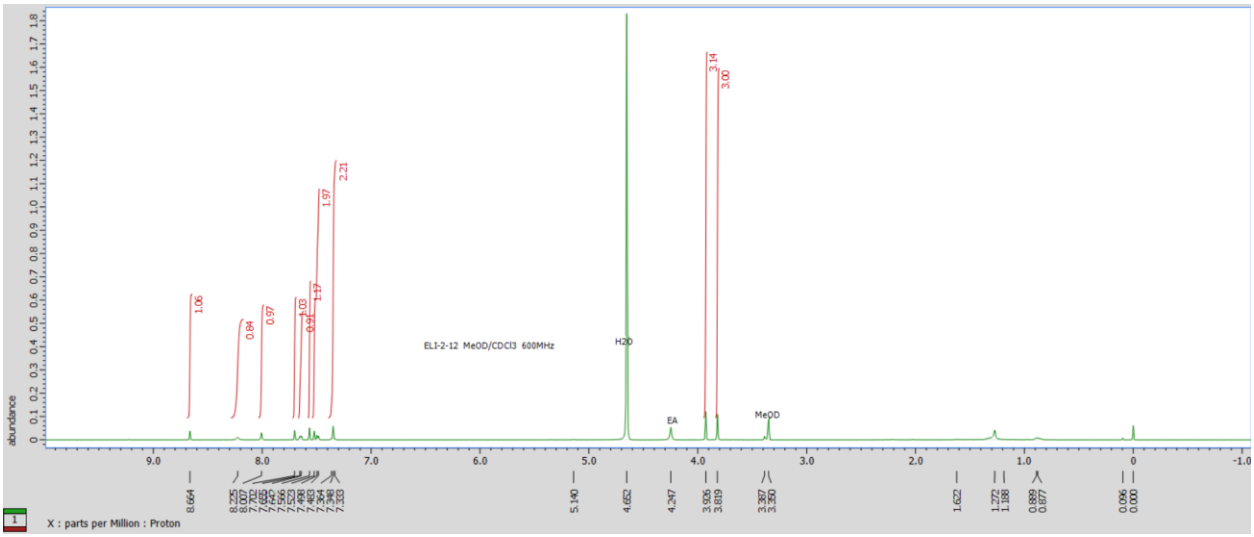
ELI-2-12 MeOD/CDCl3 600MHz
H2O
EA
MeOD
abundance
X : parts per Million : Proton

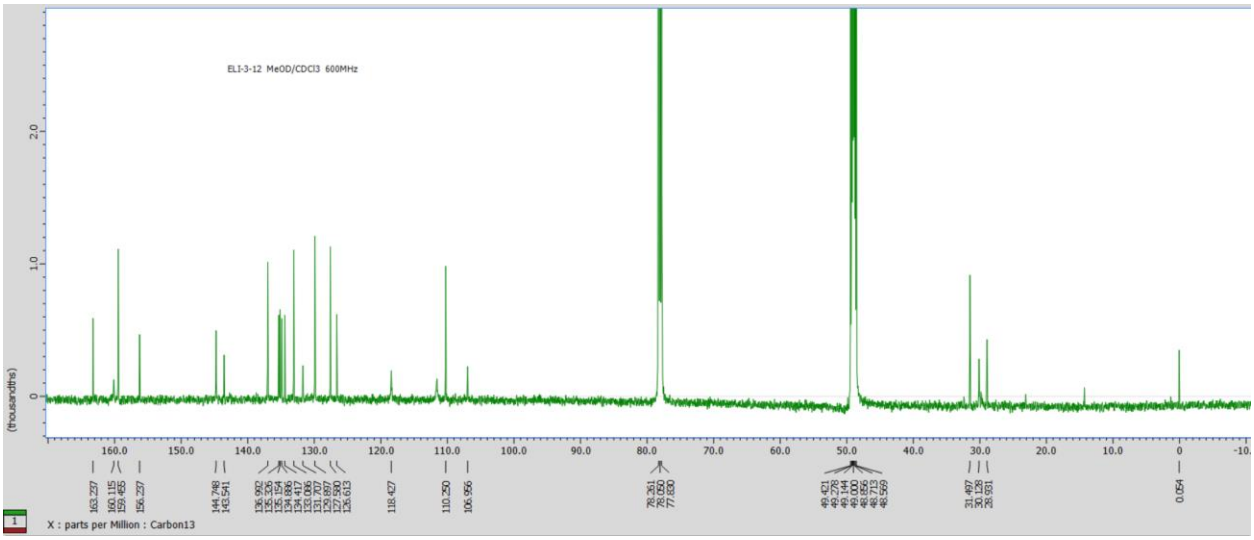
ELI-3-12 MeOD/CDCl3 600MHz
(thousandths)
X : parts per Million : Carbon13

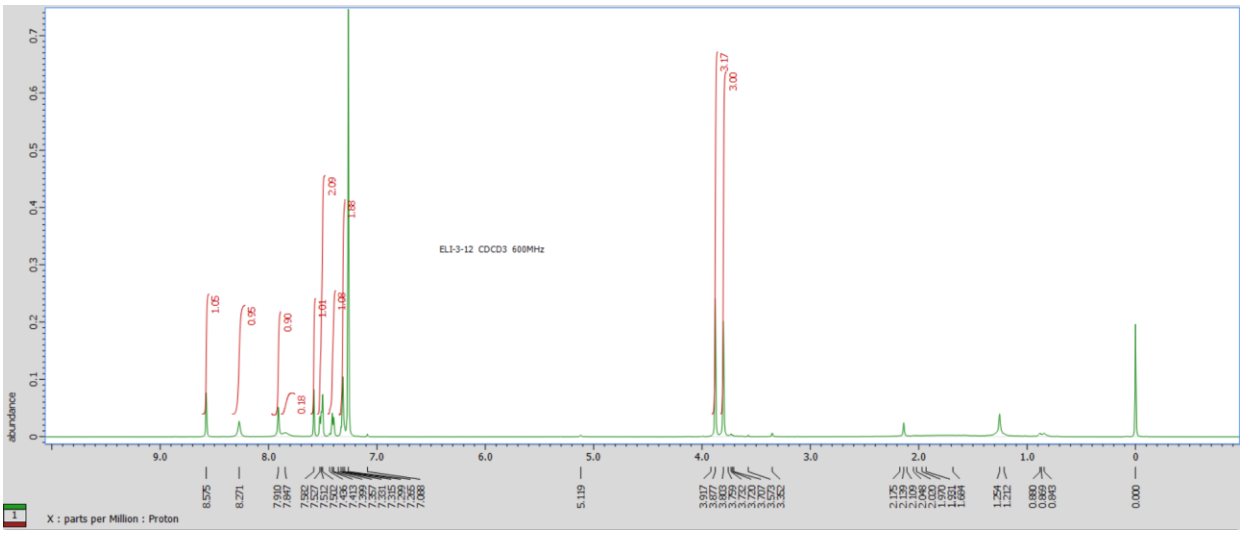
ELI-3-12 CDCD3 600MHz
abundance
X : parts per Million : Proton

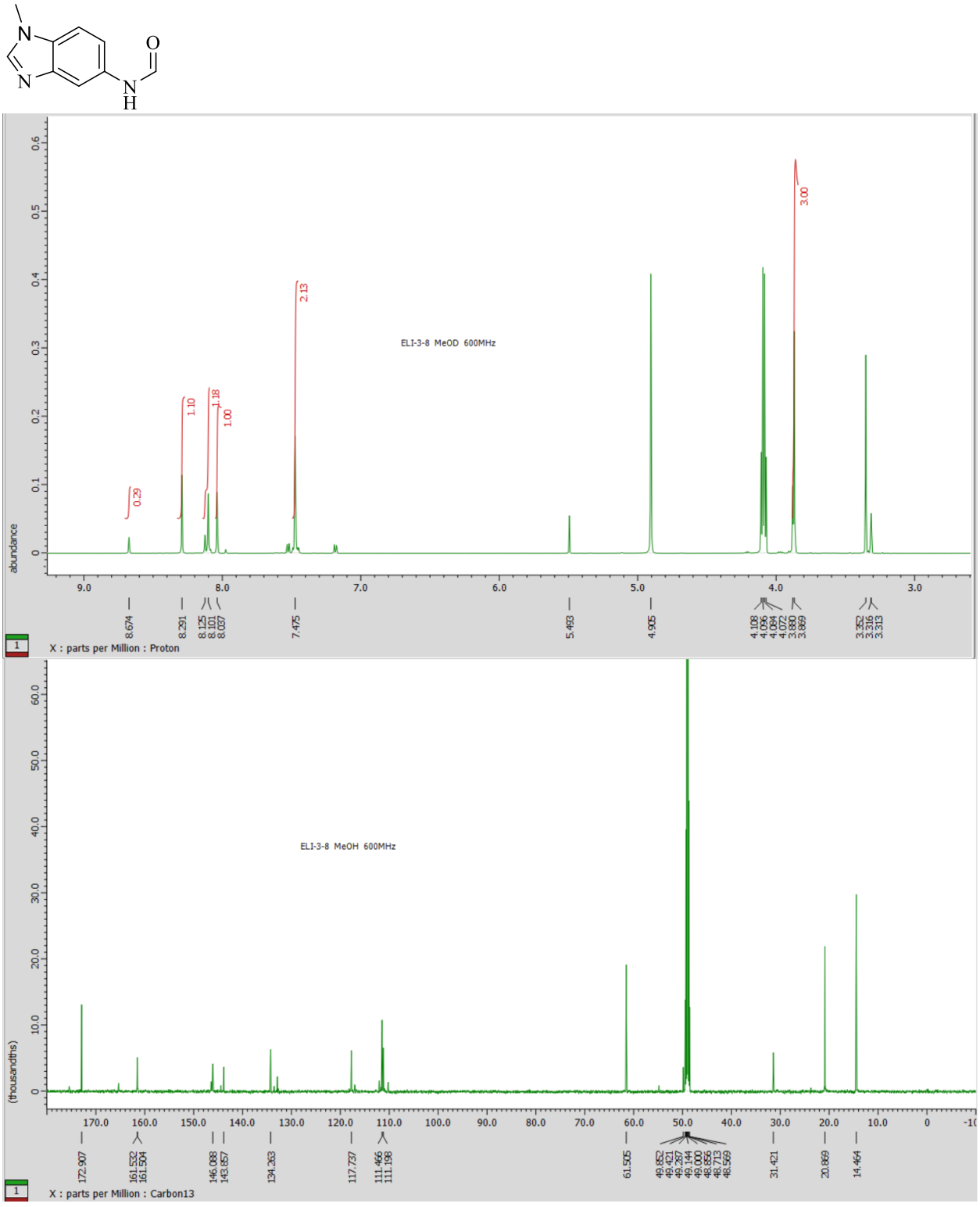

(Contains Ethyl Acetate)

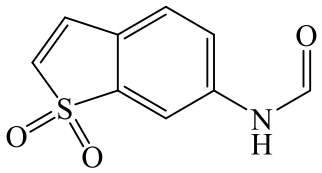
O
S
O
O
N
H

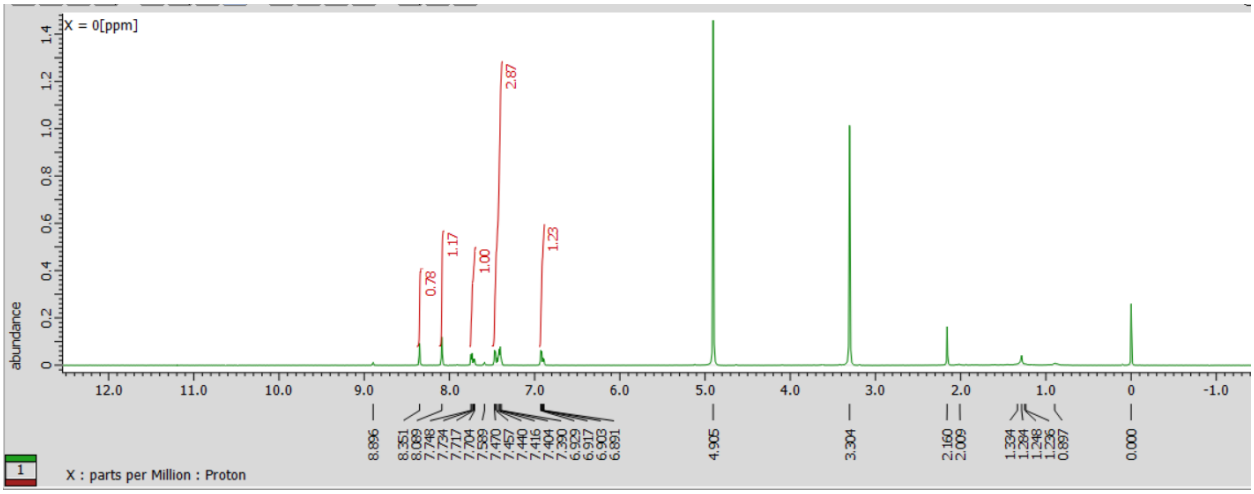
X = 0[ppm]
abundance
2.87
1.17
1.00
0.78
1.23
X : parts per Million : Proton

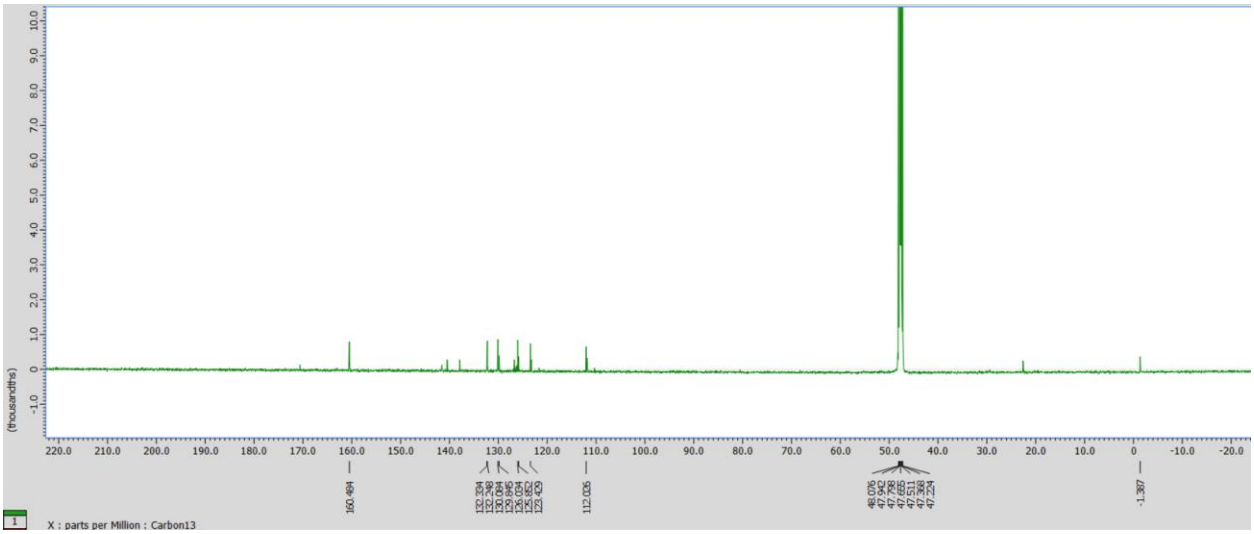
(thousandths)
X : parts per Million : Carbon13

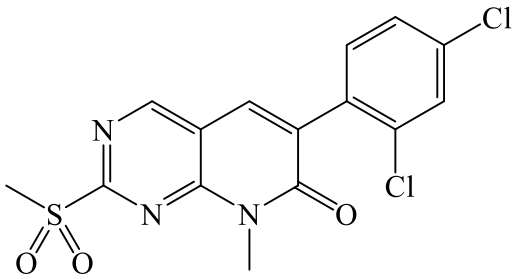
Cl
N
Cl
S
N
N
O
O
O

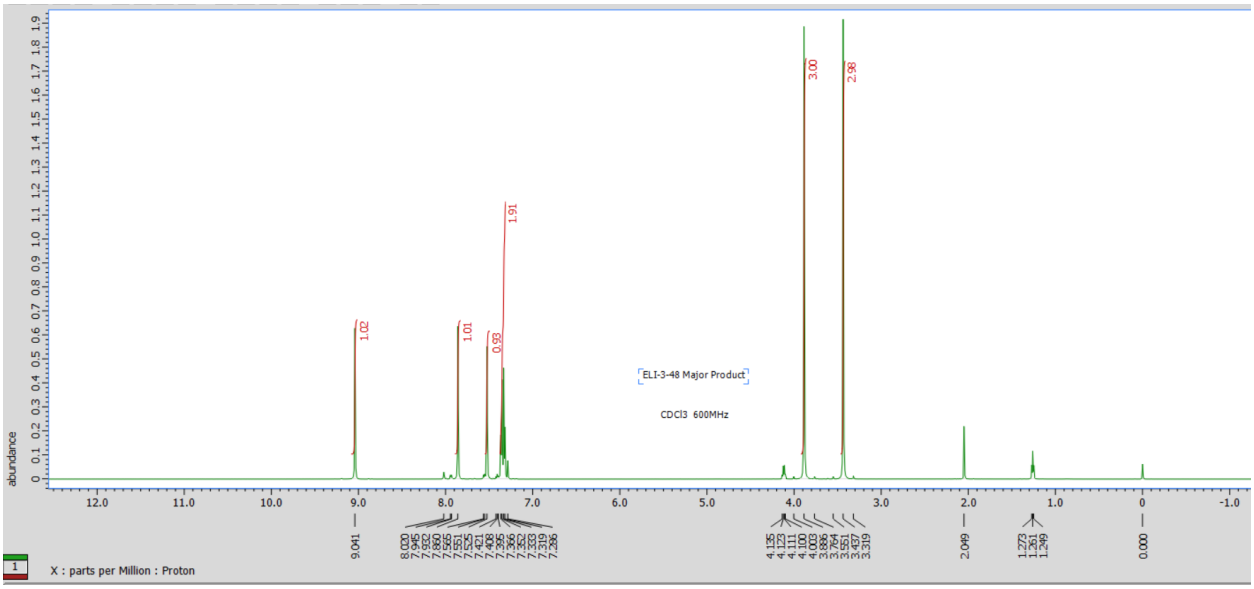
abundance
1.02
1.01
0.93
1.91
3.00
2.98
ELI-3-48 Major Product
CDCl3 600MHz
X : parts per Million : Proton

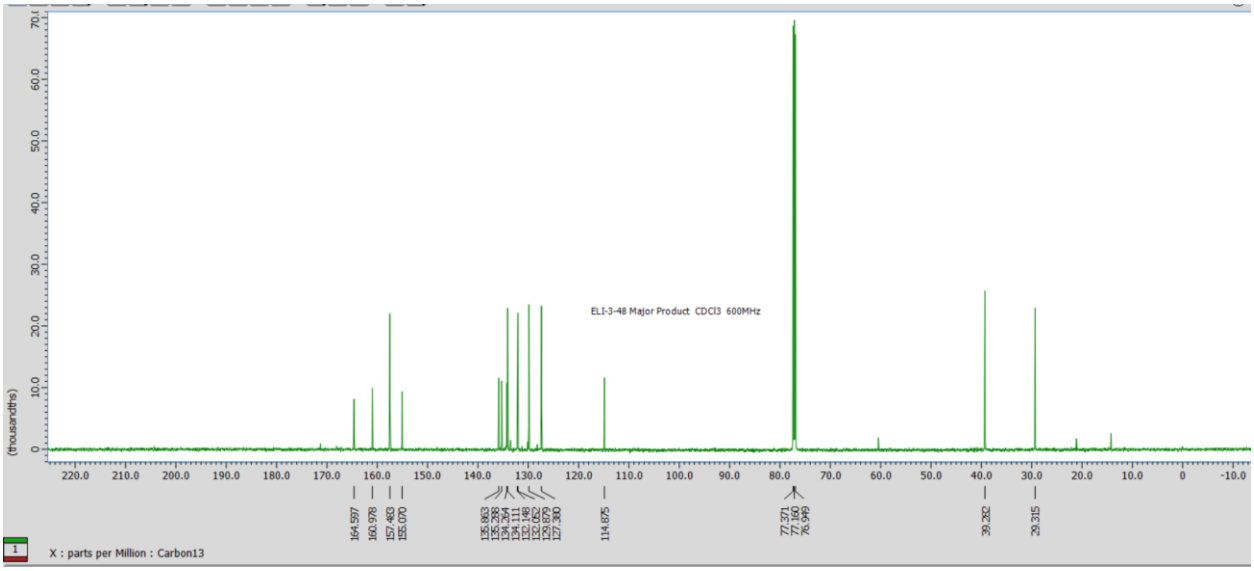
(thousandths)
ELI-3-48 Major Product CDCl3 600MHz
X : parts per Million : Carbon13

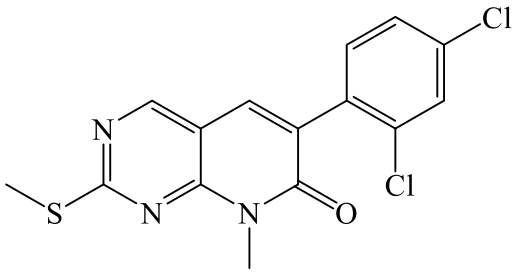
Cl
N
Cl
S
N
N
O

ELI-3-42

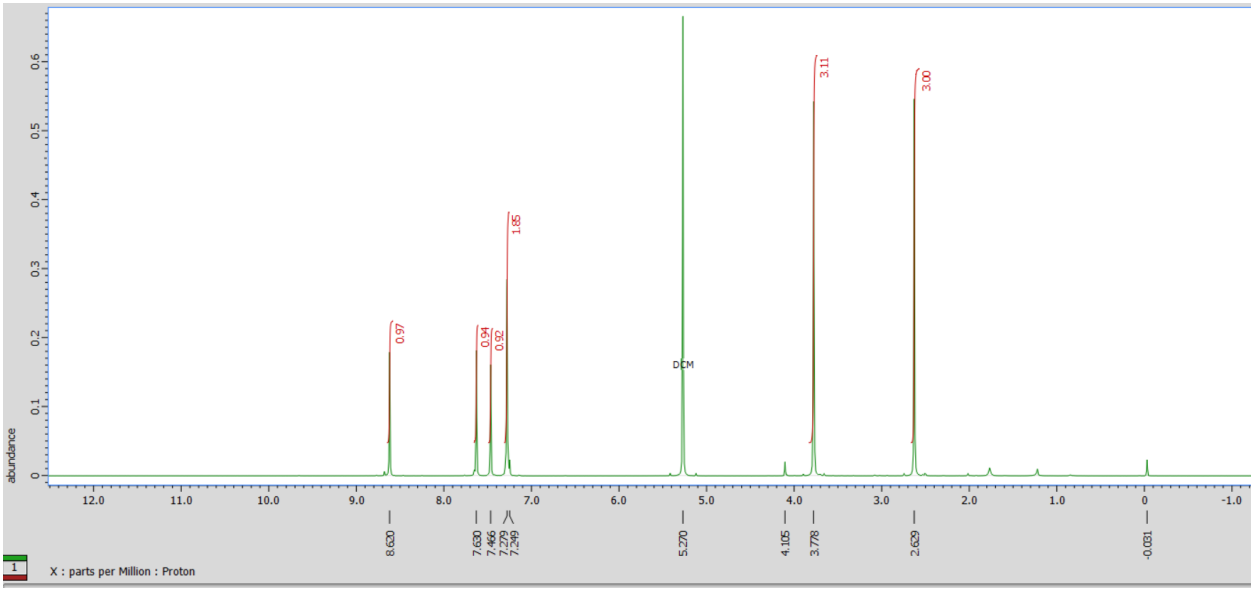
abundance
0.97
0.94
0.92
1.85
DCM
3.11
3.00
8.630
7.630
7.466
7.299
7.249
5.270
4.105
3.778
2.629
-0.031
X : parts per Million : Proton

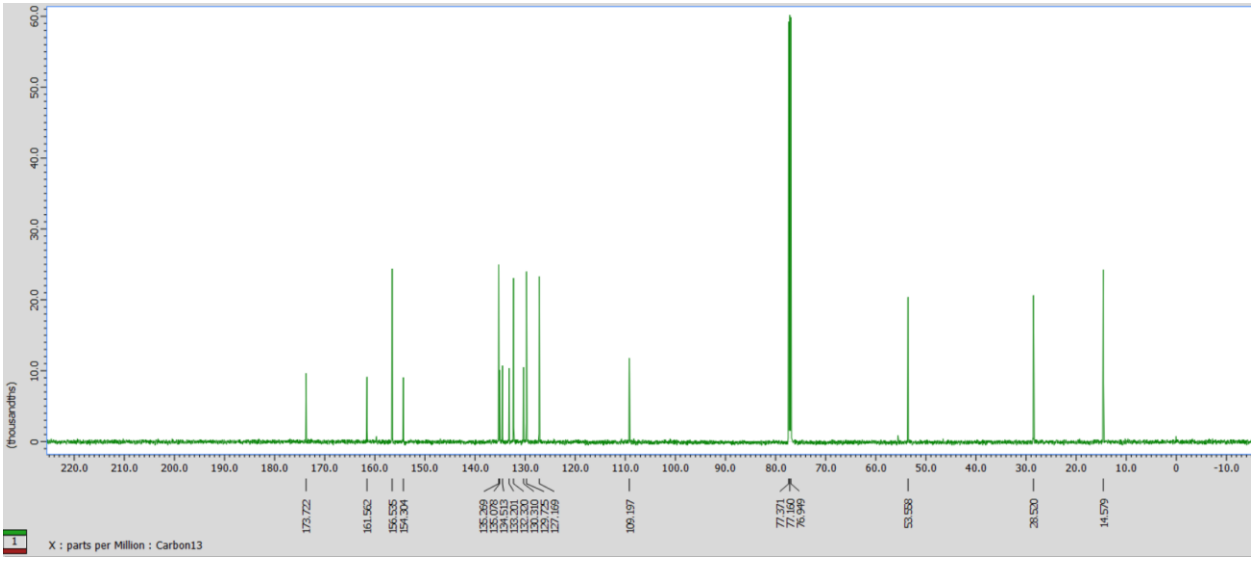
(thousandths)
173.722
161.562
156.535
154.304
135.399
135.078
134.513
133.201
131.310
130.310
129.755
127.169
109.197
77.371
77.160
76.949
53.558
28.530
14.579
X : parts per Million : Carbon13

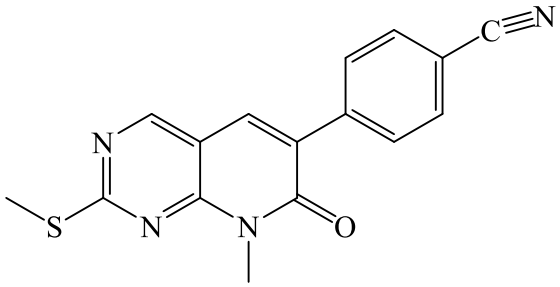
N
C≡N
S
N
N
O

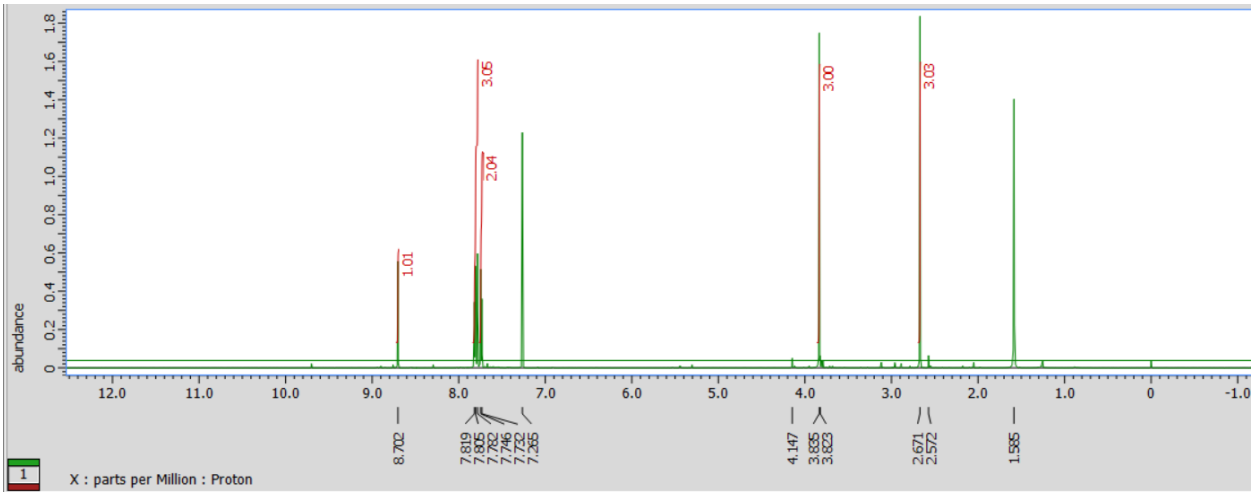
abundance
1.01
3.05
2.04
3.00
3.03
X : parts per Million : Proton

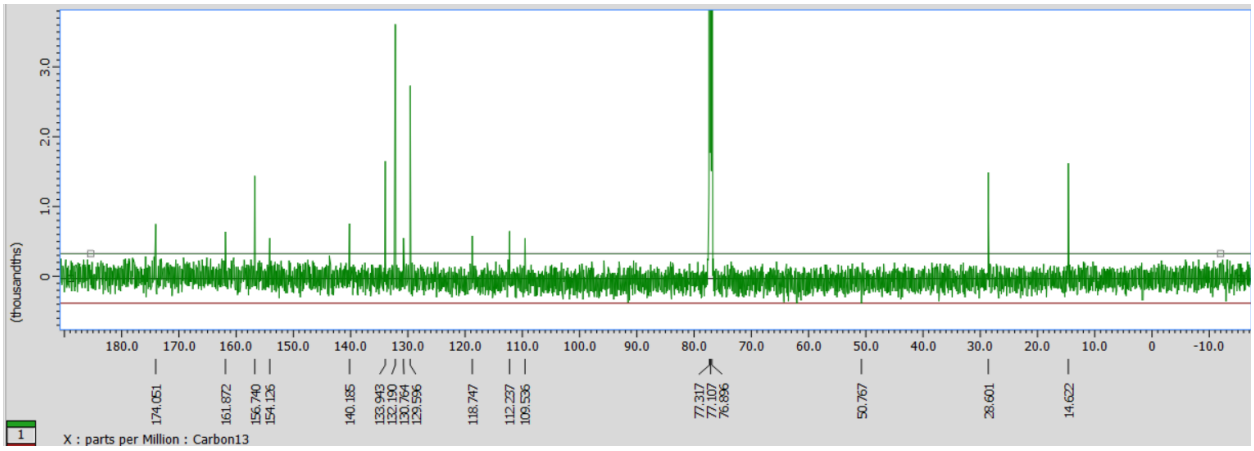
(thousandths)
X : parts per Million : Carbon13

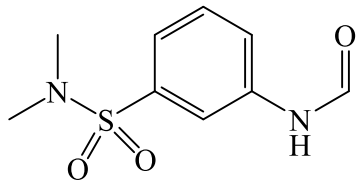
O
N
S
O
O
N
H

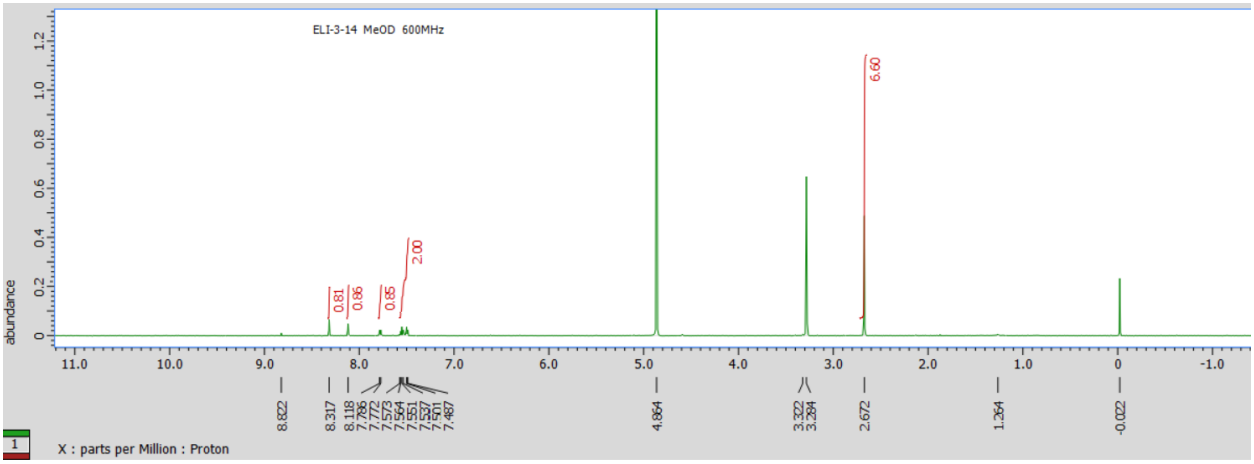
ELI-3-14 MeOD 600MHz
abundance
0.81
0.86
0.85
2.00
6.60
11.0
10.0
9.0
8.0
7.0
6.0
5.0
4.0
3.0
2.0
1.0
0
-1.0
8.822
8.317
8.118
7.786
7.772
7.573
7.564
7.537
7.501
7.487
4.864
3.322
3.294
2.672
1.264
-0.022
X : parts per Million : Proton

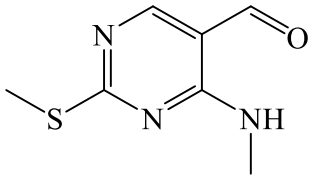
N
O
S
N
NH

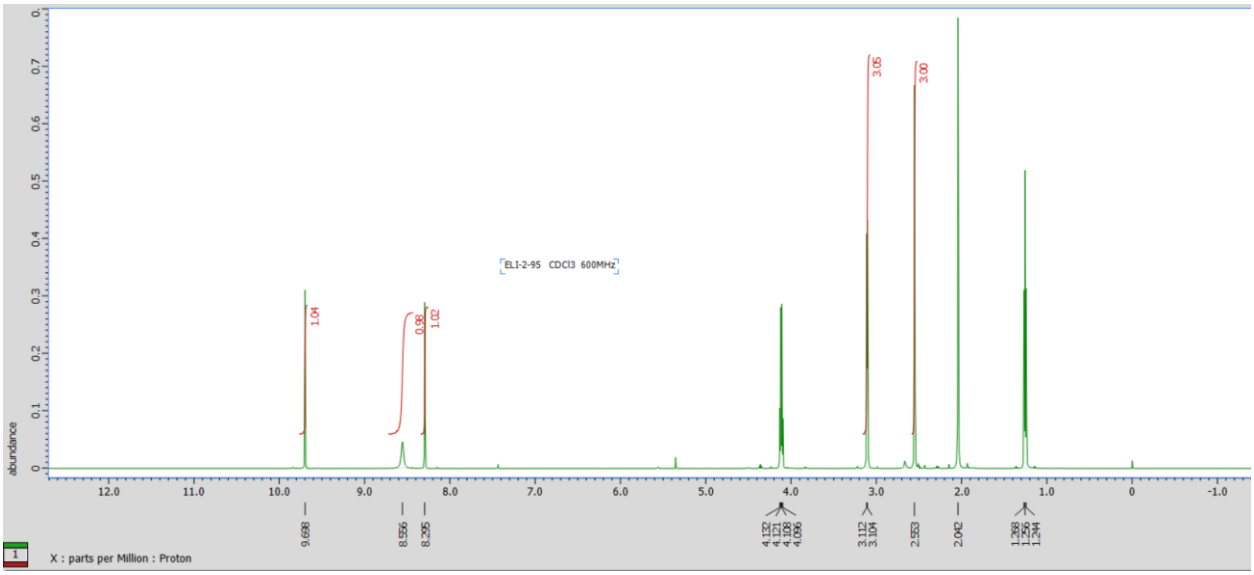
ELI-2-95 CDCl3 600MHz
1.04
0.98
1.02
3.05
3.00
abundance
X : parts per Million : Proton

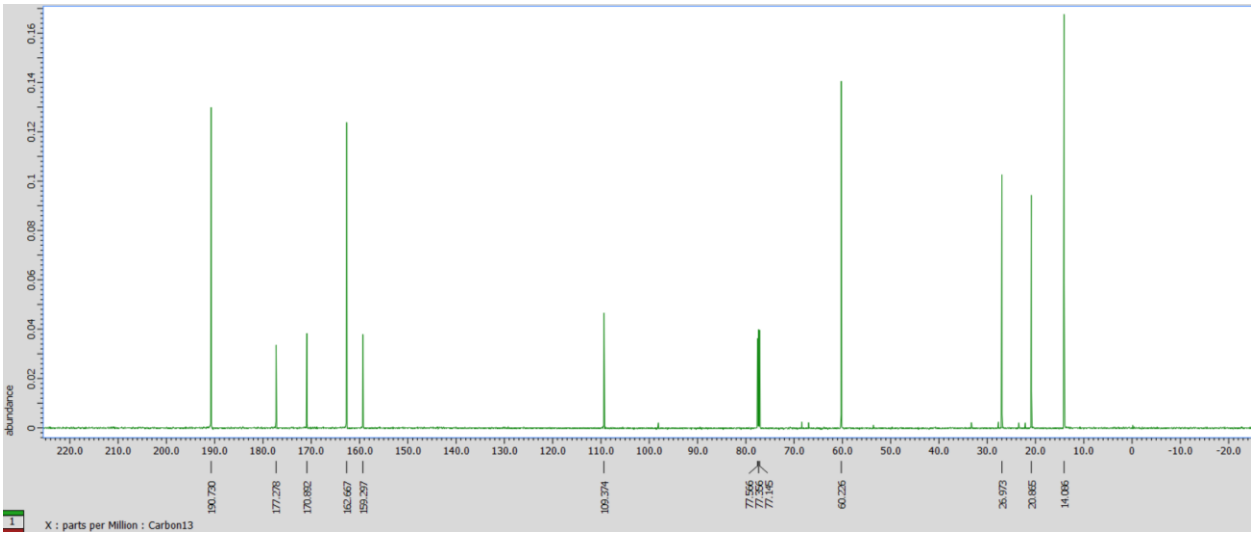
abundance
X : parts per Million : Carbon13

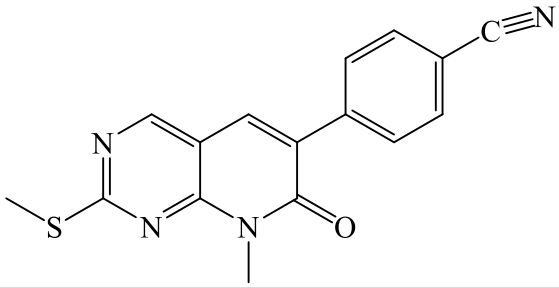
C≡N
N
S
N
N
O

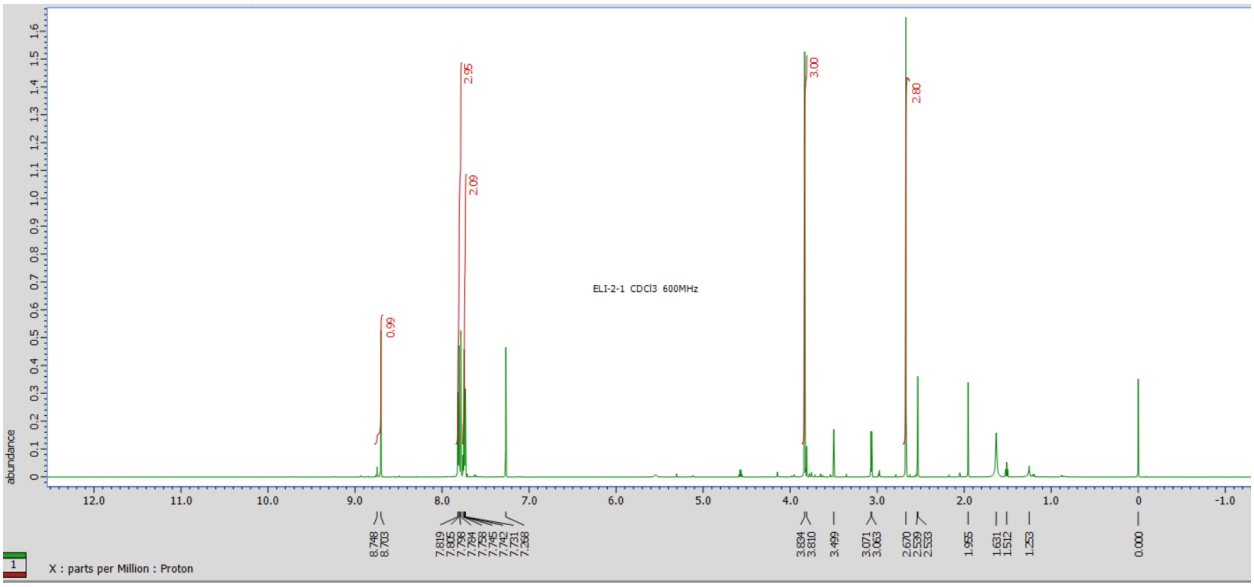
ELI-2-1 CDCl3 600MHz
abundance
X : parts per Million : Proton
0.99
2.95
2.09
3.00
2.80

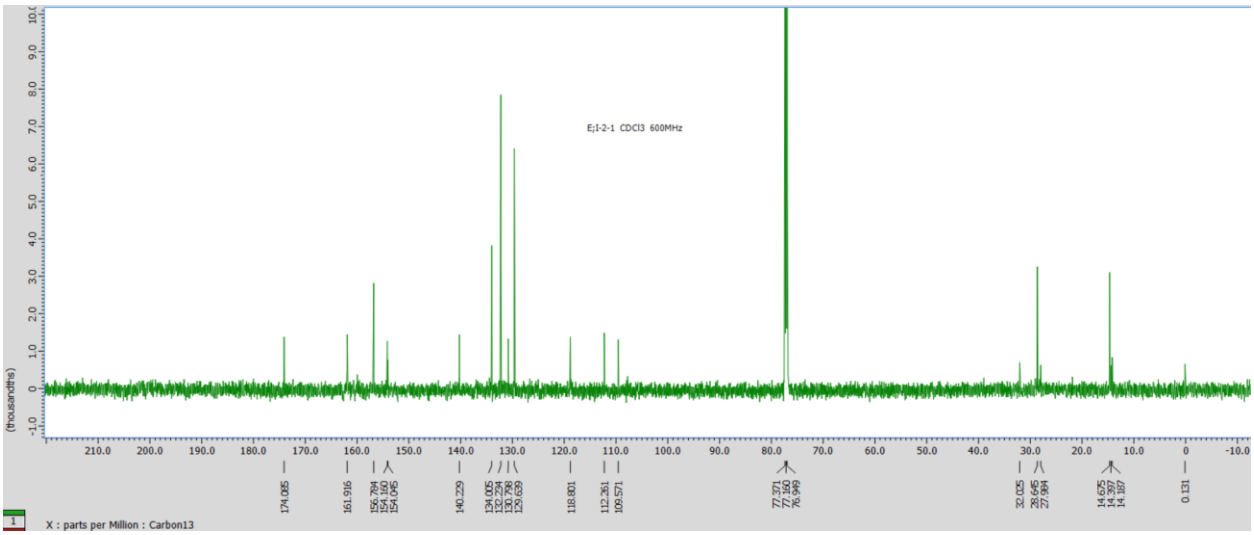
E;I-2-1 CDCl3 600MHz
(thousandths)
X : parts per Million : Carbon13

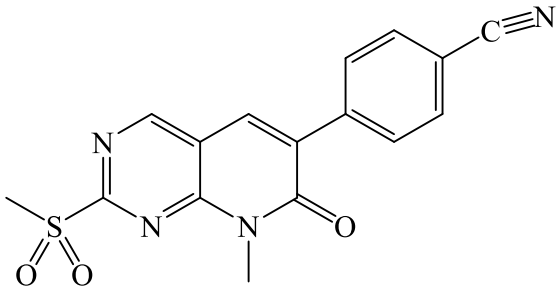
C≡N
N
S
O
O
N
N
O

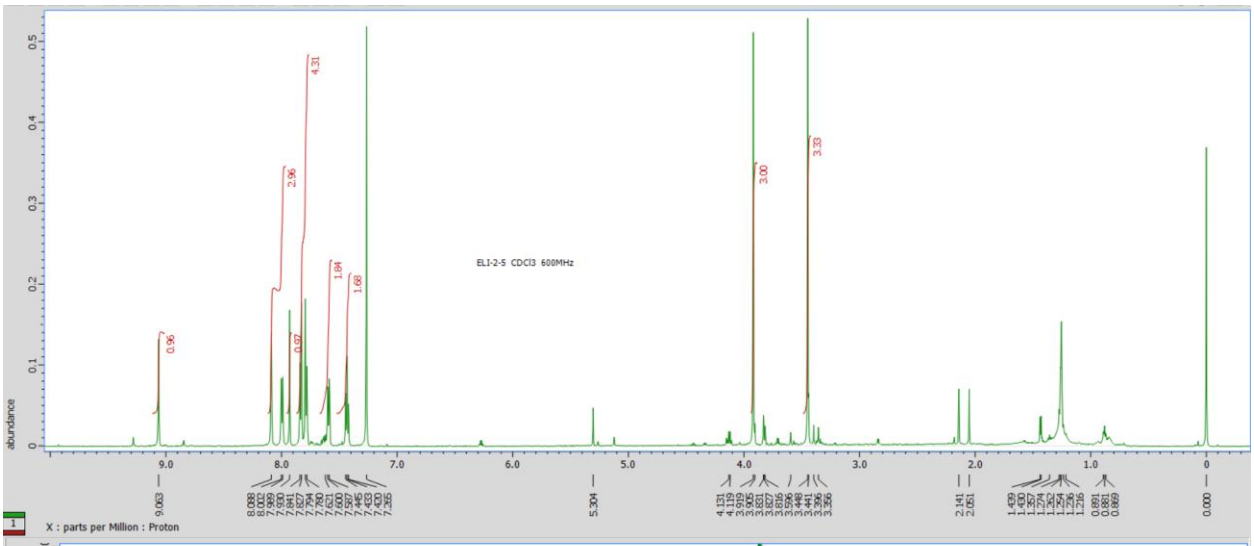
ELI-2-5 CDCl3 600MHz
abundance
X : parts per Million : Proton

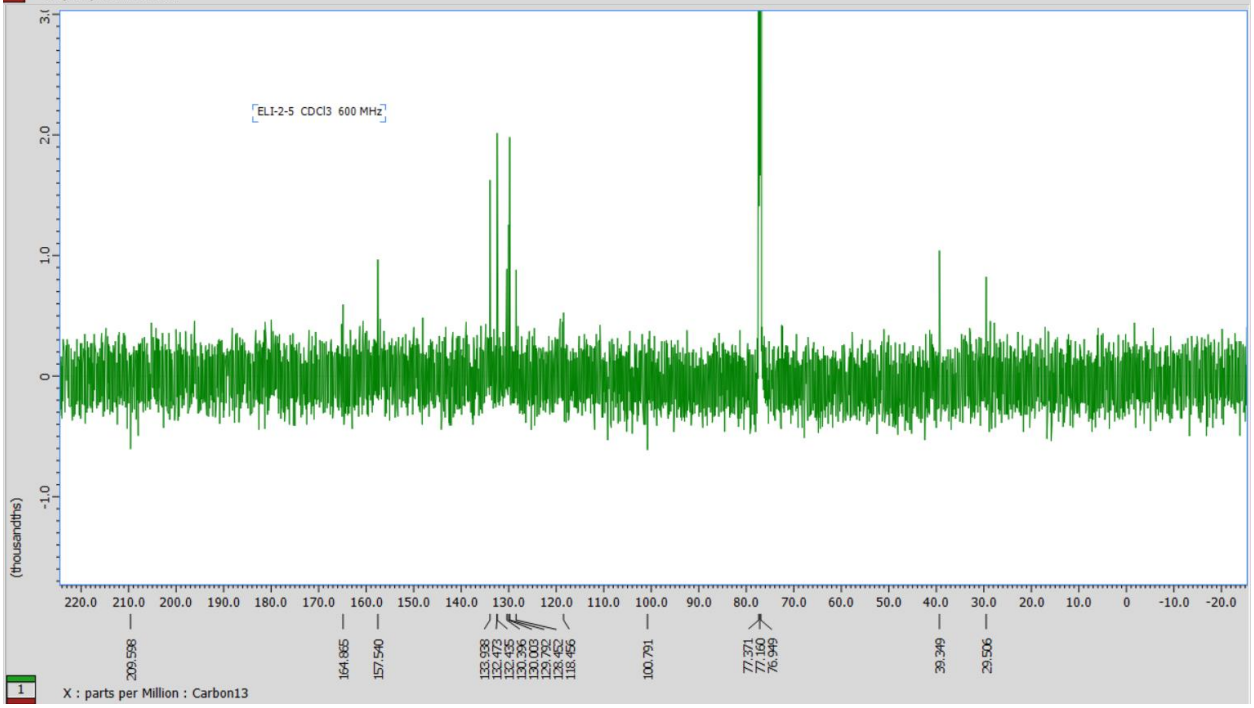
ELI-2-5 CDCl3 600 MHz
(thousandths)
X : parts per Million : Carbon13

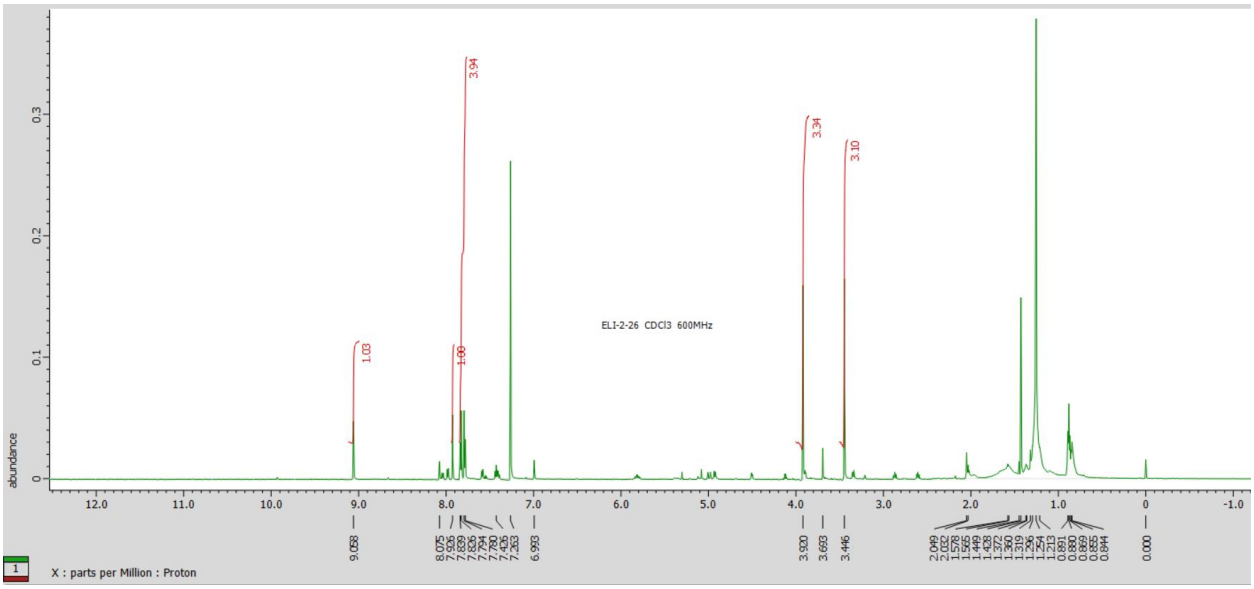
ELI-2-26 CDCl3 600MHz
abundance
X : parts per Million : Proton

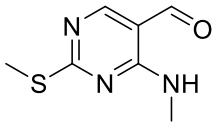
N
O
S
N
NH

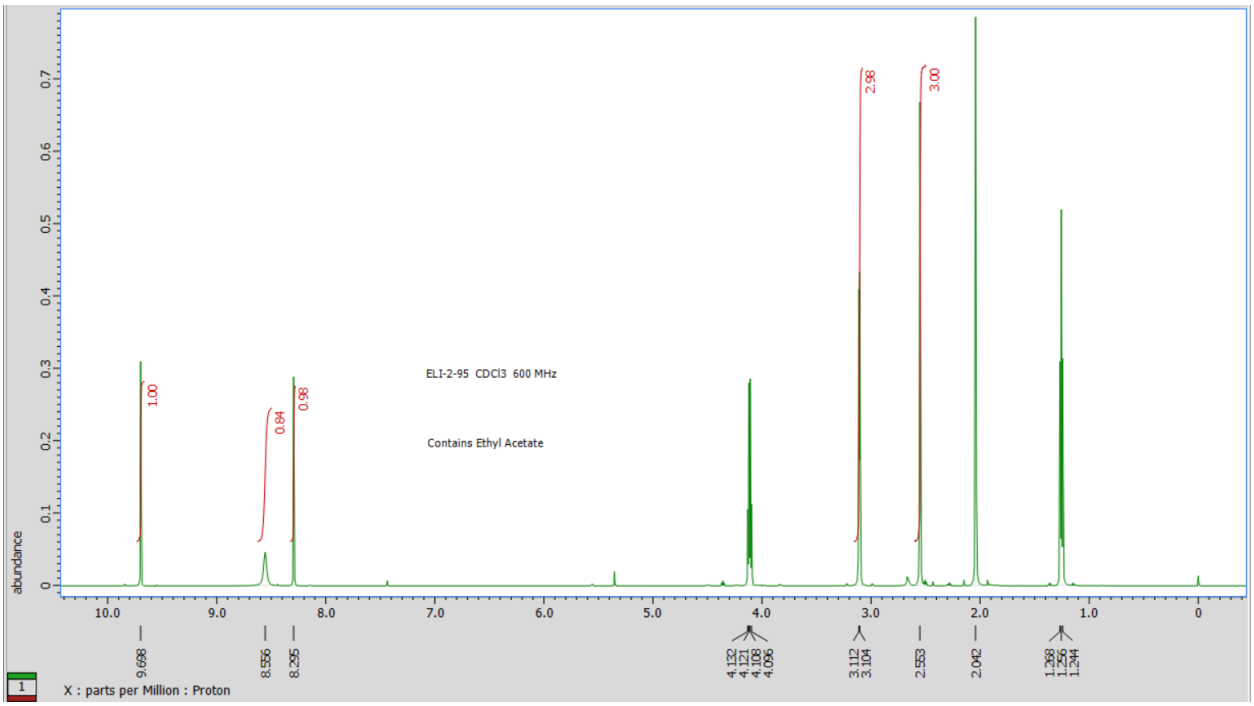
ELI-2-95 CDCl3 600 MHz
Contains Ethyl Acetate
1.00
0.84
0.98
2.98
3.00
abundance
X : parts per Million : Proton

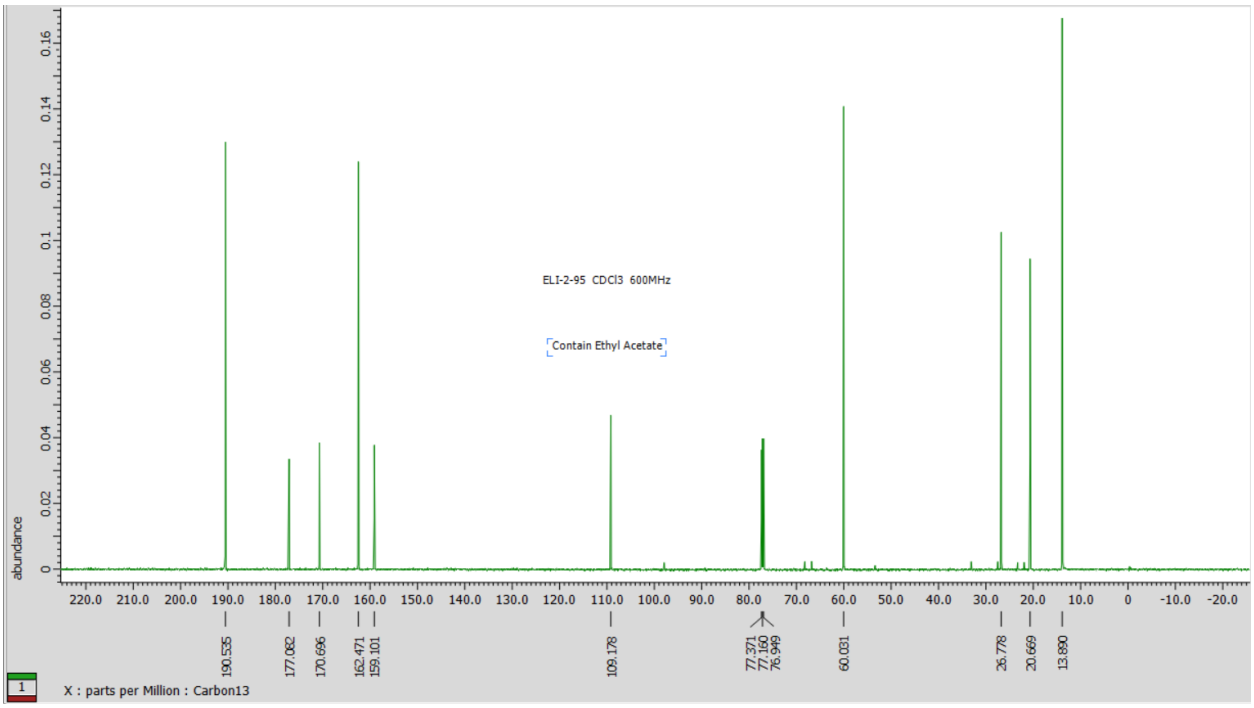
ELI-2-95 CDCl3 600MHz
Contain Ethyl Acetate
abundance
X : parts per Million : Carbon13

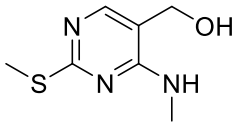
N
OH
S
N
NH

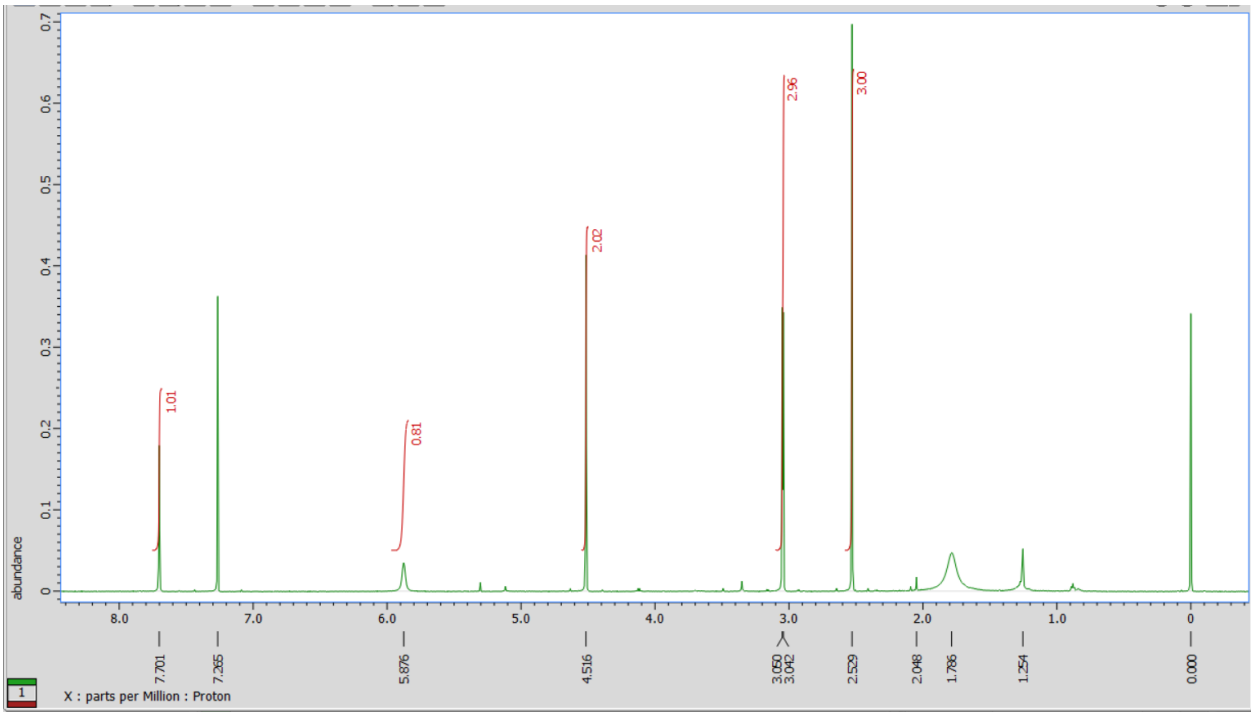
abundance
1.01
0.81
2.02
2.96
3.00
X : parts per Million : Proton

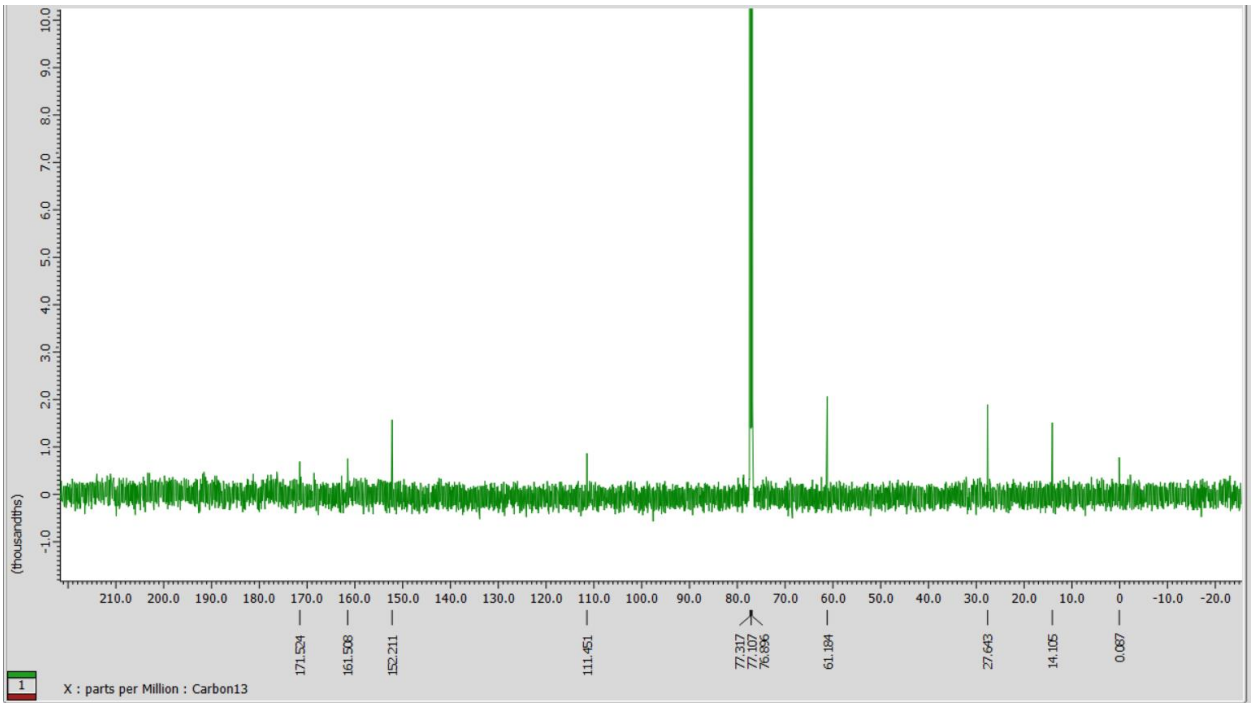
(thousandths)
X : parts per Million : Carbon13

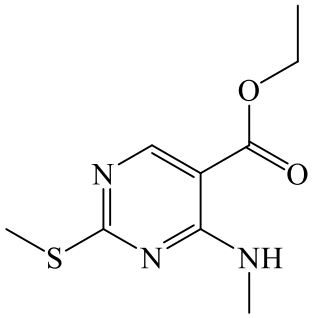
O
O
N
S
N
NH

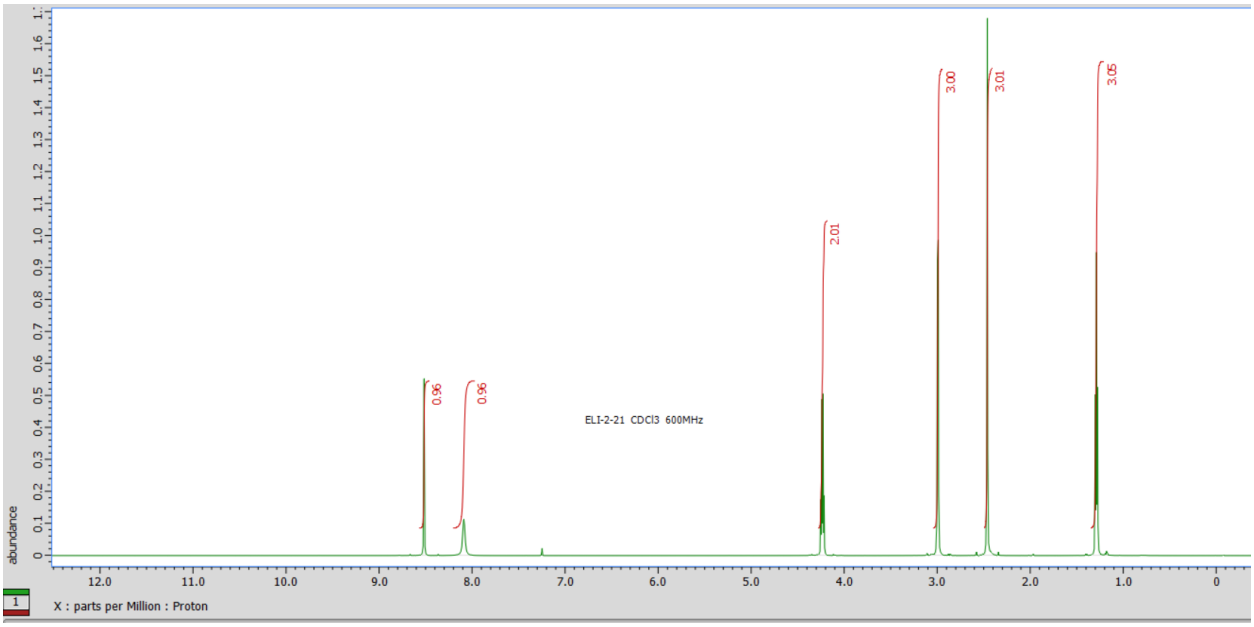
ELI-2-21 CDCl3 600MHz
0.96
0.96
2.01
3.00
3.01
3.05
abundance
X : parts per Million : Proton

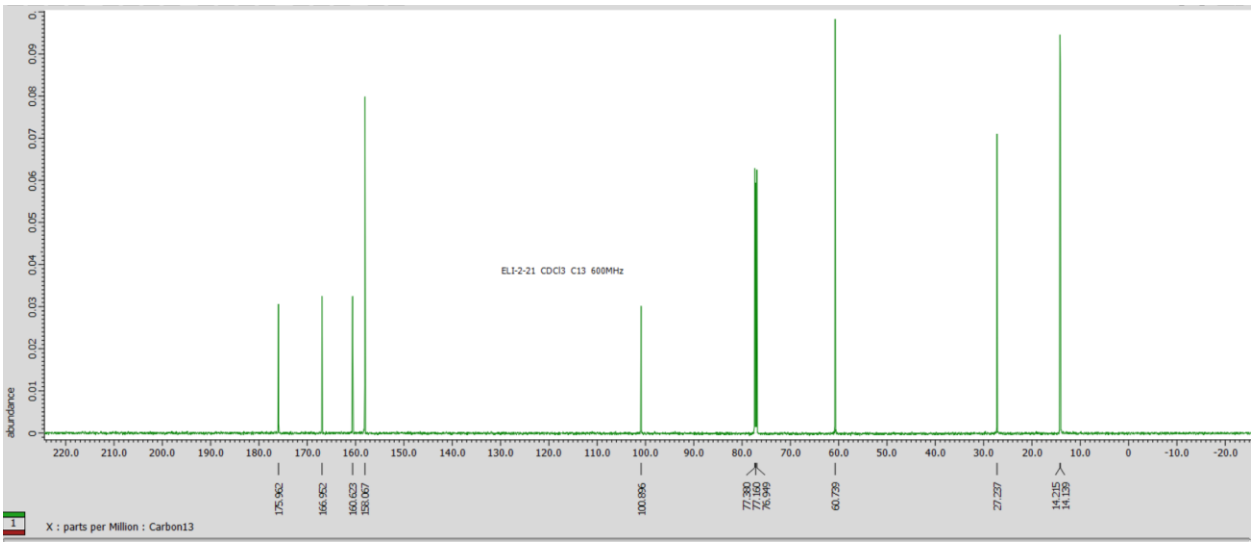
ELI-2-21 CDCl3 C13 600MHz
175.962
166.952
160.623
158.067
100.896
77.380
77.160
76.949
60.739
27.297
14.215
14.139
abundance
X : parts per Million : Carbon13

8.2. High-resolution mass spectroscopy data

ELI-CDPK-2

Target Compound Screening Report

Results Acquired by The University of Texas at Austin Mass Spectrometry Facility

Data File	MSF21-ELI-CDPK-2_hrESIpos2.d	**Sample Name**	ELI-CDPK-2	**Comment**	ELI-CDPK-2
Position	P1-D9	**Instrument Name**	Instrument 1	**User Name**	
Acq Method	FIA_pos.m	**Acquired Time**	11/11/2021 12:53:25 PM	**DA Method**	KS.m

MS Zoomed Spectrum

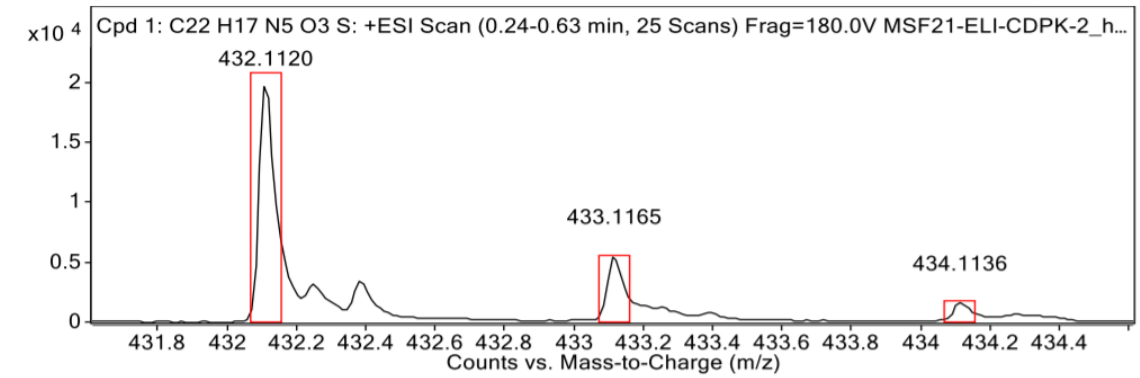

MS Spectrum Peak List

Obs. m/z	Calc. m/z	Charge	Abundance	Formula	Ion Species	Tgt Mass Error (ppm)
432.1120	432.1125	1	20299	C22H17N5O3S	(M+H)+	1.17
433.1165	433.1153	1	5706	C22H17N5O3S	(M+H)+	-2.62
434.1136	434.1129	1	1808	C22H17N5O3S	(M+H)+	-1.75
435.1692	435.1138	1	754	C22H17N5O3S	(M+H)+	-127.44
460.2695			871086			

--- End Of Report ---

ELI-CDPK-4

Target Compound Screening Report

Results Acquired by The University of Texas at Austin Mass Spectrometry Facility

Data File	MSF21-ELI-CDPK-4_hrESIpos1.d	**Sample Name**	ELI-CDPK-4	**Comment**	ELI-CDPK-4
Position	P1-E2	**Instrument Name**	Instrument 1	**User Name**	
Acq Method	FIA_pos.m	**Acquired Time**	11/11/2021 12:04:06 PM	**DA Method**	KS.m

MS Zoomed Spectrum

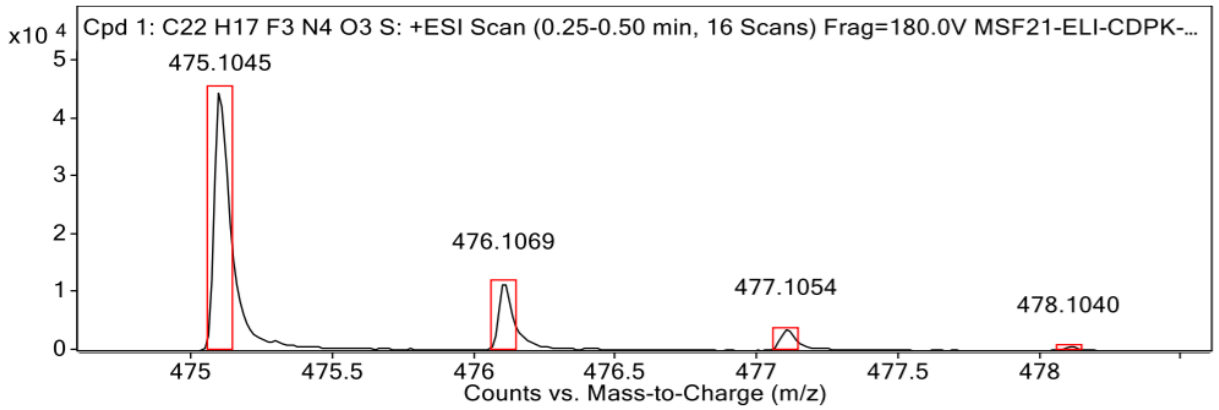

MS Spectrum Peak List

Obs. m/z	Calc. m/z	Charge	Abundance	Formula	Ion Species	Tgt Mass Error (ppm)
475.1045	475.1046	1	45445	C22H17F3N4O3S	(M+H)+	0.21
476.1069	476.1075	1	11711	C22H17F3N4O3S	(M+H)+	1.37
477.1054	477.1050	1	3820	C22H17F3N4O3S	(M+H)+	-0.93
478.1040	478.1060	1	766	C22H17F3N4O3S	(M+H)+	4.26
479.1337	479.1074	1	153	C22H17F3N4O3S	(M+H)+	-54.96

--- End Of Report ---

ELI-CDPK-6

Target Compound Screening Report

Results Acquired by The University of Texas at Austin Mass Spectrometry Facility

Data File	MSF21-ELI-CDPK-6_hrESIpos1.d	**Sample Name**	ELI-CDPK-6	**Comment**	ELI-CDPK-6
Position	P1-E3	**Instrument Name**	Instrument 1	**User Name**	
Acq Method	FIA_pos.m	**Acquired Time**	11/11/2021 12:05:48 PM	**DA Method**	KS.m

MS Zoomed Spectrum

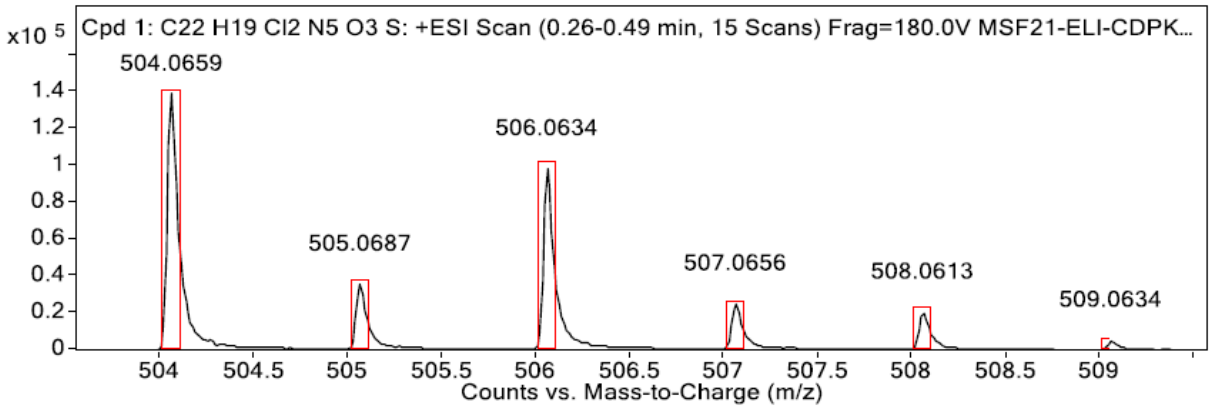

MS Spectrum Peak List

Obs. m/z	Calc. m/z	Charge	Abundance	Formula	Ion Species	Tgt Mass Error (ppm)
504.0659	504.0658	1	139726	C22H19Cl2N5O3S	(M+H)+	-0.02
505.0687	505.0687	1	35501	C22H19Cl2N5O3S	(M+H)+	-0.01
506.0634	506.0633	1	98314	C22H19Cl2N5O3S	(M+H)+	-0.26
507.0656	507.0658	1	24914	C22H19Cl2N5O3S	(M+H)+	0.48
508.0613	508.0612	1	20326	C22H19Cl2N5O3S	(M+H)+	-0.23
509.0634	509.0632	1	5009	C22H19Cl2N5O3S	(M+H)+	-0.3
510.0614	510.0611	1	1417	C22H19Cl2N5O3S	(M+H)+	-0.65

--- End Of Report ---

ELI-CDPK-7

Target Compound Screening Report

Results Acquired by The University of Texas at Austin Mass Spectrometry Facility

Data File	MSF21-ELI-CDPK-7_hrESIpos1.d	**Sample Name**	ELI-CDPK-7	**Comment**	ELI-CDPK-7
Position	P1-E4	**Instrument Name**	Instrument 1	**User Name**	
Acq Method	FIA_pos.m	**Acquired Time**	11/11/2021 12:07:31 PM	**DA Method**	KS.m

MS Zoomed Spectrum

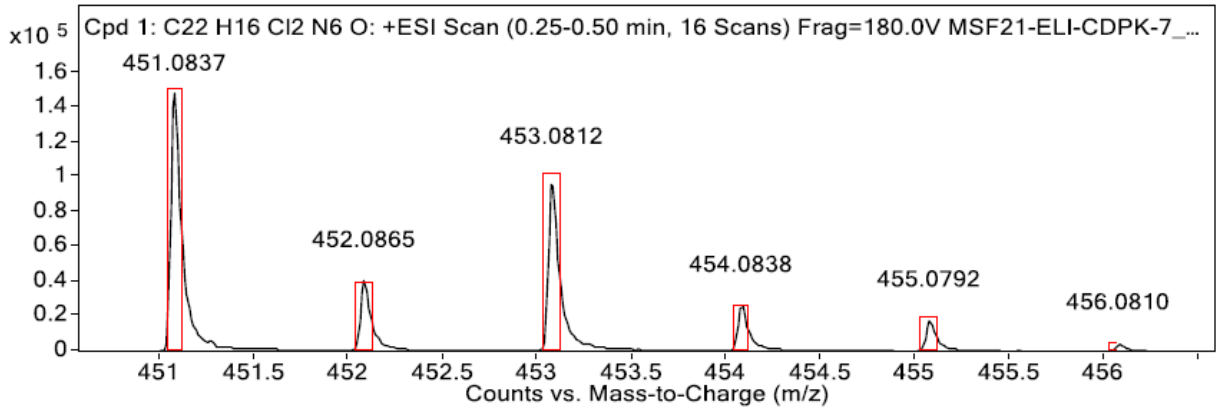

MS Spectrum Peak List

Obs. m/z	Calc. m/z	Charge	Abundance	Formula	Ion Species	Tgt Mass Error (ppm)
451.0837	451.0835	1	149920	C22H16Cl2N6O	(M+H)+	-0.32
452.0865	452.0864	1	40368	C22H16Cl2N6O	(M+H)+	-0.31
453.0812	453.0810	1	99741	C22H16Cl2N6O	(M+H)+	-0.42
454.0838	454.0836	1	26073	C22H16Cl2N6O	(M+H)+	-0.51
455.0792	455.0792	1	17616	C22H16Cl2N6O	(M+H)+	0
456.0810	456.0811	1	4491	C22H16Cl2N6O	(M+H)+	0.26
457.0792	457.0835	1	600	C22H16Cl2N6O	(M+H)+	9.61
458.0919	458.0861	1	143	C22H16Cl2N6O	(M+H)+	-12.73

--- End Of Report ---

ELI-CDPK-8*

*this is the compound that coupled twice with the heterocycle

Target Compound Screening Report

Results Acquired by The University of Texas at Austin Mass Spectrometry Facility

Data File	MSF21-ELI-CDPK-8_hrESIpos2.d	**Sample Name**	ELI-CDPK-8	**Comment**	ELI-CDPK-8
Position	P1-E5	**Instrument Name**	Instrument 1	**User Name**	
Acq Method	FIA_pos.m	**Acquired Time**	11/11/2021 12:55:13 PM	**DA Method**	KS.m

MS Zoomed Spectrum

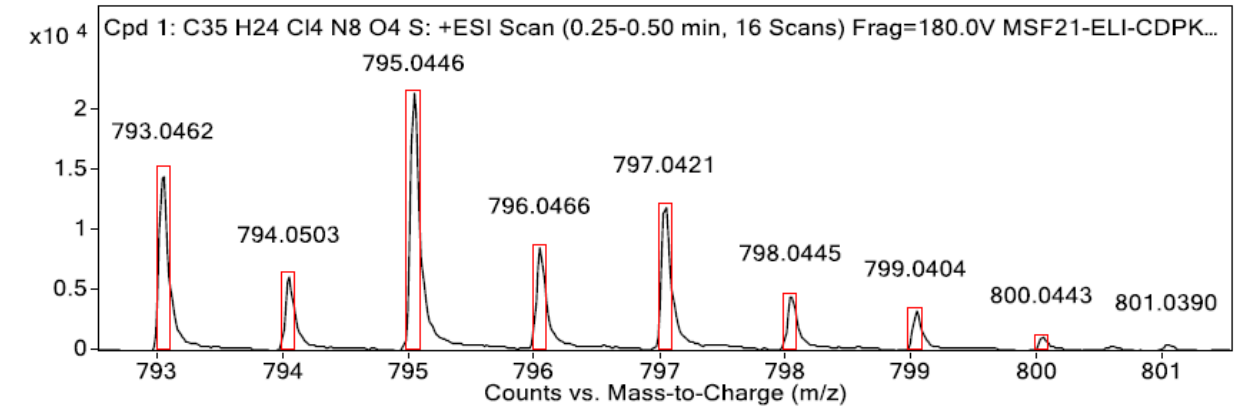

MS Spectrum Peak List

Obs. m/z	Calc. m/z	Charge	Abundance	Formula	Ion Species	Tgt Mass Error (ppm)
305.0205			29702			
793.0462	793.0468	1	14793	C35H24Cl4N8O4S	(M+H)+	0.72
794.0503	794.0497	1	6182	C35H24Cl4N8O4S	(M+H)+	-0.76
795.0446	795.0444	1	21534	C35H24Cl4N8O4S	(M+H)+	-0.24
796.0466	796.0469	1	8574	C35H24Cl4N8O4S	(M+H)+	0.42
797.0421	797.0422	1	12010	C35H24Cl4N8O4S	(M+H)+	0.16
798.0445	798.0442	1	4644	C35H24Cl4N8O4S	(M+H)+	-0.36
799.0404	799.0404	1	3348	C35H24Cl4N8O4S	(M+H)+	-0.03
800.0443	800.0418	1	1136	C35H24Cl4N8O4S	(M+H)+	-3.18
801.0390	801.0392	1	527	C35H24Cl4N8O4S	(M+H)+	0.29

--- End Of Report ---

ELI-CDPK-9**

Target Compound Screening Report

Results Acquired by The University of Texas at Austin Mass Spectrometry Facility

Data File	MSF21-ELI-CDPK-9_hrESIpos1.d	**Sample Name**	ELI-CDPK-9	**Comment**	ELI-CDPK-9
Position	P1-E6	**Instrument Name**	Instrument 1	**User Name**	
Acq Method	FIA_pos.m	**Acquired Time**	11/11/2021 12:10:59 PM	**DA Method**	KS.m

MS Zoomed Spectrum

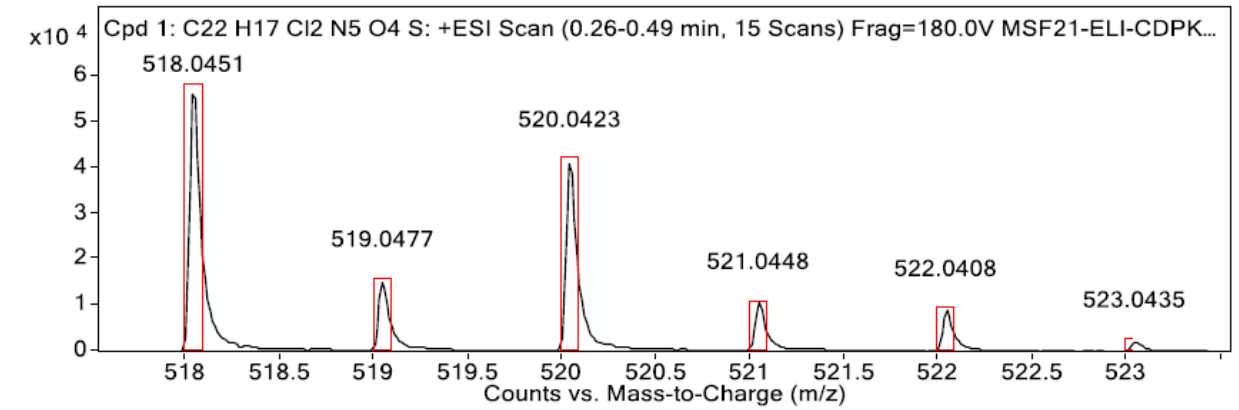

MS Spectrum Peak List

Obs. m/z	Calc. m/z	Charge	Abundance	Formula	Ion Species	Tgt Mass Error (ppm)
518.0451	518.0451	1	57997	C22H17Cl2N5O4S	(M+H)+	-0.04
519.0477	519.0479	1	15428	C22H17Cl2N5O4S	(M+H)+	0.47
520.0423	520.0426	1	41588	C22H17Cl2N5O4S	(M+H)+	0.48
521.0448	521.0451	1	10601	C22H17Cl2N5O4S	(M+H)+	0.69
522.0408	522.0405	1	9049	C22H17Cl2N5O4S	(M+H)+	-0.6
523.0435	523.0425	1	2218	C22H17Cl2N5O4S	(M+H)+	-1.79
524.0445	524.0405	1	597	C22H17Cl2N5O4S	(M+H)+	-7.67
525.0579	525.0413	1	107	C22H17Cl2N5O4S	(M+H)+	-31.72

--- End Of Report ---

**The parent compound was not found. However, a hydroxy amine adduct was observed, possibly arising from ammonium acetate in the model phase.

8.3. UV plate reader data

Captisol levels

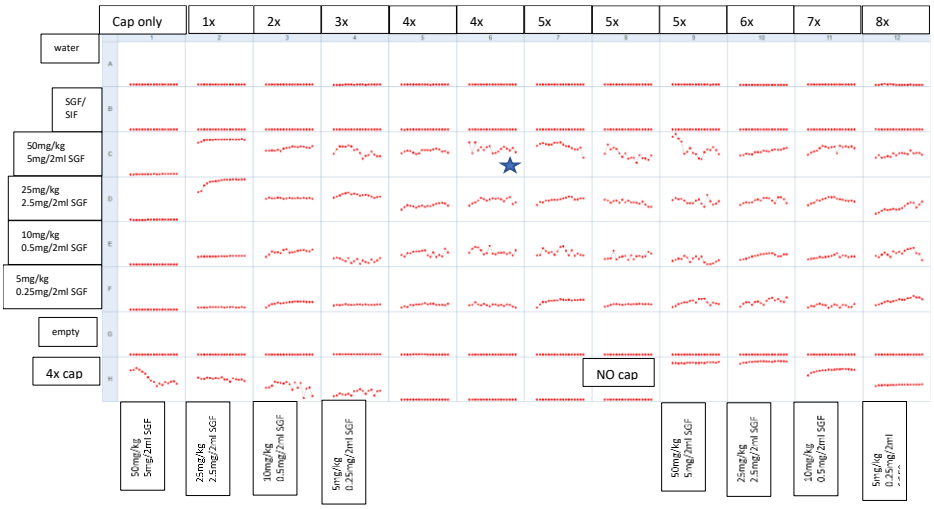

Star indicates a cat hair on the plate

Will repeat 4x & 5x cap with new SIF, triplicate + tween + methyl cellulose @ 50 mg/kg (tween shown above)

Increase frequency of read from q15min to q5min (“dots” or reads are closer together in the top plate)

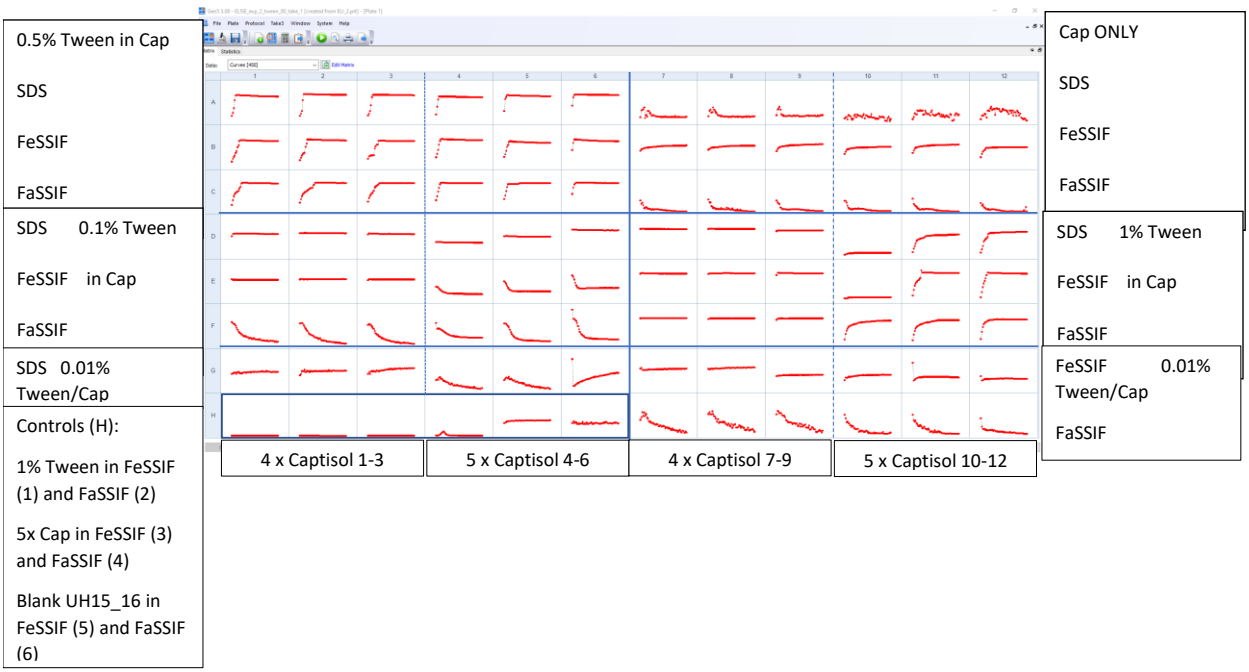

Introducing Tween 80

Methyl Cellulose

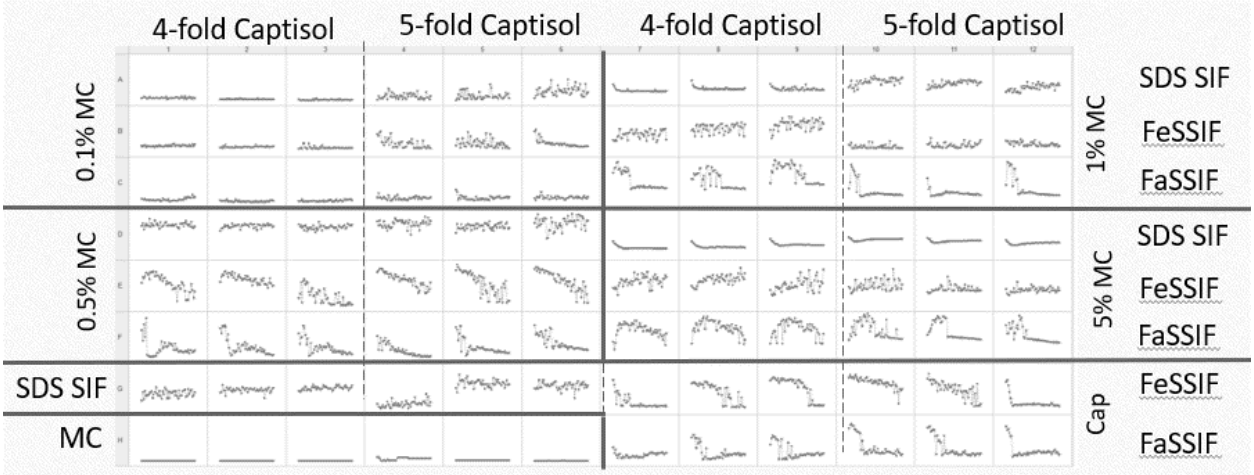

Increasing Tween 80

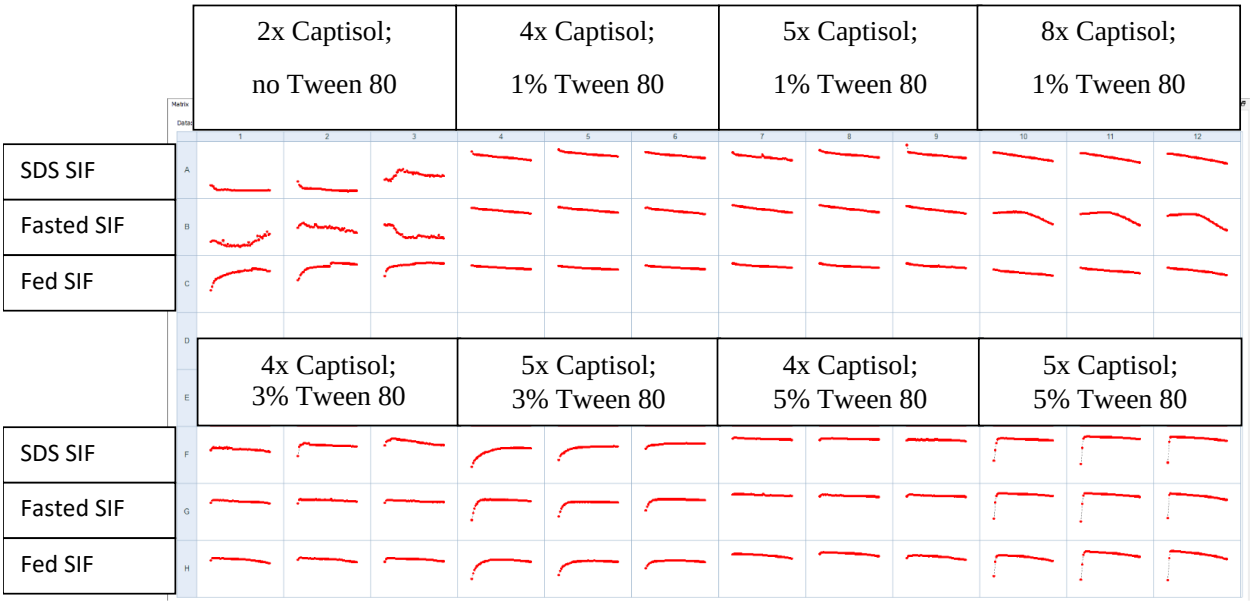

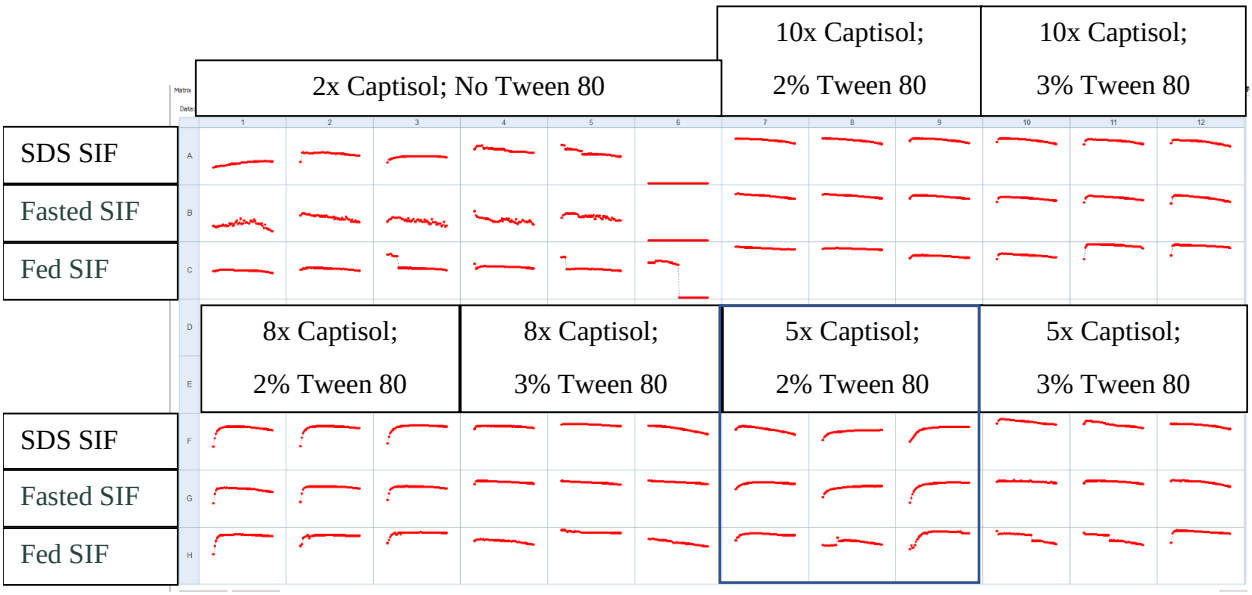

Lowering Tween 80 Tween 80 – toxicity concerns

8.4 HPLC Data

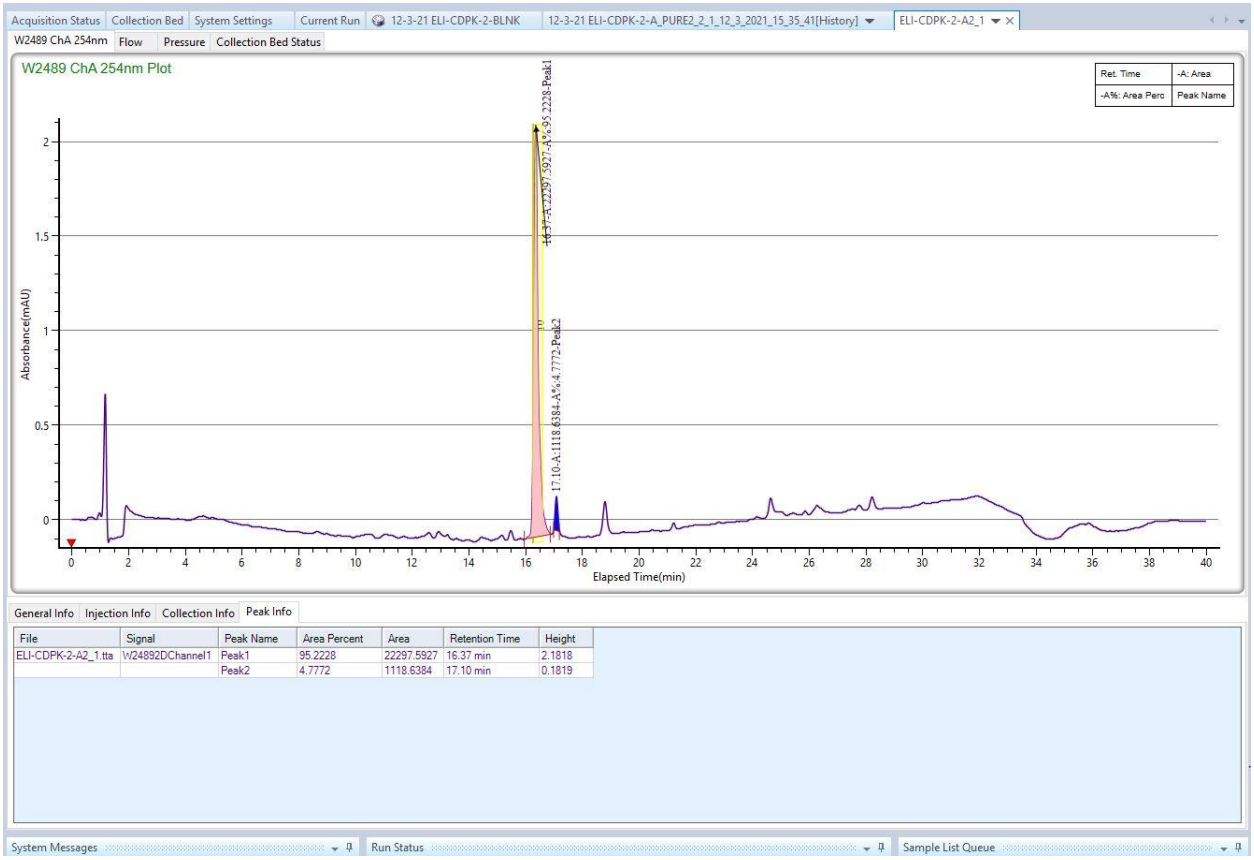

Peak at 19 mins is from column

ELI-CDPK-4

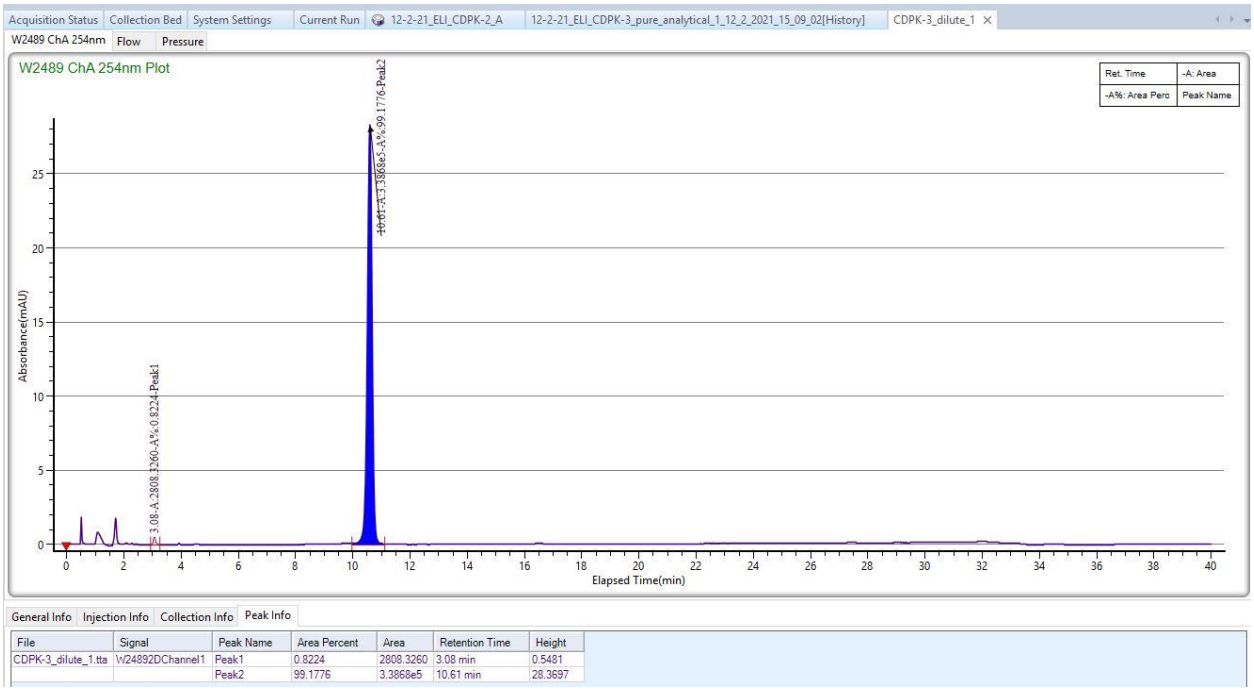

File	Signal	Peak Name	Area Percent	Area	Retention Time	Height
CDPK-3_dilute_1.tta	W2489 2DChannel1	Peak1	0.8224	2808.3260	3.08 min	0.5481
		Peak2	99.1776	3.3868e5	10.61 min	28.3697

ELI-CDPK-6

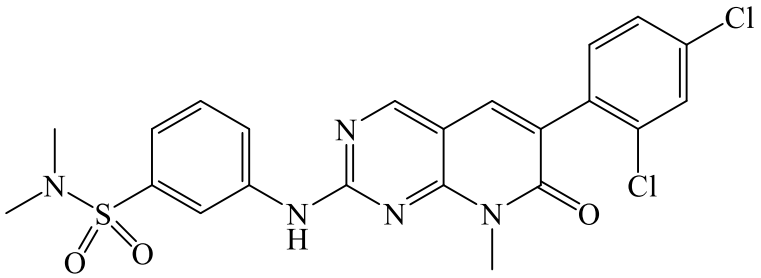
Cl
Cl
N
S
O
O
N
H
N
N
N
O

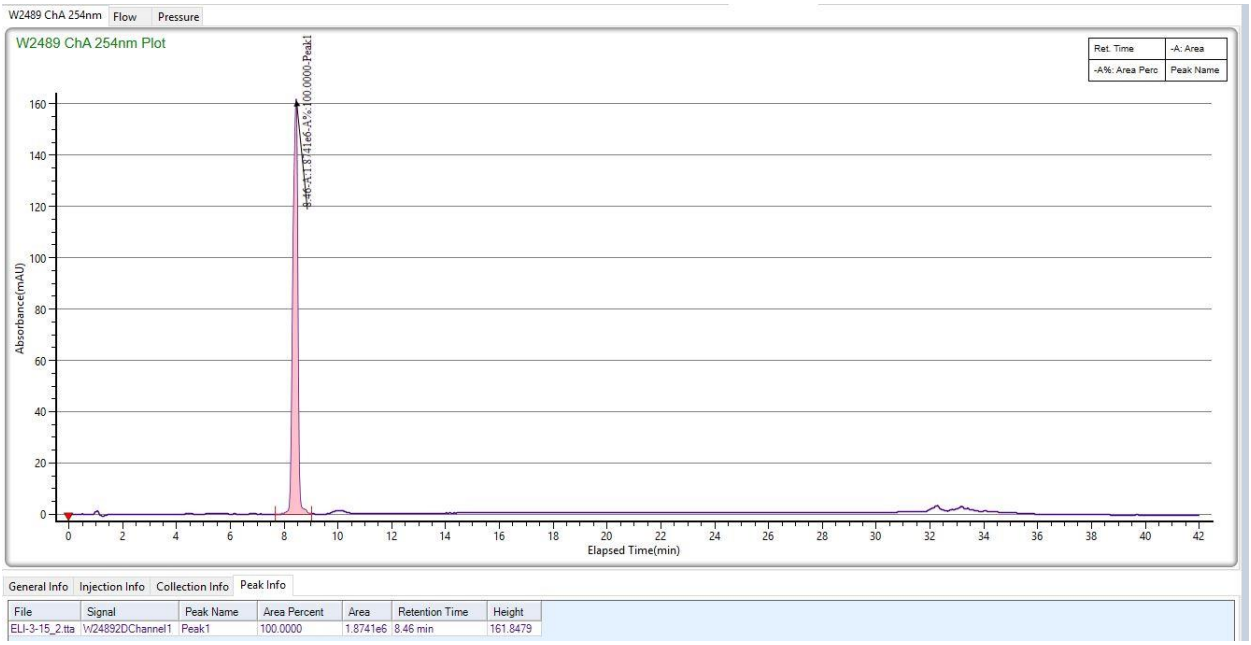
W2489 ChA 254nm
Flow
Pressure
W2489 ChA 254nm Plot
Ret. Time
-A: Area
-A%: Area Perc
Peak Name
Absorbance(mAU)
Elapsed Time(min)
General Info
Injection Info
Collection Info
Peak Info
File
Signal
Peak Name
Area Percent
Area
Retention Time
Height
ELI-3-15_2.tta
W24892DChannel1
Peak1
100.0000
1.8741e6
8.46 min
161.8479

ELI-CDPK-7

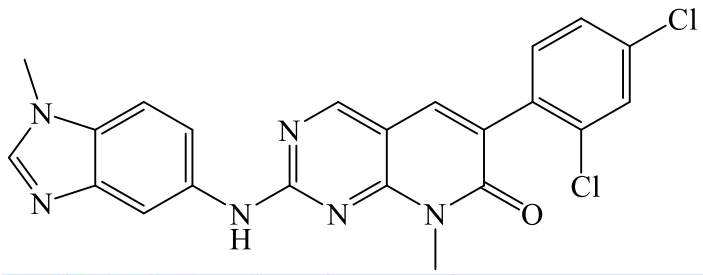
Cl
Cl
N
N
N
H
N
N
N
O

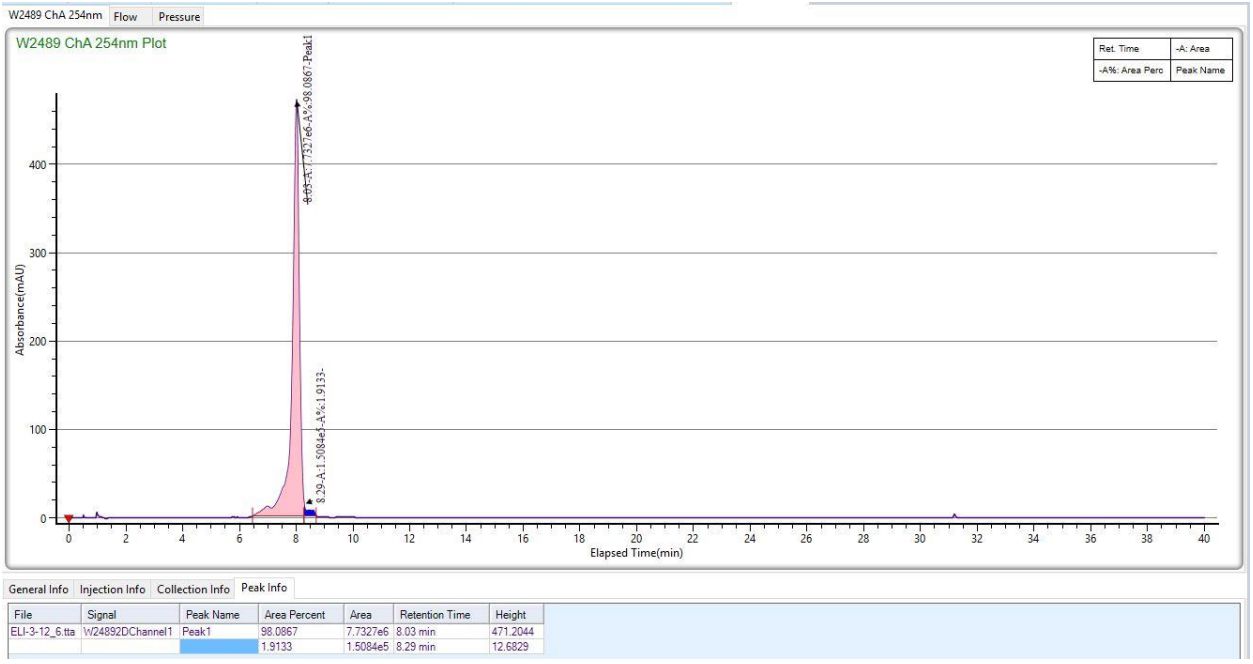
W2489 ChA 254nm
Flow
Pressure
W2489 ChA 254nm Plot
Ret. Time
-A: Area
-A%: Area Perc
Peak Name
Absorbance(mAU)
Elapsed Time(min)
General Info
Injection Info
Collection Info
Peak Info
File
Signal
Peak Name
Area Percent
Area
Retention Time
Height
ELI-3-12_6.tta
W2489ZDChannel1
Peak1
98.0867
7.7327e6
8.03 min
471.2044
1.9133
1.5084e5
8.29 min
12.6829

ELI-CDPK-8

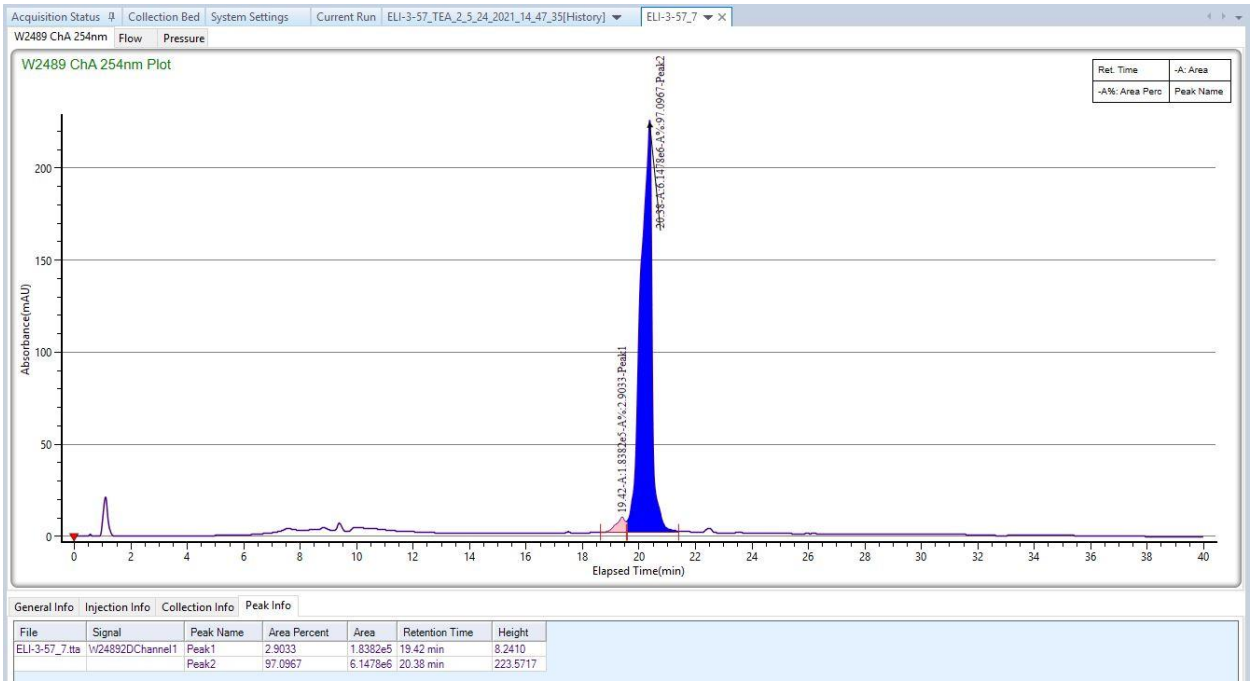

File	Signal	Peak Name	Area Percent	Area	Retention Time	Height
ELI-3-57_7.tta	W24892DChannel1	Peak1	2.9033	1.8382e5	19.42 min	8.2410
		Peak2	97.0967	6.1478e6	20.38 min	223.5717

ELI-CDPK-9

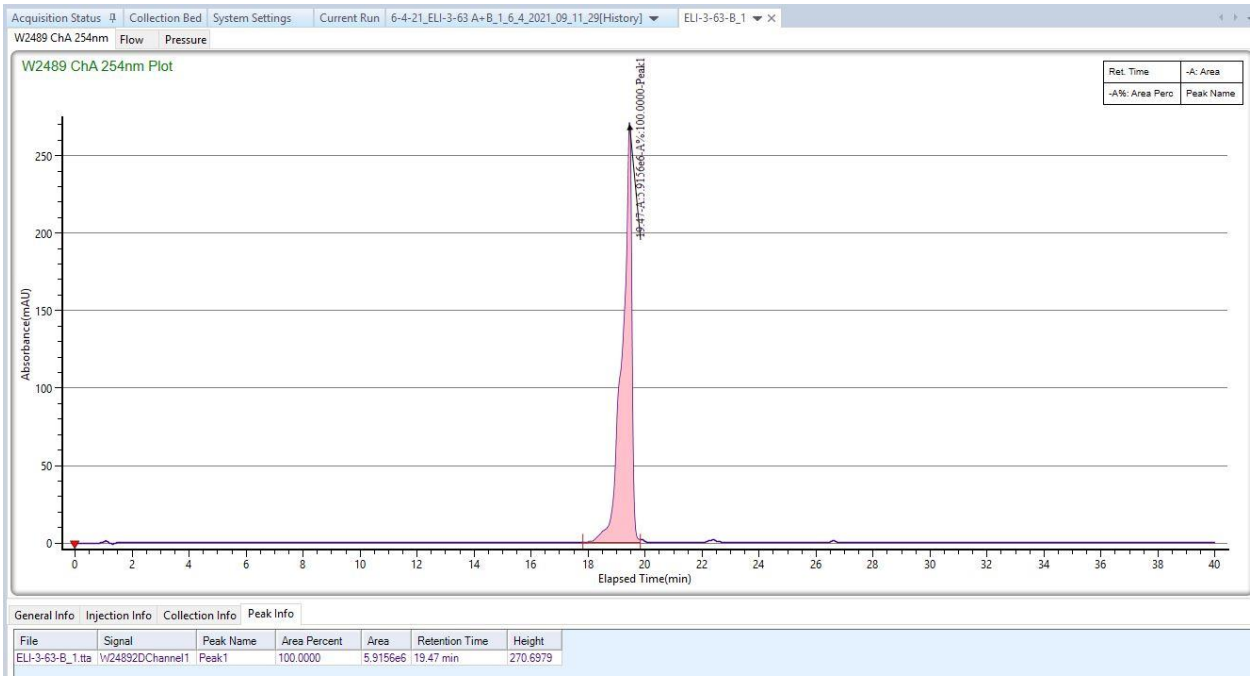
Acquisition Status
Collection Bed
System Settings
Current Run
6-4-21_ELI-3-63 A+B_1_6_4_2021_09_11_29[History]
ELI-3-63-B_1
W2489 ChA 254nm
Flow
Pressure
W2489 ChA 254nm Plot
Ret. Time
-A: Area
-A%: Area Perc
Peak Name
19.47-A:5.9156e6-A%:100.0000-Peak1
Absorbance(mAU)
Elapsed Time(min)
General Info
Injection Info
Collection Info
Peak Info
File
Signal
Peak Name
Area Percent
Area
Retention Time
Height
ELI-3-63-B_1.tta
W2489DChannel1
Peak1
100.0000
5.9156e6
19.47 min
270.6979

8.5. AUC calculations

AUC calculations for IV Formulation

	Ave		
Time(h)	**Conc (nM)**	Conc ng/mL	AUC/interval
0	**0**	0	27.056
0.08	**1424**	676.4	111.11523
0.25	**1328.08**	630.838	176.241625
0.5	**1640.2**	779.095	376.2
1	**1527.8**	725.705	625.86
2	**1107.4**	526.015	877.895
4	**740.8**	351.88	592.61
6	**506.8**	240.73	401.945
8	**339.4**	161.215	1780.68
24	**129.2**	61.37	

AUC 4942.546855 ng*h/mL

AUC calculations for Oral Formulation 1

	Ave		
Time(h)	**Conc (nM)**	Conc ng/mL	AUC/interval
0	**0**	0	0.79325
0.5	**6.68**	3.173	2.4711875
1	**14.13**	6.71175	7.0395
2	**15.51**	7.36725	13.1575
4	**12.19**	5.79025	10.697
6	**10.33**	4.90675	9.8135
8	**10.33**	4.90675	55.214
24	**4.2**	1.995	
		0	0
		0	0

AUC 98.3926875 h*ng/mL

AUC calculations for Oral Formulation 2

	Ave		
Time(h)	**Conc (nM)**	Conc ng/mL	AUC/interval

0	**0**	0	0.2375
0.25	4.0	1.9	0.6353125
0.5	6.7	3.1825	2.01875
1	10.3	4.8925	6.76875
2	18.2	8.645	25.8875
4	36.3	17.2425	26.7425
6	20.0	9.5	23.1325
8	28.7	13.6325	34.96
10	44.9	21.3275	203.8225
24	16.4	7.79	

AUC 323.9678125 h*ng/mL

AUC calculations for Oral Formulation 3

	Ave		
Time(h)	**Conc (nM)**	Conc ng/mL	AUC/interval
0	**0**	0	4.975625
1	21.0	9.95125	8.6884625
2	15.6	7.425675	6.7936875
3	13.0	6.1617	5.2005375
4	8.9	4.239375	4.099725
5	8.3	3.960075	11.12233875
8	7.3	3.4548175	8.76413
10	11.2	5.3093125	9.6935625
12	9.2	4.38425	9.26725
14	10.3	4.883	67.0225
24	17.9	8.5215	

AUC 130.6521938 h*ng/mL